2019

A co-culture microplate platform to quantify microbial interactions and growth dynamics

BOSTON UNIVERSITY

COLLEGE OF ENGINEERING

Thesis

A CO-CULTURE MICROPLATE PLATFORM TO QUANTIFY MICROBIAL INTERACTIONS AND GROWTH DYNAMICS

by

CHARLES JO

B.S.E., Duke University, 2017

Submitted in partial fulfillment of the

requirements for the degree of

Master of Science

2019

Approved by

First Reader

Daniel Segrè, Ph.D.
Professor of Biology
Professor of Biomedical Engineering
Professor of Physics

Second Reader

Ahmad S. Khalil, Ph.D.
Associate Professor of Biomedical Engineering

Third Reader

Horacio M. Frydman, Ph.D.
Associate Professor of Biology

Fourth Reader

Allyson E. Sgro, Ph.D.
Assistant Professor of Biomedical Engineering

DEDICATION

I dedicate this work to my dream. When dragons fly, I will rest.

ACKNOWLEDGEMENTS

I would like to acknowledge each and every member of the Segrè Lab for their support, guidance, and camaraderie. I joined the lab in early 2018 with limited lab experience – I had never even streaked an agar plate before I joined! Prof. Daniel Segrè and the community he fostered have encouraged my growth both as a researcher and as a person. I am incredibly blessed and grateful for the opportunity to learn alongside these talented individuals.

In particular, I want to acknowledge David Bernstein of the Segrè Lab. He pioneered the initial concept and prototype of the BioMe device, as well as leading the computational modeling work. Without his committed mentorship, thoughtful discussions, consistent support, and incredibly bright mind, the success of this project would have been impossible. I also wish to acknowledge the staff of Boston University's Engineering Product Innovation Center and of the Singh Imagineering Lab (Tinker), who were instrumental in the successful manufacturing of the BioMe prototypes.

Finally, I want to thank those who refuse to give up on me – my family, both given and found. Each and every one of you have shown me how to venture life's journey with enthusiasm, grit, focus, and positivity. Thank you for seeing my potential and not my accolades. To all of you, I am sincerely grateful.

A CO-CULTURE MICROPLATE PLATFORM TO QUANTIFY MICROBIAL INTERACTIONS AND GROWTH DYNAMICS

CHARLES JO

ABSTRACT

This thesis reports the development of BioMe, a co-culture microplate platform that enables high-throughput, real-time quantitative growth dynamics measurements of interacting microbial batch cultures. The primary BioMe components can be 3D-printed, allowing ease of fabrication and DIY accessibility in the microbiome community. A pairwise 3D-printed iteration of the BioMe device was used in diffusion and co-culture experiments. Genetically engineered *Escherichia Coli* lysine and isoleucine auxotroph strains were used to characterize the diffusion of amino acids across the porous membranes. Results demonstrated a nonlinear relationship between growth rate and pore size and also distinct diffusion behavior for lysine and isoleucine. Pairwise syntrophic co-culture experiments demonstrated synergistic but repressed interaction between these two paired auxotrophs. Investigation of the effect of varying initial amino acid conditions on growth dynamics demonstrated that small changes in initial media condition can consistently affect patterns of yield and growth rate of constituent microbial species.

TABLE OF CONTENTS

LIST OF TABLES

LIST OF FIGURES

LIST OF ABBREVIATIONS

BU…….…….. Boston University

CAD……..……...Computationally-Aided Design

CNC……..……...Computer Numerical Control

EPIC……Engineering Product Innovation Center (BU)

FBA…….……. Flux Balance Analysis

FDM……..….Fused Deposition Modeling (3D-Printing)

OD……..……...……Optical Density

SLA……..……...Stereolithography (3D-Printing)

SLS……..……Selective Laser Sintering (3D-Printing)

(1) INTRODUCTION

Microbial Community Interactions

The metabolism of an individual microbe is remarkably complex and variable, encompassing a plethora of metabolic processes that enable the survival and proliferation of a single organism [6, 7]. However, in the natural world, these individual metabolisms do not proceed in isolation. They are constantly interacting with the metabolisms and cellular processes of surrounding microorganisms, whether they be bacteria, fungi, viruses, or host cells – like our own [20, 53]. Highly intricate and multi-dimensional interaction networks emerge, whereby countless distinct species concurrently interact in varying fashions and degrees [16, 68]. Together, these interactions actively shape community structure and function, which is instrumental in an ecosystem's health and stability [5, 11, 22, 27, 57]. Welcome to the burgeoning field of microbiome research.

There are numerous possible mechanisms of microbial interactions, which can be broadly categorized into two classes: direct and indirect interactions [48]. Direct interactions require cell to cell contact and include mechanisms like bacterial conjugation, intercellular nanotubes, and cell-recognition systems [56, 68]. This thesis will focus on indirect interactions, which are diffusion-mediated and contact independent. These include mechanisms like competition, chemical signaling (including quorum sensing), horizontal gene transfer, and cross-feeding [62, 77]. Cross-feeding, also known as syntrophy, is a relationship wherein an organism depends on the products of another to survive and proliferate. A variety of cross-feeding motifs are possible, with many resulting in the cooperation and mutualism of its constituent members [52, 62]. Indeed, these symbiotic

relationships can be further characterized by its positive or negative effect on each community member: competition (-/-), mutualism (+/+), parasitism (+/-), and commensalism (+/0) [41].

Despite the explosion in metagenomic, metabolomic, and metaproteomic data in the microbiome space, the sheer complexity of naturally-occurring microbiota makes it challenging to uncover causal relationships in these systems [9, 18, 46]. So how do we begin to unravel the nature and effects of these interactions? How about their mechanisms of interaction? These types of questions are partially responsible for the naissance of synthetic ecology: the rational design, construction, and investigation of engineered microbial consortia [2, 4, 24, 82]. Researchers can leverage this bottom-up approach to selectively investigate inter-specific interactions of interest to infer the nature of these relationships in more complex natural environments.

In 2014, Mee et al. utilized these principles of synthetic ecology to study simplified instances of cross-feeding in genetically modified bacteria [45]. In a portion of their study, they generated strains of *E. Coli* which were genetically recombineered to host a single amino acid auxotrophy, by knocking out a single gene essential for the amino acid's production. These mutants were unable to survive without external supply of their deficient amino acid, but by performing pairwise co-cultures of complementary auxotrophs, they identified positive syntrophic interactions in a subset of these combinations. One such successful combination was that of the lysine auxotroph (ΔK) and the isoleucine auxotroph (ΔI), which were acquired and used for the experiments within this thesis.

Co-Culture Methods & Systems

In order to study the interspecific relationships that arise between microorganisms, it is necessary to co-culture the microbial species in such a way to allow for all or specific interaction mechanisms. Unfortunately, current co-culture methods face the great difficulty of disentangling the individual growth of constituent species in a community with high-resolution and minimal operational challenge [48]. A prevalent method is mixed co-culture, where distinct microbial species are cultured in the same vessel [26]. In order to quantify community composition, genomic assays (ex: qPCR/16S sequencing) or phenotypic plate assays (ex: serial dilution and morphological differentiation) are required. This is limited by the sheer logistical challenge of performing an assay at each discrete timepoint, all the while disrupting the sample. [26]. This method also fails to reduce the system complexity by allowing both direct and indirect mechanisms of interaction.

Conditioned media exchange is another co-culturing method, wherein a microbial species is cultured in a vessel and the filtered supernatant media is transferred to another distinct microbial culture. This is limited by its inherent unidirectional and consecutive (nonconcurrent) process [48]. Co-cultures can also be performed directly on agar plates [32]. However, this effectively requires a phenotypic means of differentiating the bacterial species and limits robust quantification of growth dynamics. [26].

In light of these pervasive method limitations and the recent renaissance in microbiome research, engineers throughout the world have recognized the need for devices and instruments that can enable improved co-culture studies. Given the enormous variety of emerging co-culture systems, a brief overview of two categories is provided.

One such category is microfluidic systems [26]. An example is the NMMI (Nanoporous Microscale Microbial Incubator) [23]. Single cells are randomly seeded into porous chambers of a hydrogel incubator, which physically isolate the cells but allow for diffusion of metabolites and other small molecules. Another example is the kChip [36]. In short, communities of varying sizes and a random assortment of bacterial species can be generated on a massive scale via the isolation and merging of droplet-encased microbes. The greatest limitation of these complex microfluidic systems is the high-level of experience and expertise required, restricting its accessibility and widespread application.

A second category of co-culture systems are membrane partitioned devices. A wonderful case study is the iChip [3, 51]. Designed to address the "great plate count anomaly", a chip was developed to embed microorganisms in their natural environment, separating them via a porous membrane. A larger pool of organisms was cultivated due to the presence of required native nutrients. A second example is the device reported in 2017 by Moutinho et al., which described the development and successful application of a co-culture plate, conceived independent of our own development of the BioMe plate [48]. This device, pictured in Figure A1, enabled real-time optical measurements of pairwise co-cultures separated by a vertical diffusible membrane.

The BioMe co-culture platform aims to extend and enhance the concept put forward by Moutinho et al.'s co-culture plate, by improving on its limitations of accessibility (cost and manufacturing), throughput (>8 co-cultures), and design flexibility for higher-dimensional co-cultures (3+ species).

(2) BIOME DEVELOPMENT

Design & Components

Seven key design principles guided the development of the BioMe plate:

(1) Enable widespread compatibility with available lab equipment – general architecture of a standard 96-well microtiter plate.

(2) Facilitate DIY fabrication by biologists, ecologists, and non-engineers - cost-effective and easy to manufacture.

(3) Leakage-proof. Reliable experimental results and prevention of equipment damage.

(4) Biocompatible and inert. Limited environmental modulation of cultures.

(5) Sterilizable and reusable. Cost-effective, contamination-free repetitive use.

(6) Prevent cross-contamination within and between co-culture samples. Confidence in decoupled bacterial cultures, without additional assays.

(7) Flexible physical framework that can accommodate higher-order co-culture architecture. Potential investigation of complex microbial communities.

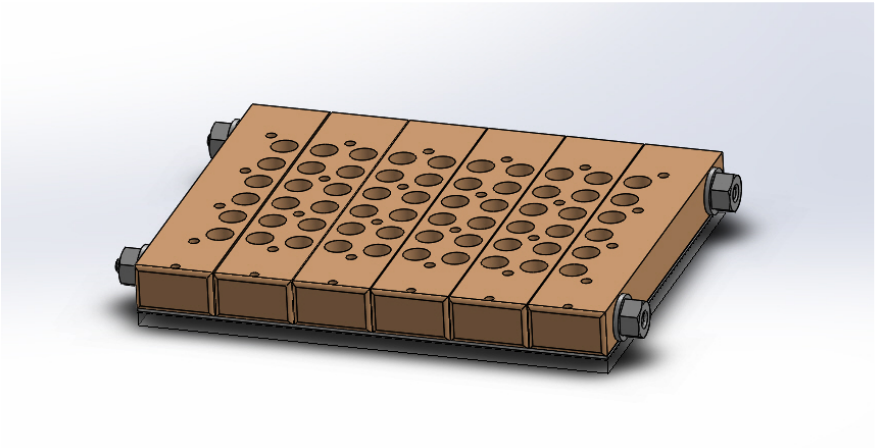

Figure 1: SolidWorks CAD image of the BioMe plate with pairwise co-culture architecture for the observation of paired microbial species interactions

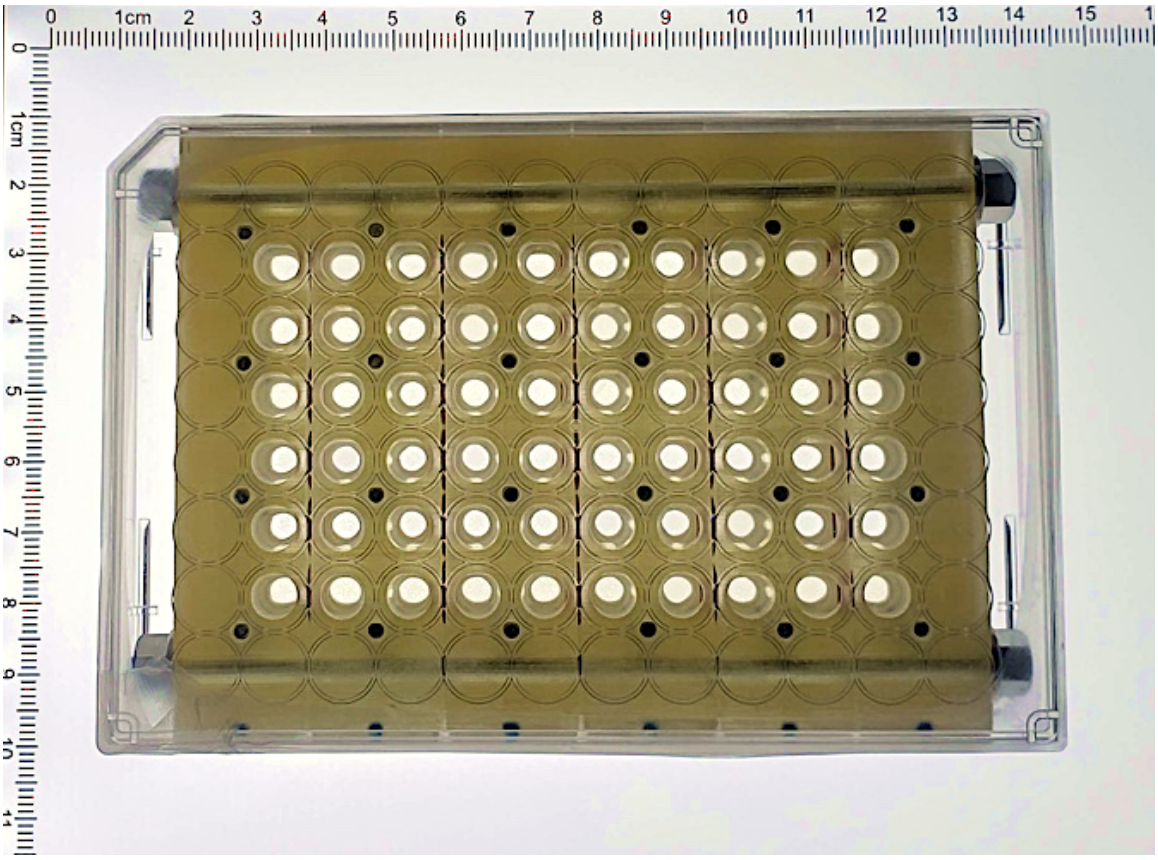

Figure 2: Fully assembled BioMe pairwise plate

The BioMe co-culture platform enables high-throughput, high-resolution quantitative growth dynamic measurements for distinct constituent species within microbial communities. The multi-component device relies on porous membranes assembled between consecutive plate segments, isolating species to specific wells. This affords the ability to measure the growth of individual microbial species and their dynamic interactions via diffusion-mediated mechanisms. This includes, but is not limited to: resource competition, symbiotic cross-feeding, horizontal gene transfer, and quorum sensing. The batch cultures can be measured directly in the device using standard plate readers, allowing complete and undisrupted visualization of bacterial growth curves.

The general BioMe design fragments the microtiter plate structure into fundamental modular components: six primary body segments, and an optically clear base. Edge body segments (x2) are composed of 6 wells and middle body segments (x4) are composed of 12 wells, for a total of 60 wells and 30 pairwise co-culture assays in the same device. A column of O-rings and membranes are positioned between each body segment and then fastened together by rods and nuts to produce a lateral seal. A vertical seal between the assembled body segments and the transparent base is created by gasket and screws. The core BioMe device is then fit into a bottom tray, which acts as a fail-safe in the event of leakage. A standard 96-well microplate lid is used to cover the device to prevent external contamination of the system. Parafilm may be used to seal the assembly to prevent extensive evaporation throughout lengthy experiments.

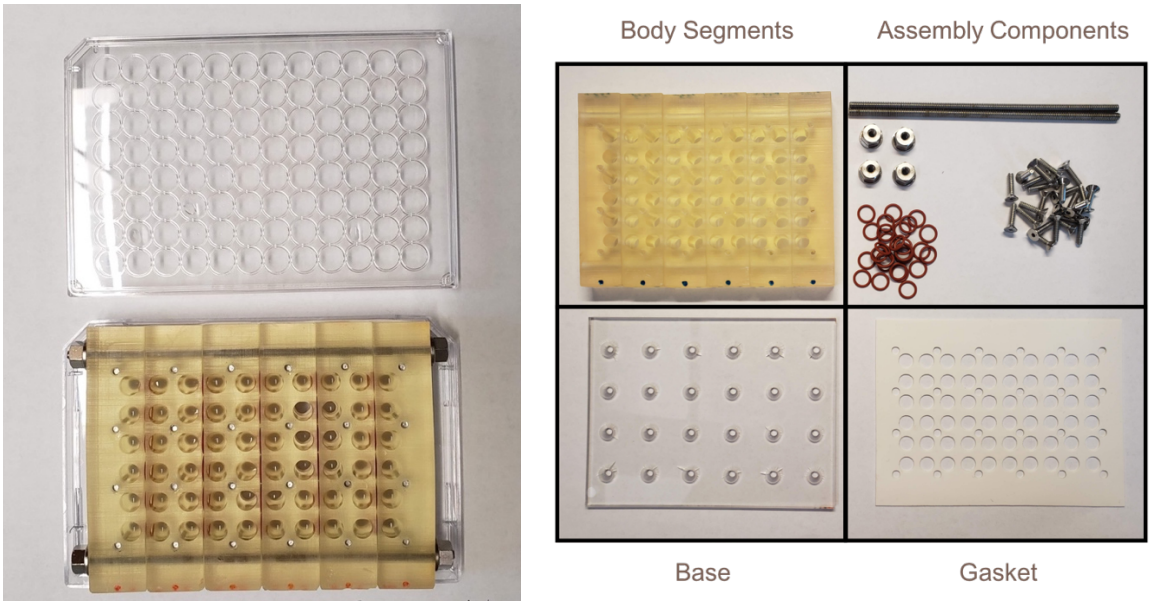

Figure 3: (Left) Assembled BioMe plate pictured with the bottom tray and top lid (Right) Overview of all primary components for the assembly of the BioMe plate

Materials for each BioMe component are listed below in Table 1 and procurement sources and catalogue numbers for each material is provided in Table A1. An exploration of the selection and troubleshooting process for component materials is provided in the "Development & Validation" section of this chapter.

Table 1: List of components and respective material used in the BioMe plate

Component	Material
Primary Body Segments	Machined: Semi-Clear White Polypropylene, 3/8" Thick 3D-Printed: Dental SG Resin
Optically Clear Base	Clear, Scratch-, UV-, and Impact Resistant Polycarbonate, 1/8" Thick
Gasket	Food-Grade High-Temperature Silicone Rubber Sheet, 1/32" Thick, 40A Durometer (Medium Soft)
O-Rings	High-Temperature Silicone O-Ring, 1mm wide, 6mm Inner Diameter
Rods	18-8 Stainless Steel Threaded Rod, 6-32 Thread Size, 6" Long
Nuts	18-8 Stainless Steel Flange Nut, 6-32 Thread Size
Screws	316 Stainless Steel Hex Drive Flat Head Screw, 82° Countersink, 4-40 Thread Size, 1/2" Long
Semi-Permeable Membranes	Hydrophilic Polycarbonate Membranes. PVP-Treated, Track-etched. Custom 7.94mm diameter.
Bottom Tray	Fisherbrand Lid for 96/384 Well Plate, Clear, Polystyrene
Top Lid	Costar 96 Well Cell Culture Plate Flat Bottom – Lid, Non Pyrogenic, Polystyrene

Five different varieties of membranes were tested and validated for use in the device: null (no pores), 0.03, 0.1, 0.2, and 0.4 µm pore sizes. The null, 0.03, and 0.1 micron membrane filters have a nominal thickness of 6µm and the 0.2 and 0.4 micron filters have a nominal thickness of 6-12µm. The pores are absolutely-rated, precisely cylindrical, and narrowly distributed, allowing their surfaces to capture 100% of particles larger than pore

sizes. These membranes are coated with polyvinylpyrrolidone (PVP) to better process aqueous samples. These membranes are thus engineered to be hydrophilic and polar in nature and cannot be reused, as it may result in degeneration of coating and loss of hydrophilicity.

The design of the body segments specifically dictates the number of species allowed to interact. The images so far provided have demonstrated the design for pairwise co-culture interaction studies, as used for the experiment described in this thesis. However, the device framework was specifically designed to be flexible and easily modified to allow higher dimensional co-cultures (ex: three-species co-culture architecture). Unfortunately, these alternative designs and topologies were not tested and validated in the scope of this thesis, although its seamless design and manufacture is plausible in the established device architecture and assembly scheme.

Certain caveats and limitations are inherent to the design of the BioMe plate, arising from the use of porous membranes and batch cultures. Implementation of the diffusive membrane imposes three constraints on experimental investigation. Firstly, the membranes limit microbial interactions to contact-independent mechanisms - this prohibits cell surface contact interactions. Alternatively, this may be viewed as an advantage of the co-culture platform, whereby the system complexity is reduced to a single class of interaction mechanisms. Secondly, the membrane impedes short-range cell-to-cell interactions, modulating the strength of cross-feeding, competition, and communication observed in well-mixed, unsegregated co-cultures. Thirdly, the intrinsic membrane material properties may bias the rate of diffusion of specific small molecules. These membrane-related

limitations are explored in detail in Chapter Three.

Additional caveats are inherent to the use of *in vitro* batch cultures. Given the initial media composition is set and not replenished, characteristic features of microbial growth are resource-limited, including maximum biomass yield, exponential phase duration, and inevitable culture death. Thus, viable microbial cultures cannot be maintained indefinitely, with the observation of interactions limited to the initial concurrent growth of the multi-species system — before sufficient nutrient depletion and waste accumulation. In lieu of these caveats, BioMe is best suited to probe the existence and relative strengths of interspecific interactions and their effects on initial community assembly and time-dependent composition.

Manufacturing

All fabrication steps of the BioMe device were conducted at either Boston University's College of Engineering's Engineering Product Innovation Center (EPIC) or the Singh Imagineering Lab (Tinker). CAD drawings for manufactured components are provided in their respective sections, with dimensions provided in millimeters.

Assembly Components (Ready-to-Use):

Assembly components used in the final iteration of the BioMe were bought ready to use. These include the O-rings, the 6-32 flange nuts, the 4-40 screws, and the semi-permeable membranes. The 6-32 rods were cut to size, from 6" to 125mm using a grind wheel.

Food-Grade Gasket (Laser-Cut):

Stock food-grade silicone rubber sheets were cut to gasket specifications using an Epilog Laser Mini 60W laser cutter (25% speed, 100% power, and maximum frequency). Direct exposure to the laser resulted in charring and ignition and subsequent warping of the silicone rubber. Trial and error demonstrated that wrapping the stock rubber sheet in dampened heavy duty wipers (shop towels) prior to laser cutting mitigated these issues. Well holes were slightly oversized (6.30mm = 105% of 6mm) in order to accommodate gasket squish upon assembly, as shown in Figure 4.

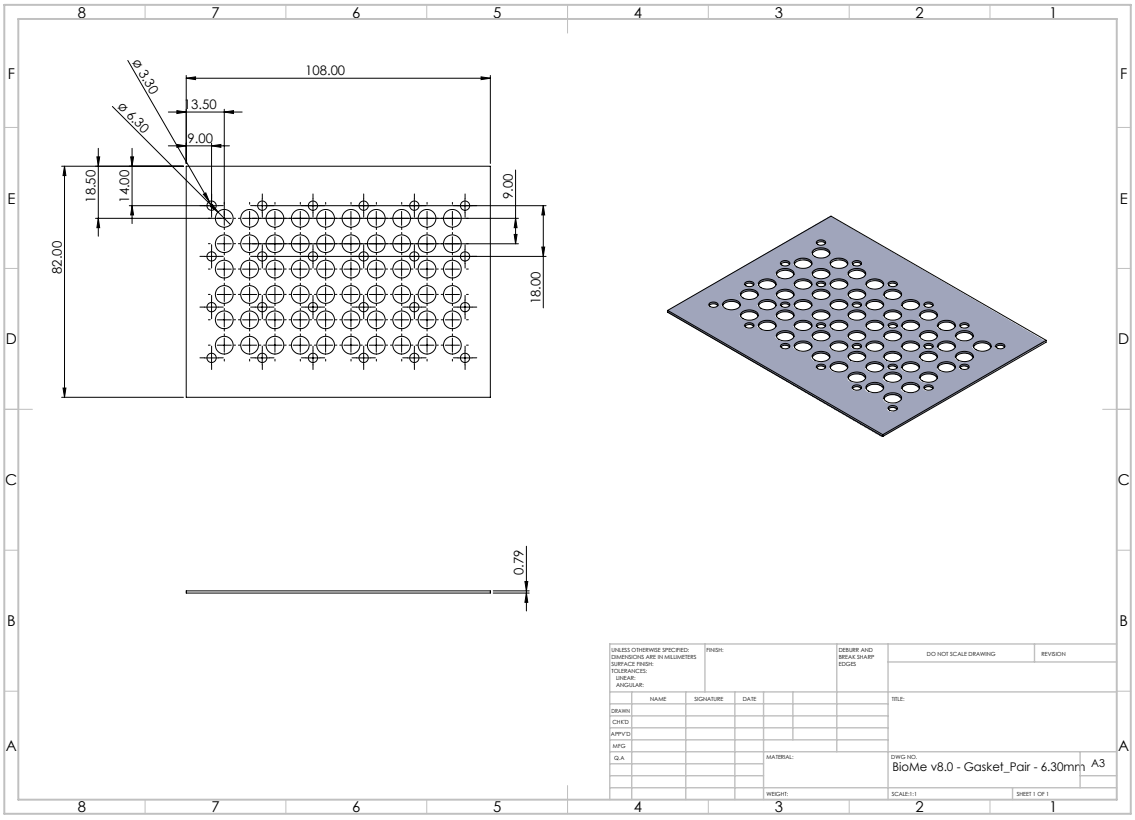

Figure 4: SolidWorks CAD drawing of laser-cut food-grade silicone gasket

Optically Clear Base (CNC Milled):

The optically clear base was machined via a single CNC mill operation. The CAD model for the base was first imported into GibsCamm software to specify the geometry and dimensions of the component. With geometry established, drilling operations for (1) through holes for the screws, (2) 82º countersink for the holes, and (3) contouring to cut to size were sequentially outlined. A 1/8" drill bit was used for steps 1 and 3, and a standard counterbore drill bit was used for the 82º countersink. The sequence of operations was crucial, as through holes were necessary prior to countersinking and cutting to size may pop the stock loose before conclusion of operations. Given the designed depth of the countersink, the drill bit would be required to drill past the bottom of the stock. Thus, sacrificial polycarbonate stock was securely taped to the bottom of the target stock to prevent destruction of the CNC mill tabletop. The CAD drawing is shown in Figure 5.

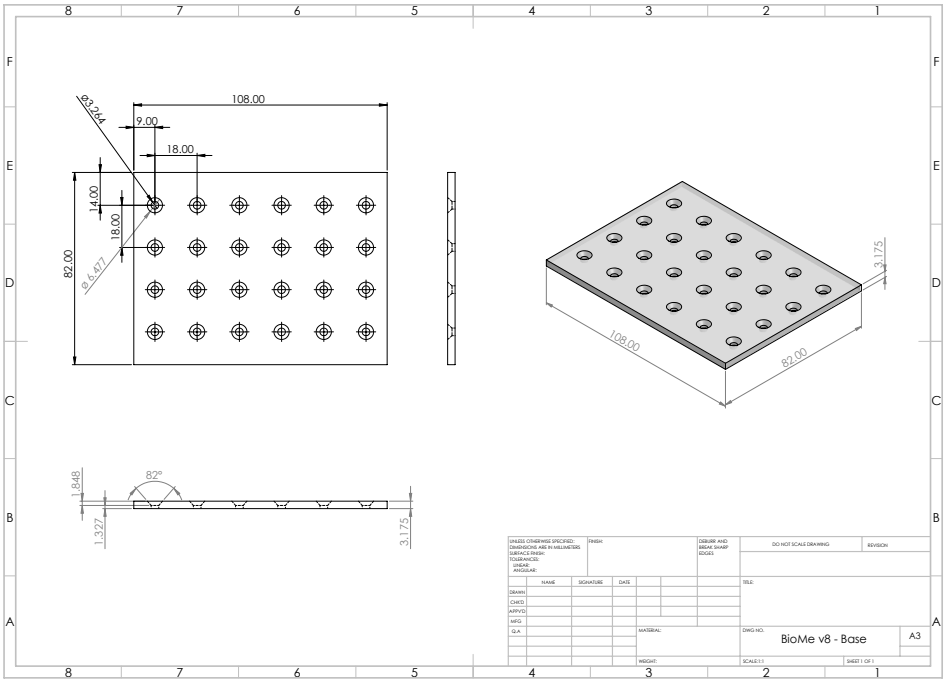

Figure 5: SolidWorks CAD drawing of optically clear base

Body Segments (Machined):

Fabrication of the primary body segments proved most difficult, with a total of six operational steps to yield the final device component. As with the base, GibsCamm software was used to detail the operations of the CNC mill. Given the CNC mill used was a standard three-axis milling machine, the milling of the vertical holes for the wells and the horizontal holes for the tunnels were performed in primary and secondary operations, respectively. The primary drilling operation consisted of: (1) through holes for vertical wells, (2) spot holes for the screw holes, (3) indicator hole at the bottom of top face segment to indicate orientation during assembly, and (4) contouring to cut to size. The secondary drilling operation on the side face of the segment consisted of: (1) spot holes for the rod holes, and (2) through holes for the horizontal tunnels. . A 1/8" drill bit was used for through hole and contouring operations, with a standard counterbore drill bit used for the spot and indicator holes. Each individual body segment was positioned side face up and clamped into place before secondary operation proceeded. For middle body segments, this was repeated for the other side face. Once CNC milling operations were concluded, a drill press was used to complete the spot holes, drilling the tap screw holes (4-40 tap screw = #43 drill bit) and the rod holes (6-32 rods free-fit = #32 drill bit). Each body segment was then manually tapped with a 4-40 tap bit and then deburred. As demonstrated, manufacture of the primary body segment proved labor-intensive and a large obstacle for manufacture by those with limited engineering experience. The CAD drawing for the middle body segment of the final BioMe iteration (v8 – Ivy v2) is provided in Figure 6, with the drawings for both the left and right body segments given in Figures A2 & A3, respectively.

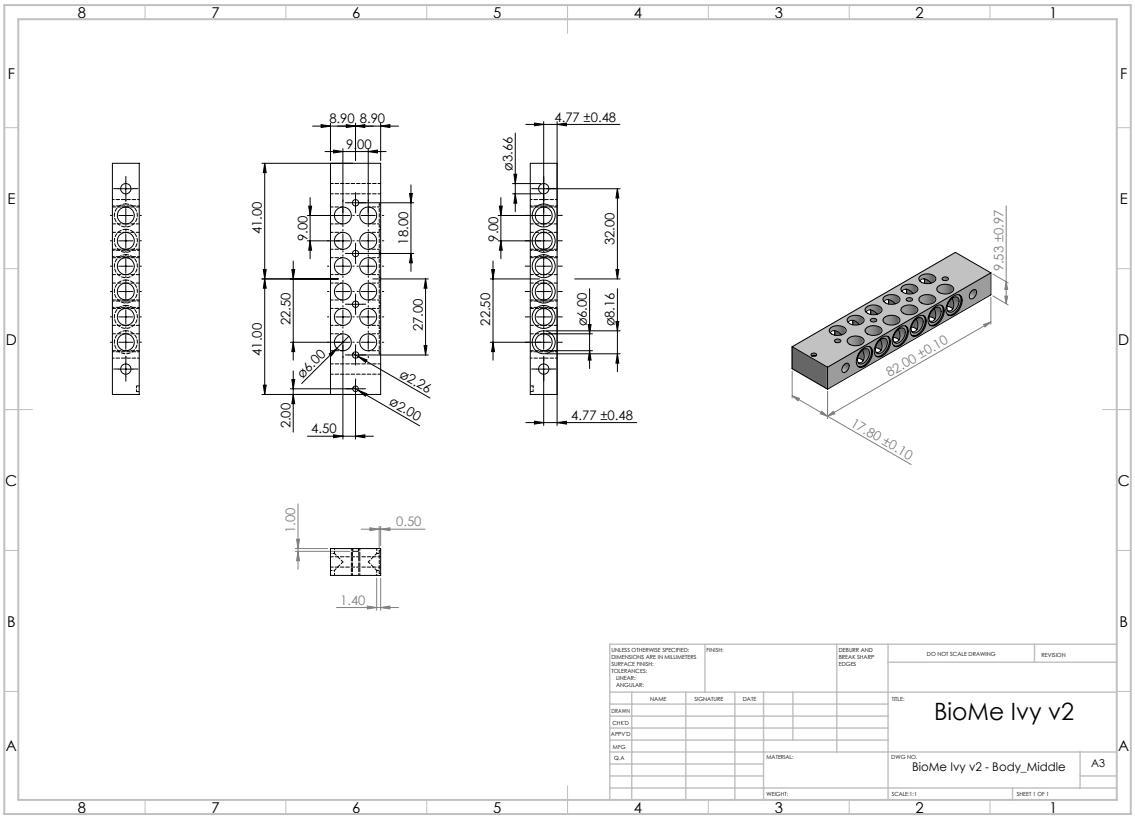

Figure 6: SolidlWorks CAD drawing of the middle body segment for both machined and 3D-printed

Body Segments (3D-Printed):

In order to improve ease of fabrication and DIY accessibility, 3D printing was explored and successfully implemented in the final iteration of the BioMe device. Various types of 3D printing exist, although many proved unfeasible due to inability to print watertight structures (ex: SLS), non-biocompatibility (ex: FDM), or necessity for unavailable equipment. FormLabs' Form2 SLA printer was chosen due to its popularity and accessibility in the 3D printing market, quality of print relative to cost of resin and equipment, and availability of a biocompatible, autoclavable liquid resin: Dental Resin SG.

Fabrication of the body segments via 3D printing was reduced to three simple steps. First, a STL model was saved directly from the Solidworks CAD model and then uploaded to the FormLabs' Pre-Form Software. The models were orientated vertically on the resin tank, without any supports to minimize post-processing and messy prints. The print was then allowed to proceed and conclude, with average print times for a whole device (6 body segments) taking ~10hrs. All that was left was to manually tap the undersized screw holes and then to sand down the body segments to required dimensions. The 3D printed pairwise variation of the BioMe plate was used for all subsequent experimental work.

Machining vs. 3D-Printing:

The decision to pursue 3D-printing was largely motivated by the desire to optimize and streamline manufacturing, in order to facilitate device fabrication by individuals with limited engineering and machining experience. However, as often faced in engineering, there are tradeoffs between the two manufacturing methods. Machining affords high resolution and fidelity to drawing specifications, with very low rates of failure. Most failure arises from improper manufacturing procedure. The downside of machining is the labor-intensive, lengthy, and multi-step process necessary to yield a final product. On the other hand, 3D-printing is relatively quick & easy once a final design is successfully modeled. Unfortunately, there are significant downsides. Firstly, the prints are lower in resolution than machining, with great limitation in printing thin wall features. Secondly, print failures are quite frequent and sporadic, especially on older Form2 printers and used resin tanks. An example of failed body segments prints are depicted in Figure A4.

Development & Validation

An iterative process of design, troubleshooting, and optimization was undertaken to produce a device that reliably operates under the seven key design principles. The following section will detail the issues and obstacles that were encountered and overcome throughout the eight stages of device iteration and its associated validation failures, troubleshooting process, and design improvements. Overall the greatest hurdles that will be addressed are: (1) Optimization of design for ease of manufacture and assembly, (2) Vertical seal and leakage, (3) Lateral seal and leakage/cross-contamination, (4) Material selection for biocompatibility and sterilization efficacy, (5) Sterilization method development and isolation of contamination root cause, (6) Dimensioning and tolerancing.

Before proceeding with a discussion of the design process, it is important to detail the vocabulary used to describe the troubles faced with contamination. Contamination is the general term used to refer to any unintended bacterial growth in the device. Cross-contamination refers to a bacterial culture either contaminating its paired co-culture well (intra-sample) or contaminating other co-cultures (inter-sample). Crossover refers to a bacterial microorganism squeezing its way through the pores of the membrane, thus contaminating the adjacent co-culture well (intra-sample). Contamination observed in experimental results was generally a result of cross-contamination due to technical errors and limitations, notably an imperfect lateral seal between body segments, O-rings, and membranes.

Validation Experiments :

Two experiments were used to validate the use of the BioMe plate: (1) Leakage & pH test, and (2) Sterilization validation. The leakage and pH test was a simple visualization test, whereby all wells of the assembled BioMe device were seeded with 250μL of 100μM phenol red, a pH indicator. The core BioMe device was then placed atop a paper towel and then fit into the bottom tray and covered with the top lid. This allowed for a simple test of leakage and environmental modulation of the culture. If no leakage was observed, the experiment was repeated with no paper towel and taking start and end point OD measurements at the acid (432nm), isosbestic (478nm), and basic (558nm) OD points for phenol red. Stability at these values indicated inert properties of the material.

Sterilization validation was used to assess the successful sterilization and reuse of the BioMe device. Bacterial cultures of *E. Coli* were grown up for 72hrs at 30°C in a static incubator, in order to allow complete growth and potential formation of biofilms. The device was then sterilized following the working sterilization method and then reseeded with fresh no-antibiotic media and incubated for 72hrs. If visualization determined no bacterial growth, each well was plated onto agar plates to confirm the lack of bacterial contamination.

Development Process – Optimization & Troubleshooting:

The first original design of the BioMe device utilized individual polycarbonate bases and O-rings to produce the vertical seal, as well as individual O-rings to produce the lateral seal. The device design is pictured in Figure 7.

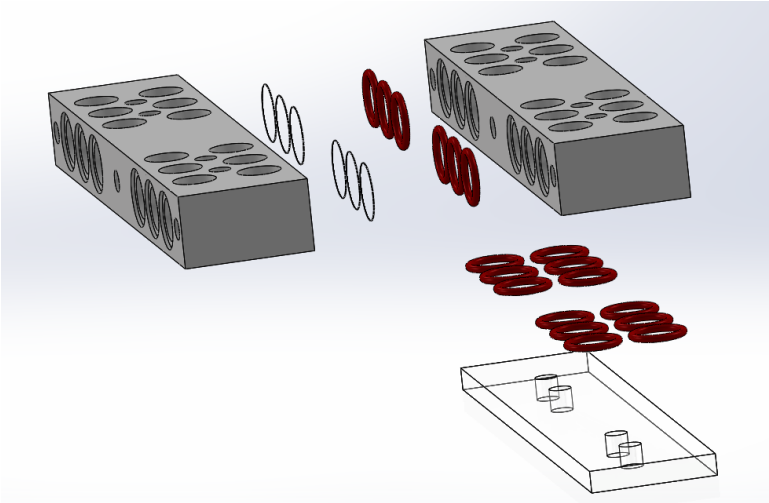

Figure 7: BioMe v1 – Original design for the co-culture platform

Thus, in order to optimize the ease of manufacturing and assembly, a universal one base and gasket system for all body segments was explored. Moving forward, the base was used as the foundation of all design, as the overall dimensions were set to allow fit into the bottom tray and congruence with 96-well plate architecture.

Problems were immediately encountered using the one base and gasket system, notably during the leakage and pH test. The phenol red samples in the BioMe device demonstrated consistent and measurable increase in pH. In order to identify the root cause of this modulation, each device component was individually tested in a beaker of phenol red. It was determined that the laser-cut red high-temperature silicone gasket was leaching its dye into the solution, not only modulating its acidity based on its absorbance but also based on simple pH strip testing. Figure 8 pictures the discoloration and pH modulation specific to the base gasket in 100μM phenol red solution. The material of the gasket was then changed to transparent high-temperature silicone gaskets, which demonstrated no modulation of the pH.

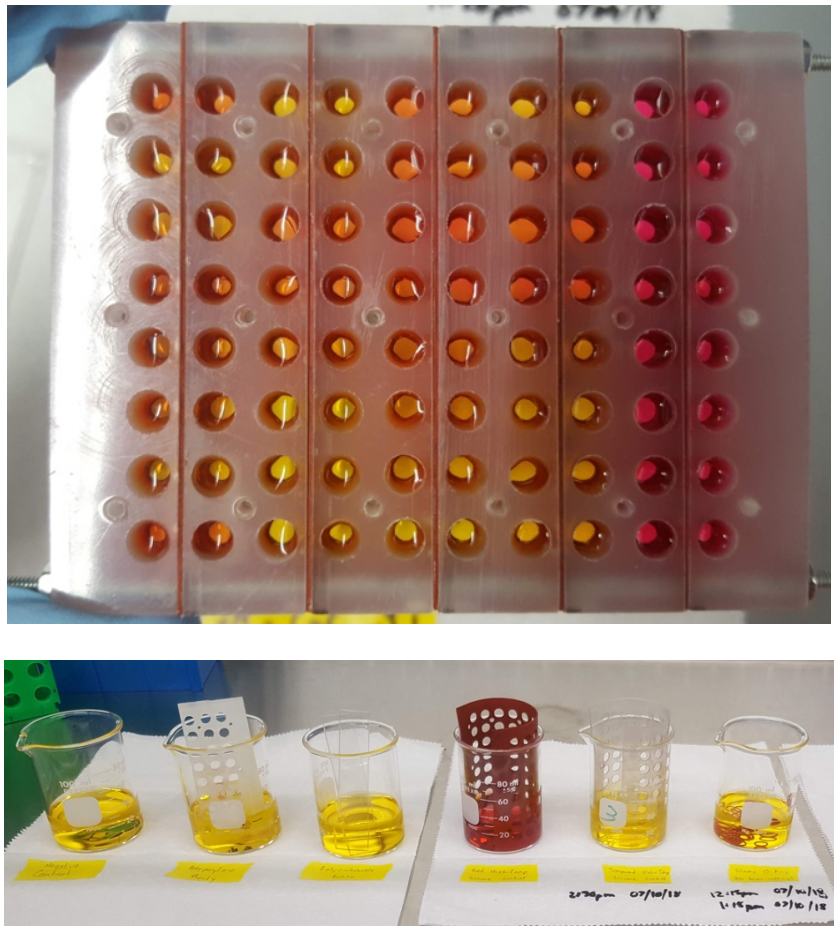

Figure 8: pH & Leakage testing of device components. (Top) Failed pH & Leakage test, with modulation of pH by device. (Bottom) Laser-cut red silicone gasket responsible for pH modulation

Leakage was pervasive in many of the early iterations of the BioMe device. In order to facilitate discussion, improvements will be discussed in terms of the vertical and lateral seal. In terms of the vertical seal, originally the design called for three 4-40 3/16" screws per body segment. However, the short length of the screw proved quite adept at stripping the threads of the tapped holes in the body segments, especially when large forces were applied to secure the seal with the base and gasket. Thus, the design was amended to accommodate four 4-40 ½" screws per body segment, which improved the robustness of the seal and prevented thread stripping.

The design sought to further optimize the ease of assembly by utilizing side gaskets for the lateral seal, rather than the individual placement of six O-rings per column. The first major obstacle was that the gasket changed the required dimensioning of the body segments, to account for the additional width of the squished gasket and enable assembly with the base and associated screw hole locations. Given that the squished dimension of the gasket was variable throughout the length of the body segment and the amount of force produced by the rod and nut fastening was unknown, trial and error was used to determine the proper dimension of the body segments. This device iteration successfully passed the leakage & pH test when the transparent silicone rubber was used. However, once the device began use for experimental work, it was discovered that the side gaskets were inadequate at preventing cross-contamination between co-culture samples (inter co-culture). It was decided that the advantage of ease of assembly was not worth the associated cross-contamination risk, thus individual O-ring design for lateral seal was brought back.

Original design also began with a total of 96-wells, hosting all edge wells both vertically and horizontally. However, there were a few issues that were discovered. First and foremost, the vertical edge wells had no co-culture counterpart, and its well volume was different than the other wells due to the lack of additional volume introduced by the side tunnel. Thus, these wells were inadequate for use as mono-culture controls; such controls were better suited for co-culture wells separated by null membranes. Moreover, the horizontal edge wells at both the top and bottom of each column proved to be susceptible to excessive evaporation and high risk of leakage throughout the course of lengthy experiments. As such, all edge wells were removed from the design. In order to

further improve the lateral seal with access to more side-face real-estate, the original 4-40 rods for lateral seal were replaced with thicker and more robust 6-32 rods. Flange nuts that spanned the whole thickness of the body segment (~10.5mm) were also chosen as the fastener of choice, to distribute the lateral load more evenly across the z-axis of the device.

The greatest obstacle encountered during validation of the device was for the sterilization of the device components upon previous use for bacterial culture. Material choice again proved to be the key to sterilization, although method development was essential in robust contamination elimination. The autoclave hosts particularly harsh conditions for most materials, given its high heat and pressure exposure of the material, indeed the very mechanism of action for sterilization of microorganisms. There are not many 3D printing resins that can withstand the harsh conditions of autoclaving. Fortunately, FormLabs has a proprietary blend of 3D printing resin, known as Dental SG Resin, that proved able. Indeed it is not only autoclaveable, but is also classified as a Class 1 biocompatible resin, with non-mutagenic, non-cytotoxic, non-systemic toxic properties.

In-house sterilization validation consistently failed for the earlier iterations of the device. It was especially difficult to isolate the source of contamination as an error in sterilization method or improper material choice. Months of sterilization method development, including an incredibly thorough sterilization via bleaching, dishwashing, autoclaving, UV exposure, and ethanol bath demonstrated contamination even after such laborious attempts. Thus, a similar root cause analysis to the pH modulation test was adopted upon thorough sterilization to test each device component for contamination. It was then determined that the base and side transparent gaskets were once again the cause

of issues. Once the transparent silicone rubber material was switched out for food-grade high-temperature silicone rubber, all subsequent contamination was solved upon sterilization. Figure 9 demonstrates contamination isolated to the beakers with the gaskets and fresh media.

Figure 9: Component-wise sterilization validation. (Top) All components. (Bottom) Laser-cut transparent gaskets were isolated as the root-cause of contamination and failed sterilization.

It is also important to note that direct exposure of the polycarbonate base to steam in the autoclave resulted in discoloration and clouding of the material. This is especially detrimental to the clarity required for reliable optical measurements. It was discovered that

wrapping the optically clear base in Kimwipes and then aluminum foil solved this discoloration and also enabled complete sterilization of the component.

The final sterilization method was optimized to reduce labor-intensity but included sterilization redundancy to ensure robust sterilization. The full sterilization procedure is included in Appendix A, but in summary, includes dishwash and autoclave prior to assembly, partial assembly with O-rings and ethanol-soaked membranes in a biosafety cabinet (BSC), ethanol bath and drying, and then full assembly with the gasket and base, also in the BSC. Short-term storage of the fully assembled device in a sterile bag demonstrated no contamination upon storage and use. Results of the sterilization validation experiment are provided below in Figure 10, demonstrating zero contamination in any of the wells via plate assay.

Figure 10: Sterilization validation v13 demonstrates no contamination in any of the wells proceeding 72hr culture and sterilization.

(3) MEMBRANE DIFFUSION CHARACTERIZATION

Overview

Experimental work with the BioMe plate began with the testing for diffusion of biological small molecules across the porous membrane. This was necessary to characterize the diffusive ability of the membranes, specifically for molecules involved in metabolic processes. Genetically engineered auxotrophs, which require an external supply of a specific amino acid, were used to test for the diffusion of amino acids across the membrane. These auxotrophs were *E. Coli – NR1* strains genetically recombineered using λ-Red recombination to knock out a gene with a CAM cassette, targeting genes essential for a specific amino acid's production [45]. The ΔK lysine and ΔI isoleucine auxotrophs were acquired and used for our experiments; ΔK was created by knockout of the lysA gene and ΔI by knockout of the ilvA. The ΔK and ΔI auxotroph can only survive and replicate in an environment where a supply of their deficient amino acid is available.

A simple diffusion experiment in the BioMe device was devised to: (1) selectively test for diffusion of lysine or isoleucine across membranes, using positive auxotrophic growth as a biological measure of successful diffusion, (2) test variable pore sizes, to observe potential crossover of the bacteria and growth rate as a function of pore size, and (3) validate sterility and cross-contamination in the device. A graphical schematic is depicted in Figure 11. A total of 5 membrane variations were tested: Null/no pores, 0.03, 0.1, 0.2, and 0.4 micron pore size. To the best of our knowledge, a systematic investigation of the effect of membrane pore size on small molecule diffusion has not been investigated in a co-culture platform.

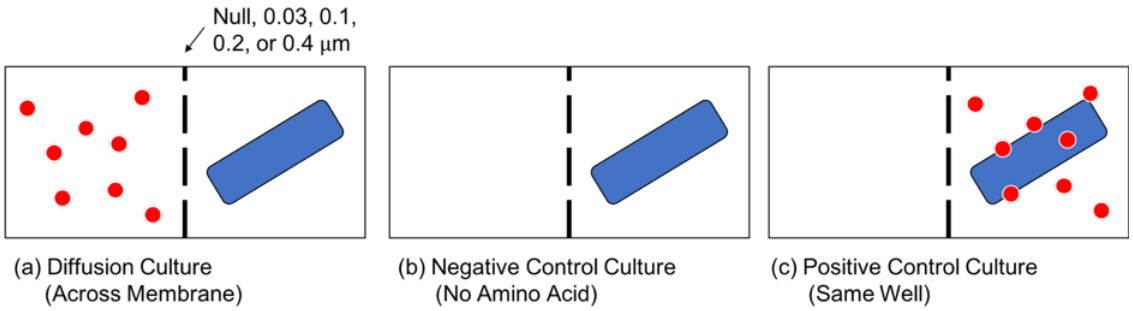

Figure 11: Schematic of Amino Acid Diffusion Exp. (Blue rod = *E. Coli* ΔK or ΔI auxotroph culture; Red dots = required amino acid: lysine or isoleucine; Dotted black line = membrane with variable pore size)

Figure 12 below provides an example overview of the resulting growth curves for the amino acid diffusion experiment. The negative control had no amino acid added to the co-culture, therefore no growth should be observed in either well. The positive control had amino acid added to the same well as the auxotroph, therefore a normal bacterial growth curve should be observed only in the auxotroph well. For the diffusion culture, the amino acid was placed in the well across the membrane from the auxotroph. Positive auxotroph growth indicates successful diffusion of the amino acid. Any growth observed in the leftmost well with only media is indicative of either cross-contamination, with the bacteria crossing into the adjacent well due to improper seal, or crossover, with the bacteria crossing into the adjacent well through the pores of the membrane.

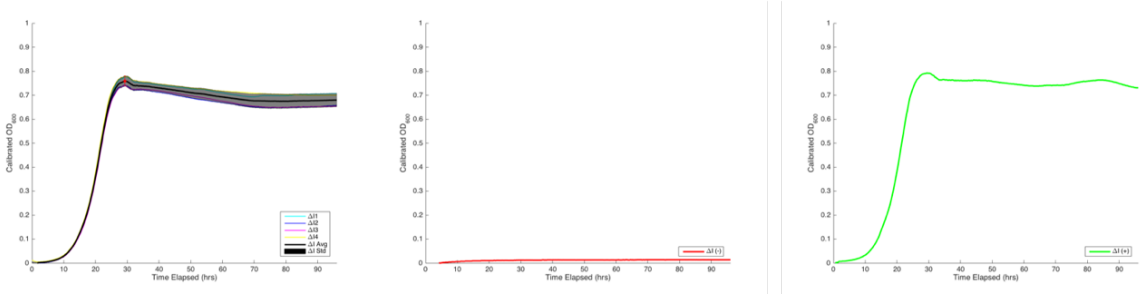

Figure 12: Overview of example Amino Acid Diffusion Exp. results. (Left) Diffusion culture with successful diffusion and positive auxotroph growth. (Middle) Negative control. (Right) Positive control.

Materials & Methods

The auxotrophs were cultured in M9 minimal media (supplemented with vitamins and antibiotic) and incubated in the plate reader at 30°C, without shaking, throughout the course of the kinetic-read experiment. The initial inoculation cultures were sampled from distinct clonal broth cultures in exponential phase (6hrs post-inoculation, LB+Cam), washed and resuspended in M9, calibrated to a set OD 0.1, and then diluted 100x. Calibration of the OD to 0.1 was calculated using Equation 1.

$$\% \text{ Culture in Dilution} = \frac{Set\ OD600 - M9\ OD600}{Culture\ OD600 - M9\ OD600} = \frac{0.1 - M9}{C - M9} \quad (1)$$

Diffusion cultures were conducted in triplicates or quadruplicates for each membrane pore size, each derived from distinct clonal colonies, with a negative and positive control for each pore size. For both the lysine and isoleucine diffusion experiments, the media of the adjacent well had enough amino acid to yield a theoretical maximum of 10^9 cells. This was calculated with Equation 2 below, where [aa] in (g/L) is the initial amino acid concentration, a.a per cell is the number of extracellular amino acid required per cell [2], theoretical yield is 10^9 cells, N_A is Avogadro's number = $6.022 \times 10^{23} \frac{aa}{cell}$, MW_{aa} is the molecular weight of the amino acid, and V_{well} is the volume of the well sample = $250\mu L$.

$$[aa] = \frac{\frac{aa\ per\ cell * theoretical\ yield}{N_A} * MW_{aa}}{V_{well}} \quad (2)$$

For the lysine diffusion experiment (aa per cell = 1.1×10^8 aa/cells, MW_{aa} = 182.65 g/mol) lysine concentration was calculated to be 1.33×10^{-1} g/L. For the isoleucine diffusion experiment (aa per cell = 7.5×7 aa/cells, MW_{aa} = 131.7 g/mol), isoleucine concentration was calculated to be 6.53×10^{-2} g/L.

Both the lysine and isoleucine diffusion experiments were performed in duplicate. The first lysine experiment was run for 55hrs and 15 mins (55:15), with the expected 96hr kinetic-read cut short due to software error; the following three experiments were run for a complete 96hrs. A BioMe plate was sterilized and assembled with different membrane pore sizes for each of its 5 pairwise columns. The same device was sterilized and reused throughout all four experiments, in order to control for variation in between distinct BioMe plates. For ΔK- Run 1 and ΔI- Run 1, the diffusion cultures were performed in triplicate and for Run 2 they were performed in quadruplicate. The device schematic and original OD_{600} data for all four experiments are given in Appendix B, Figures B1-B4. An example device schematic, for the ΔK- Run 1 experiment, is provided in Figure 13 below. Similar schematics were used for all four diffusion experiments.

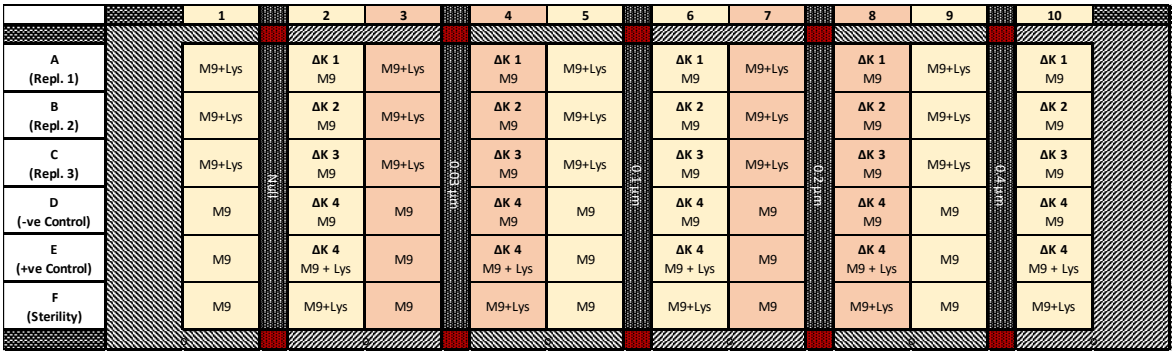

Figure 13: Example BioMe device schematic for the ΔK- Run 1 experiment.

The original OD_{600} data was then calibrated by subtracting the original OD value by the average OD of the non-contaminated wells with just media (with or without amino acid) at that specific time point. These calibrated OD_{600} growth curves were then used to determine the maximum calibrated OD_{600} attained throughout the entire kinetic growth experiment.

Logarithmic OD_{600} data was calculated by taking the natural log (ln) of the original OD_{600} data. The logarithmic OD_{600} growth curves for each biological replicate was then used to calculate maximum specific growth rate, μ_{max}. A sliding window algorithm was written using Matlab to calculate growth rate for 5hr intervals in a set time range (10-30hrs) during which end of lag phase, exponential phase, and start of stationary phase was observed. The data was constrained to the linear OD_{600} range of [0, 0.4] and to linear regression estimates with an $R^2 \geq 0.995$. The maximum growth rate for each replicate was then recorded, and averaged for all replicates within a given pore size. Data for all membrane pore sizes across all four diffusion experiments followed this pipeline of data organization, calibration, analysis, and visualization.

Results & Discussion

Contamination occurred in wells expected to exhibit no growth in three of the four diffusion experiments. There was 1 contamination event in ΔK- Run 1 and ΔK- Run 2, four events in ΔI- Run 1, and none in ΔI- Run 2. These are color-coded red in Figures B1-B4, with data omitted from analysis color-coded blue. The contaminated wells were always the left well with the amino acid supplemented media, inferring that intra-sample contamination was likely, either due to cross-contamination or crossover. Original data for the experiment with most contamination events ΔI- Run 1, are given below. As depicted, growth curves shown in red had positive growth in wells with only the media with amino acid and no initial bacterial inoculation.

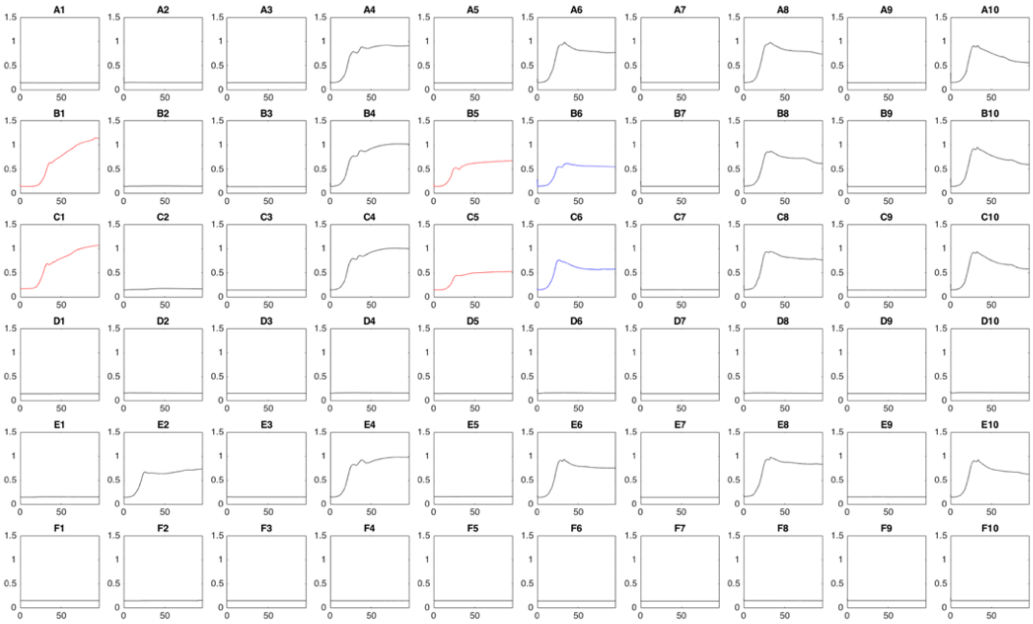

Figure 14: Original data for Δ*I* - Run 1. Contamination events (red), omitted data (blue).

There seemed to be no correlation between pore size and these contamination events. Indeed, no 0.2 or 0.4 micron pore size samples were contaminated throughout all four diffusion experiments. Crossover of either the Δ*K* and Δ*I* auxotrophs through the pores of the membrane within the 96hr time-course experiment was thus ruled out. This is supported by Figure A1, which provides an electron microscope image demonstrating the relative size difference between a 0.1 micron pore size and *E. Coli* bacteria. Thus, it seems that the contamination most likely arose due to technical error, with possible sources including improper placement of the O-ring and/or membrane, improper assembly, imperfect lateral seal, or contamination during pipetting.

Calibrated growth curves for each biological replicate, negative control, and positive control of all tested membrane pore sizes for the first run of the lysine and isoleucine diffusion experiments are provided in Figure B5 (ΔK – Run 1 & Δ*I* – Run 1). As previously mentioned, the kinetic read experiment for ΔK – Run 1 was cut short due to

software error. The Δ*I* – Run 1 growth curves demonstrated a diauxic shift near the end of the exponential phase of the bacterial growth curves for all tested biological replicates and positive control. The cause of the diauxic shift was hypothesized to be a result of incomplete washing prior to initial inoculation, such that some of the media resources from the initial LB media contaminated the minimal M9 media of the experiment. This was confirmed by the lack of diauxic shift in Δ*I* – Run 2, where thorough washing was conducted. Due to these technical and procedural errors, Run 2 for both the lysine and isoleucine diffusion experiments will be used for the bulk of the discussion and analysis.

The calibrated growth curves of the second run of the lysine (Δ*K* – Run 2) and isoleucine (Δ*I* – Run 2) diffusion experiments are provided in Figure 15 below. This demonstrates the large amount of data that can be produced in a single experimental run using the high-throughput BioMe co-culture plate.

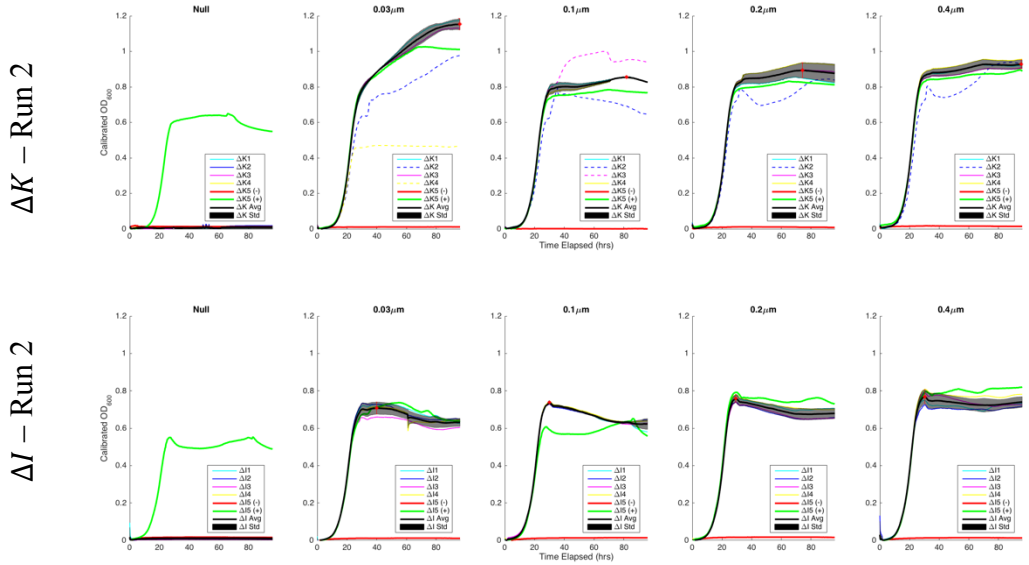

Figure 15: *E. Coli* Auxotroph Growth Curves (Run2): replicates (blue, cyan, magenta, yellow), negative control (red), positive control (green), average of replicates (black line), standard deviation of replicates (grey shading), maximum OD_{600} attained(red dot and line). Replicates that were not included in further analysis are shown in dotted lines.

Lysine and isoleucine could successfully diffuse through membranes with 0.03, 0.1, 0.2, and 0.4μm pore sizes. This is demonstrated by the positive auxotroph growth observed in all membrane pore size other than the null membrane, which should and did demonstrate no auxotroph growth. Moreover, the close resemblance between the samples and positive controls (with amino acid starting in the same well as the auxotrophs) demonstrate that the amino acids could diffuse across the membranes with ease. Slight variation was observed in between biological replicates, but standard deviation remained low.

Modulation of the membrane pore size had noticeable effects on the growth dynamics of the auxotroph growth. Notably, the growth curves for the 0.03μm pore size samples in ΔK – Run 2 demonstrated significant and atypical positive growth during the stationary phase. Curiously, even the growth dynamics of the positive controls seemed to be dictated by the membrane pore size, even though the amino acid began in the same well as the bacterial culture. This is demonstrated by the close resemblance in growth curve behavior between the positive control (green) and replicate average (black) within the same membrane pore sizes and qualitative distinction in behavior of the positive controls across pore sizes. This suggests that the difference in growth dynamics does not arise from the initial diffusion of the amino acid across the differently sized pores of the membranes, but from some other mechanism.

Natural logarithm OD_{600} data is plotted for all membrane pore sizes for the first run of the diffusion experiments in Figure B6, and for the second run in Figure 16 below. Different colors represent the average growth for each different pore size tested.

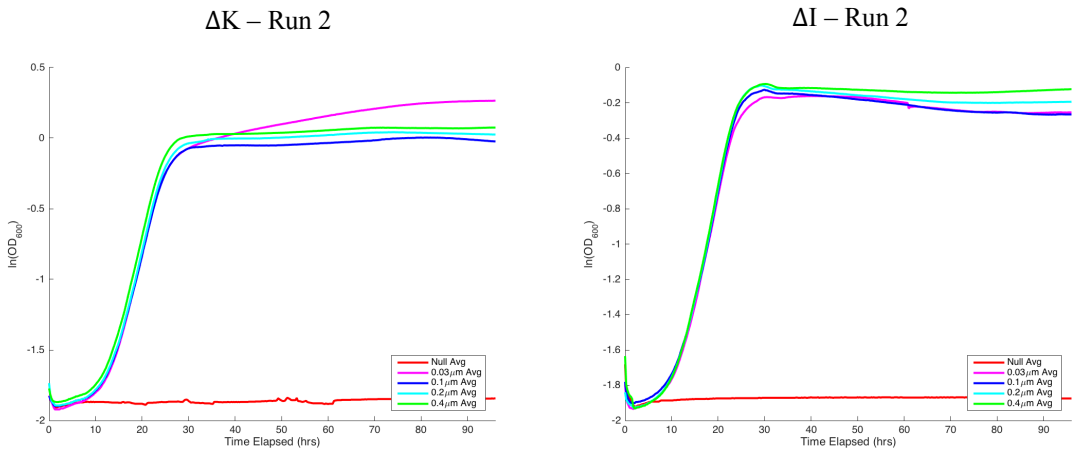

Figure 16: Semi-log plots for the average ln(OD_{600}) growth curves for all membrane pore size (Run 2) Null (red), 0.03μm (magenta), 0.1 μm (blue), 0.2 μm (cyan), 0.4 μm (green).

These semi-logarithmic plots clearly demonstrate the discernible impact of membrane pore size on auxotroph growth dynamics. Qualitative analysis of the plots demonstrates a direct relationship between yield and pore size, except for the 0.03μm pore size. This can be quantified by the maximum OD_{600} attained throughout the course of the kinetic read, which is plotted in Figure 17 below. This confirms the direct relationship between maximum yield and pore size for all conditions, except for the 0.03μm ΔK growth condition. All maximum OD_{600} values (average, standard deviation, and time @ max) is given in Table B1.

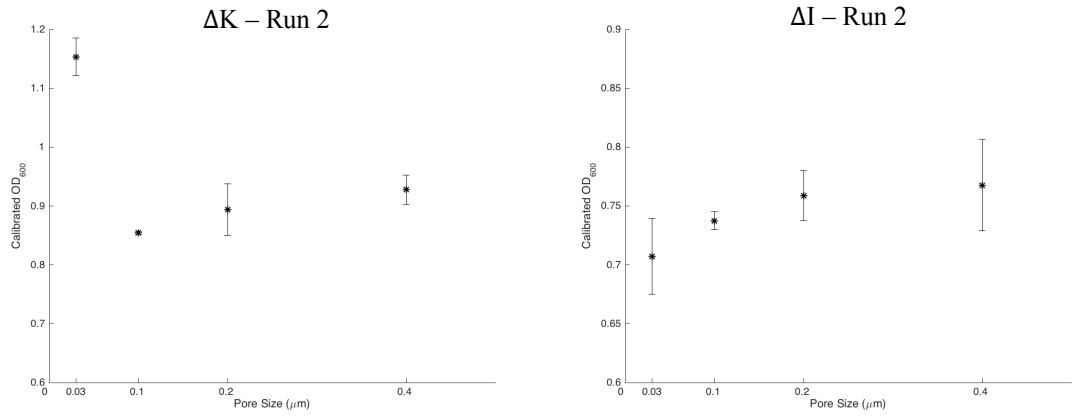

Figure 17: Maximum calibrated OD600 attained as a function of pore size (Run 2)

I hypothesize that the atypical growth dynamics of the 0.03μm ΔK condition can be attributed to lysine degradation. As previously described, these auxotrophic *E. Coli* strains were generated by single gene knockout for the production of the respective amino acid. No additional genetic modifications were made and the genomes were otherwise wildtype *E. Coli – NR1*. Although an isoleucine degradation pathway does not exist in *E. Coli*, a lysine degradation pathway does; this is depicted in Figure 18. The two terminal products of the L-lysine degradation pathway are 2-oxoglutarate and succinate, which are two intermediates of the TCA cycle – the primary pathway responsible for energy generation in most organisms, including *E. Coli*.

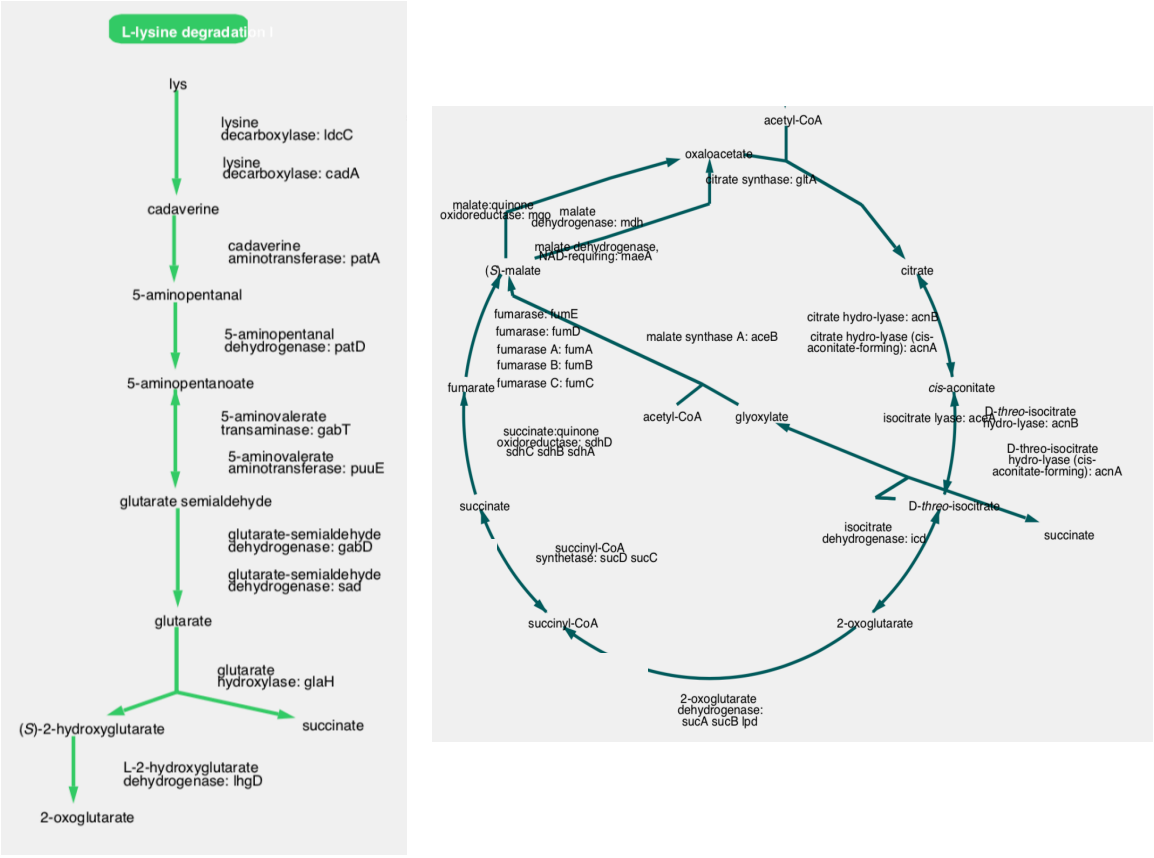

Figure 18: *E. Coli* metabolic pathways (Left) Lysine degradation pathway. (Right) TCA cycle [7]

Table 2: Relative volumes with respect to the 0.03μm pore volume

0.03µm	0.1 µm	0.2 µm	0.4 µm
1	11	44 - 89	178 - 356

The large relative difference in volume between 0.03μm and the 0.1μm and an additional source of energy via lysine degradation may serve to explain the atypical behavior of the 0.03μm ΔK condition. The relative volumes for the membrane pores as a function of their diameter is provided in Table 2, accounting for the nominal thickness of the sourced membranes. The smaller pore size may be better suited at sequestering the lysine degradation products in the culture well, enabling sustained positive growth throughout the stationary phase – not observed in any other pore size for either lysine or isoleucine. Additional testing is required to test the hypothesis.

The log OD_{600} data was used to find the maximum specific growth rate, μ_{max}, as a function of the pore size. Average values with standard deviation are plotted in Figure 19. Values of μ_{max}, R^2, and sample size, n, are tabulated in Table B2. An increasing, monotonic relationship between pore size and max specific growth rate is observed. Once again, the only exception is the 0.03μm ΔK condition. This is confirmed by analysis of the ΔK – Run 1 data, whereby the growth rate for 0.03 μm pore size is higher than the 0.1 μm pore size. The otherwise direct relationship between pore size and μ_{max} seems to suggest that the auxotroph growth rate is proportional to the diffusion rate of the amino acid across the membrane.

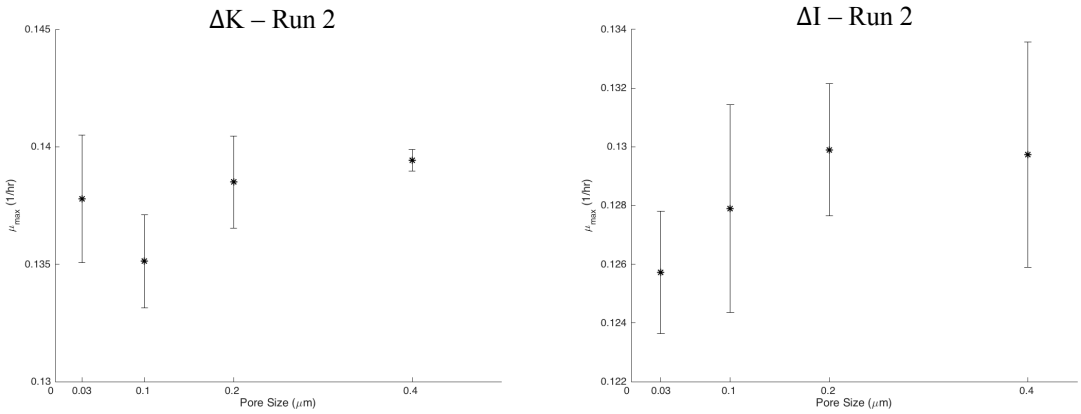

Figure 19: Maximum specific growth rate, μ max, as a function of pore size (Run 2)

In lieu of the assumption that growth rate is indicative of diffusion rate of the amino acid, I hypothesize that the material properties of the membranes selectively bias the diffusion rates of different electrostatically charged small molecules. Lysine has a positively charged lysyl side chain and isoleucine has a non-polar, uncharged hydrocarbon side chain. It is possible that the difference in electrostatic properties due to the different side chains on lysine and isoleucine accounts for the difference in growth rates. For the small $0.03\,\mu m$ pore size, the positive charge of the lysine side chain on top of the zwitterionic characteristics of these amino acids may accelerate its diffusion across the membrane, respective to its larger 0.1μm pore size.

This possible yet surprising interplay of electrostatic forces and random walk diffusion across these membranes may be most noticeable at the smallest membrane pore size. Electrostatic forces may grow relatively stronger as the pores become tighter, but random walk diffusion across becomes increasingly likely as the pores grow larger. This interplay of Brownian Motion and electrical charges may help to explain the atypical behavior for the growth curves of the $0.03\mu m$ ΔK condition.

(4) SYNTHETIC SYNTROPHY CO-CULTURE

Overview

The diffusion experiments successfully demonstrated that amino acids can diffuse easily across the porous membranes. This motivated the subsequent syntrophic co-culture experiments between the complementary amino acid auxotrophs. The ΔK lysine auxotroph and the ΔI isoleucine auxotroph were previously shown to exhibit mutualistic syntrophic exchange, enabling positive growth in a well-mixed co-culture [45]. Thus, an experiment was devised to recapitulate those results in the BioMe plate. The graphical schematic for the co-culture experiment is provided below in Figure

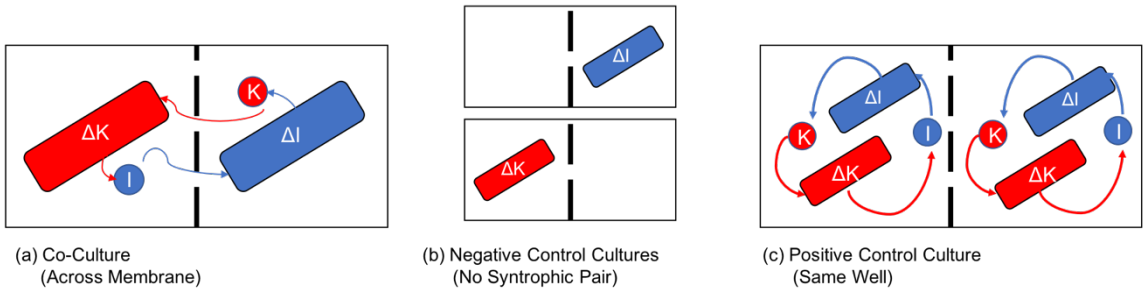

Figure 20: Graphical schematic of the Synthetic Syntrophy Co-culture Exp. (Red rod = E. Coli ΔK; Blue rod = ΔI; Red dot = secreted lysine; Blue dot = secreted isoleucine; Dotted black line = membrane)

In this system, the auxotrophs are incapable of producing respective amino acids necessary for their own survival and reproduction. They rely on the sharing of the required amino acid by an auxotrophic counterpart, though the exact mechanisms of the secretion and uptake are largely unknown [35, 45]. It is important to note a crucial difference between the diffusion experiments and the paired syntrophic co-culture experiments. The diffusion experiments were seeded with a surplus of amino acid, such that maximum yield was largely limited by glucose availability; a large amino acid concentration gradient was

established at the membrane interface, enabling high rates of diffusion across the pores. However, secretion rates of amino acids in *E. Coli* are notably lower and a continuous process rather than an initial fixed amount of amino acid [54].

Two variations of the experiment were devised. The first experiment tested different membrane pore sizes to determine whether pore size and nutrient availability modulated system growth. The second experiment tested different initial amino acid concentrations to determine whether initial conditions could alter community structure and growth dynamics.

Materials & Methods

Four co-culture experiments were run in total. The first experiment ($\Delta K \& \Delta I$ – Var. Pore Size 1) observed the differences in growth dynamics as a function of pore size. Three clonal replicates were run for all co-culture samples, with both negative controls (one for each auxotroph) without auxotrophic counterpart, and a positive control with both auxotrophs seeded in the same well. In the case of the positive control, it is impossible to deconvolve the individual growth of either the ΔK or ΔI auxotrophs – an advantage of the BioMe platform. The second experiment ($\Delta K \& \Delta I$ – Var. AA 1) observed the differences in growth for variable initial amino acid amounts.

A second run of experiments sought to replicate the previous experiments but for longer kinetic-read durations. The first run of experiments was planned to be 96hrs in length. Unfortunately, software cut the second experiment short to 54hrs and 30mins. Although measures were taken to prevent the software freezing by adjusting power settings,

operating software update schedules, and other system settings, the plate reader software would occasionally freeze within the 54hrs–55hrs interval. The second run of experiments both successfully ran for a week (168hrs). The device schematics are provided in Appendix B8–B11.

For the variable initial amino acid experiments, the pore size was fixed to be $0.2\mu m$. 5 different initial amino acid conditions were investigated: (1) No amino acid seed, (2) both lysine and isoleucine provided @ 10^3 cell yield, (3) both @ 10^6 cell yield, (4) lysine @ 10^6 cell yield, and (5) isoleucine @10^6 cell yield. Equation 2 was previously used to determine concentrations necessary for 10^9 cell yield (lysine: 1.33×10^{-1} g/L; isoleucine: 6.53×10^{-2} g/L). The media for all conditions were subsequently prepared via serial dilution. Due to shortage of null membranes, only the four porous membranes were tested (0.03, 0.1, 0.2, and $0.4\mu m$) in $\Delta K \& \Delta I$ – Var Pore Size 1.

Due to the inability to confidently assess contamination events in the first run, a phenotypic plating assay was developed. M9+Lys+Cam and M9+Ile+Cam agar plates were prepared for selective growth of either the ΔK or ΔI auxotrophs, respectively. $5\mu L$ of culture samples from all wells were plated for assessment of positive growth; any unexpected positive colony formation was indicative of contamination. This method was also used in $\Delta K \& \Delta I$ – Var. AA 2.

Results & Discussion

Variable Pore Size

The first experiment observed the growth dynamics of the syntrophic pair for varying membrane pore sizes. The OD_{600} growth curves are provided in Figure 21. Given that the growth of the microbial species was isolated to a specific well, it was possible to measure growth curves for both the Δ*K* and Δ*I* auxotrophs, unlike well-mixed co-cultures – the positive control. As expected, null membranes prevented any growth from occurring.

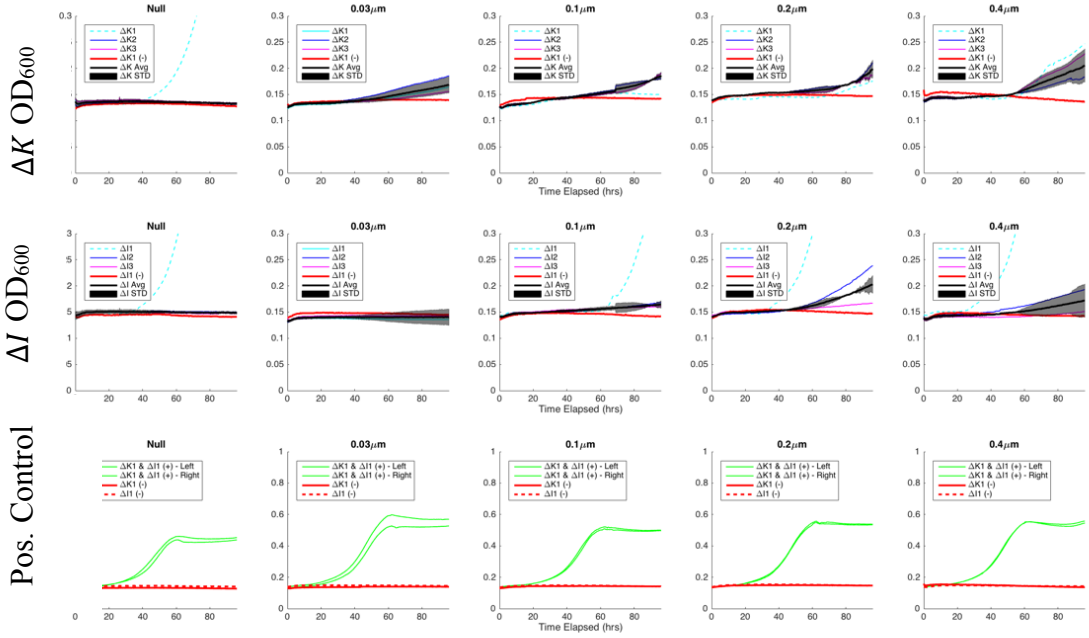

Figure 21: Δ*K*&Δ*I* – Var. Pore Size 1: Original OD_{600} growth curves. (*Top Row*) OD_{600} growth curves of the Δ*K* auxotroph (y-axis = [0 0.3]), (*Middle Row*) OD_{600} growth curves of the Δ*I* auxotroph (y-axis = [0 0.3]), (*Bottom Row*) OD_{600} growth curves of the positive control co-culture, where Δ*K* and Δ*I* auxotrophs are in the same well (y-axis = [0 1]). Data omitted for analysis is depicted by dotted lines.

There was a striking decrease in observable growth for the membrane-partitioned co-culture samples. Although same well positive controls demonstrated typical microbial growth curves, with stationary phase reached by 60hrs, qualitative analysis of the

membrane-partitioned co-cultures demonstrates a very slow exponential growth, observable near the end of the 96hr kinetic-read.

Although only slight initial growth of the membrane-partitioned co-culture was observed, enough data was collected to infer the effects of membrane pore size on average microbial growth rate. In this experiment, 5 contamination events were observed. The paired wells of the contaminated co-culture sample were omitted for analysis. There were always at least a sample size of two (n=2) paired co-cultures for each membrane pore size. Figure 22 provides a semi-logarithmic plot of ΔK and ΔI growth for all membrane pore sizes, and the maximum OD and maximum specific growth rate (μ_{max}) for both ΔK and ΔI as a function of membrane pore size.

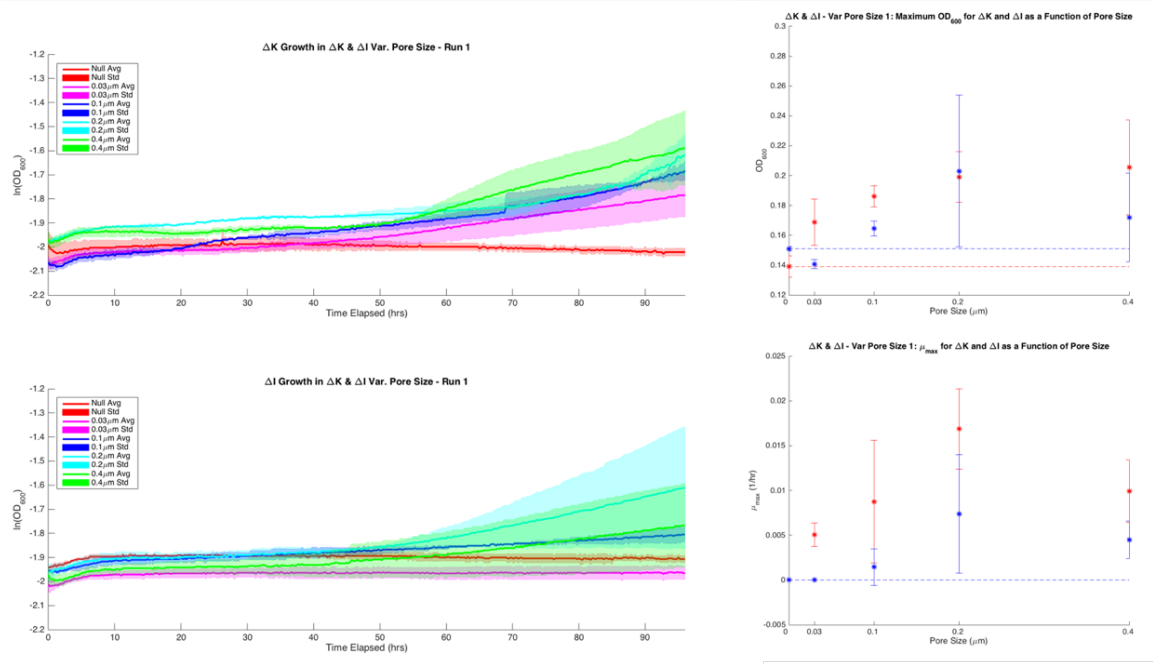

Figure 22: ΔK&ΔI – Var. Pore Size 1: Semi-logarithmic ln(OD_{600}) growth curves for (*Top-Left*) ΔK auxotroph and (*Bottom-Left*) ΔI auxotroph. (*Top-Right*) Maximum OD_{600} (average $\pm$ std) attained by the respective auxotrophs; ΔK in red and ΔI in blue. (*Bottom-Right*) Maximum specific growth rate, u_{max}, (average $\pm$ std) attained by the respective auxotrophs; ΔK in red and ΔI in blue.

Generally, the ΔK auxotrophs had a higher maximum yield and higher μ_{max} for all membrane pore sizes. The only exception is for the $0.2\mu m$ pore size, where ΔI reached a comparable maximum OD as ΔK. The relationship between max specific growth rate and membrane pore size was nonlinear and non-monotonic. The highest μ_{max} was achieved by the co-culture samples with the $0.2\mu m$ membrane. However, more samples are required to make a confident assessment of the trend.

Variable Initial Amino Acid

The original intent of the variable initial amino acid experiment was to determine whether the positive syntrophy cycle could be "kickstarted" by an initial amount of amino acid. Similar to what was observed in the variable pore size experiment, the growth was incredibly minimal for the membrane-partitioned co-culture. The original OD_{600} data is visualized in Figure B12. No contamination was observed in any of the wells. Moreover, the positive controls do not reach stationary phase by the conclusion of the 54hr time-course. The semi-log plots provided in Figure 23 are able to capture the slow growth dynamics much better.

Interestingly, a trend that was observed earlier where ΔK had a higher max OD_{600} and μ_{max} than ΔI was reversed when any amount of initial amino acid was provided. As expected from previous results, the ΔK auxotroph had a higher OD_{600} yield than the ΔI in the condition with no initial amino acid seed provided. The distinction was greatest when solely isoleucine was provided, and the max OD_{600} and μ_{max} were comparable when just lysine was provided.

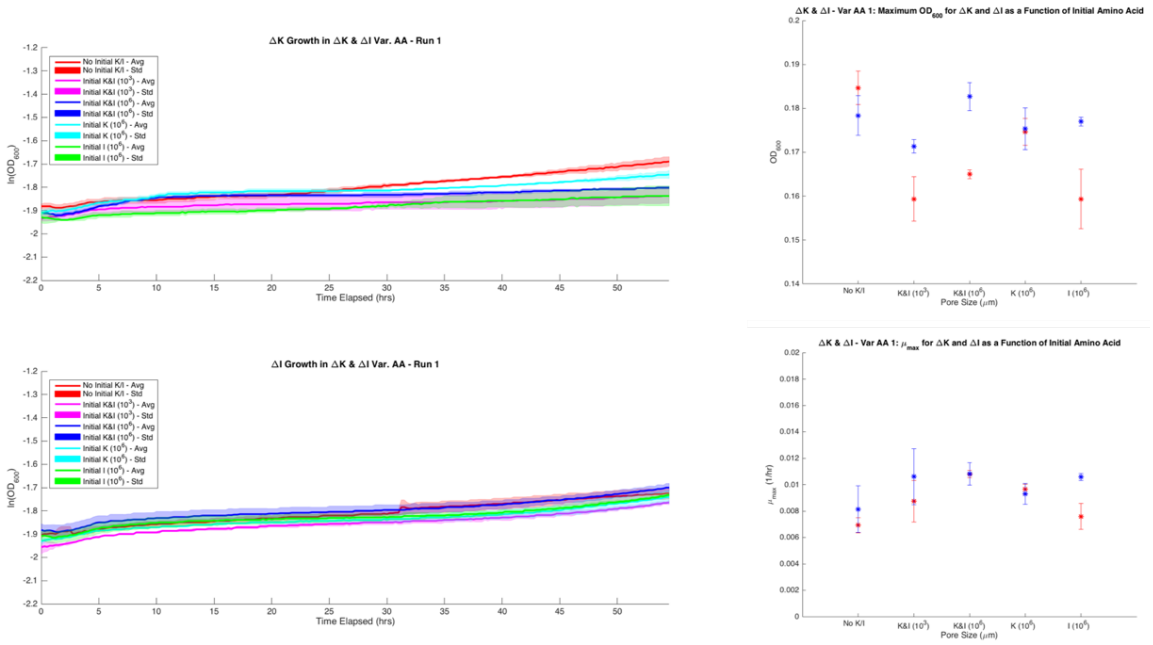

Figure 23: ΔK&ΔI – Var. AA 1: Semi-logarithmic ln(OD_{600}) growth curves for (*Top-Left*) ΔK auxotroph and (*Bottom-Left*) ΔI auxotroph. (*Top-Right*) Maximum OD_{600} (average $\pm$ std) attained by the respective auxotrophs; ΔK in red and ΔI in blue. (*Bottom-Right*) Maximum specific growth rate, u_{max}, (average $\pm$ std) attained by the respective auxotrophs; ΔK in red and ΔI in blue.

Week-Long Experiments

For the second week-long run of the variable pore size experiment, results demonstrated a high rate of cross-contamination. The device schematic and original data for both week-long runs are given in Figures B10-B11, with the organized data provided in Figure B13-B14. For the variable pore size experiment, only one set of membrane-partitioned samples remained without cross-contamination. This was confirmed by both qualitative analysis of original OD_{600} readings and by phenotypic plate assay. The single set of sample data followed a similar data analysis pipeline. The semi-log auxotroph growth curves, plots of maximum OD and of μ_{max} are given in Figure 24. The maximum OD_{600} yield and μ_{max} for ΔK were consistently higher than that of ΔI for all membrane pore sizes,

confirming the results from the first run.

Both runs also support that larger membrane pore sizes favor ΔK biased community composition. Within the given data set, there existed a direct relationship between membrane pore size and maximum OD_{600} and μ_{max} for ΔK, although the growth rate for ΔI seemed to plateau for the 0.1, 0.2, and 0.4μm membrane pore sizes.

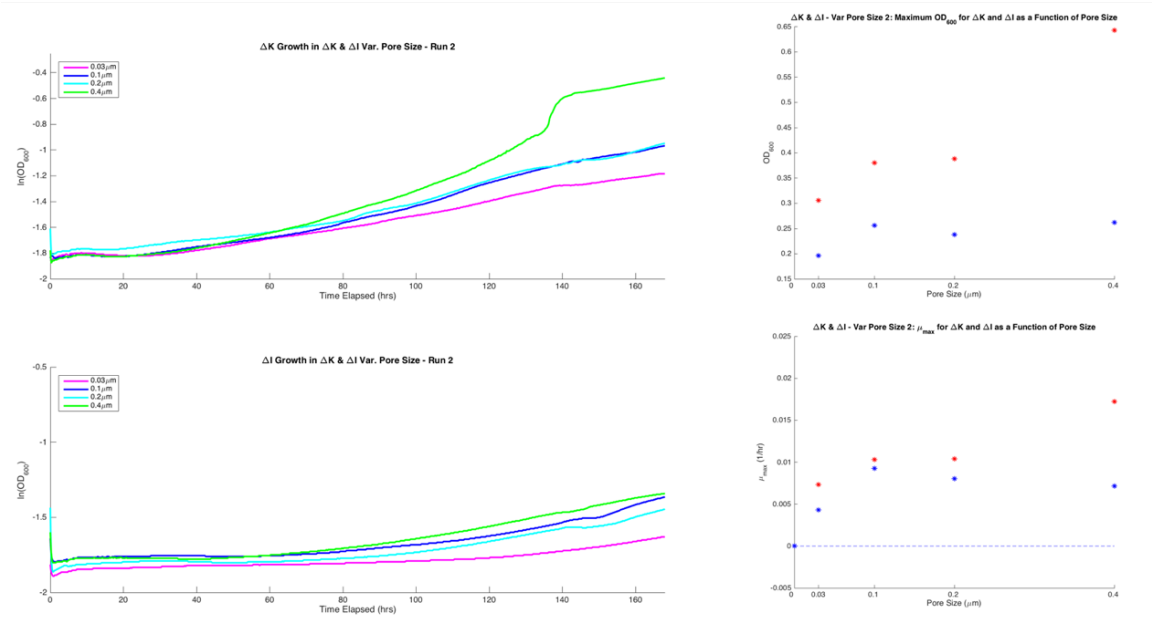

Figure 24: ΔK&ΔI – Var. Pore Size 2: Semi-logarithmic ln(OD_{600}) growth curves for (*Top-Left*) ΔK auxotroph and (*Bottom-Left*) ΔI auxotroph. (*Top-Right*) Maximum OD_{600} (average $\pm$ std) attained by the respective auxotrophs; ΔK in red and ΔI in blue. (*Bottom-Right*) Maximum specific growth rate, u_{max}, (average $\pm$ std) attained by the respective auxotrophs; ΔK in red and ΔI in blue.

The second week-long run of the variable initial amino acid experiment also demonstrated high rates of cross-contamination. The majority of membrane-partitioned samples were cross-contaminated towards the later hours of the kinetic-experiment. Enough samples were gathered to have 1+ samples for each initial amino acid condition. The original OD_{600} plots are shown in Figure 3.17 and the semi-log plots, and max OD_{600} and μ_{mas}as a function of initial amino acid condition are shown in Figure 25.

The second run also demonstrated the outperformance of the Δ*I* strain relative to the ΔK strain, reversing the trend observed in no amino acid conditions. The presence of any initial amount of lysine or isoleucine caused the system to favor the Δ*I* strain, with both the highest max OD_{600} and μ_{max} attained when just the isoleucine was provided. Both max OD_{600} and μ_{max} were most similar when no initial amino acid was provided. Both runs seem to indicate an inhibitory effect of lysine to the ΔK species and a stimulatory effect of isoleucine to the ΔI species. This potentially describes a simple means of adjusting initial environmental conditions to directly affect respective yields and growth rates between a pairwise syntrophic co-culture.

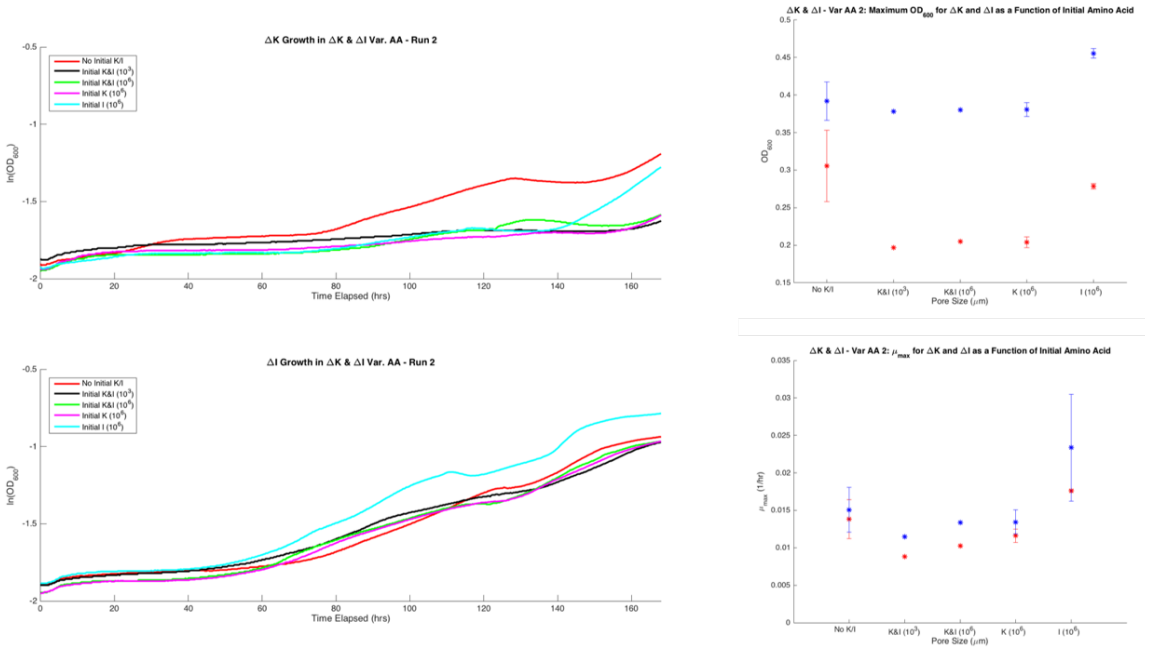

Figure 25: Δ*K*&Δ*I* – Var. AA 2: Semi-logarithmic ln(OD_{600}) growth curves for (*Top-Left*) Δ*K* auxotroph and (*Bottom-Left*) Δ*I* auxotroph. (*Top-Right*) Maximum OD_{600} (average ± std) attained by the respective auxotrophs; Δ*K* in red and Δ*I* in blue. (*Bottom-Right*) Maximum specific growth rate, u_{max}, (average ± std) attained by the respective auxotrophs; Δ*K* in red and Δ*I* in blue.

The recurring events of contamination require an in-depth analysis. It can be confidently stated that the contamination is arising from cross-contamination, either inter or intra-sample, due to the latency in contamination and positive control-like growth in the contaminated well. Indeed, none of the contamination events seemed to occur early into the time-course experiment. Potential sources of contamination include improper seal allowing for one-event contamination of paired wells or the crossover of the organism through the pores of the membrane.

Unknowingly, the BioMe plate was utilized in relatively testing conditions. There are less than 10 reported week-long co-cultures at this volume range [26]. Furthermore, the media in each well are nutrient-rich due to the slow growth of the auxotrophs, creating the perfect condition for cross-contamination if a microbe were to permeate across or around the membrane.

Moreover, I hypothesize that a certain subset of these "contamination" events are not contamination at all, but rather examples of gained genomic fitness. Examples of mechanism include horizontal gene transfer, with the vectors passing through the pores of the membranes, or a mutation to regain wildtype ability to produce the knocked out amino acid. Although further validation is required to demonstrate lack of cross-contamination due to the technical issues of improper sealing or crossover, it is possible that the harsh selective forces placed upon the genetic mutants are encouraging them to either uptake surrounding genetic material or metabolically adapt to reinstate amino acid production. Previous research has demonstrated that forced media pressure can induce faster rates of horizontal gene transfer within *E. Coli* [10].

(5) ONGOING & FUTURE WORK

Computational Modeling

This drastic impediment to growth in the membrane-partitioned syntrophic co-culture was unexpected. In order to explore this phenomenon further, a theoretical model was developed to investigate elements of the positive syntrophic feedback system in further detail. In particular, whether the experimental results could be recreated *in silico* under the conditions of low secretion rates and low across-membrane diffusion rates. A graphical schema of the theoretical framework of the model is provided in Figure 26.

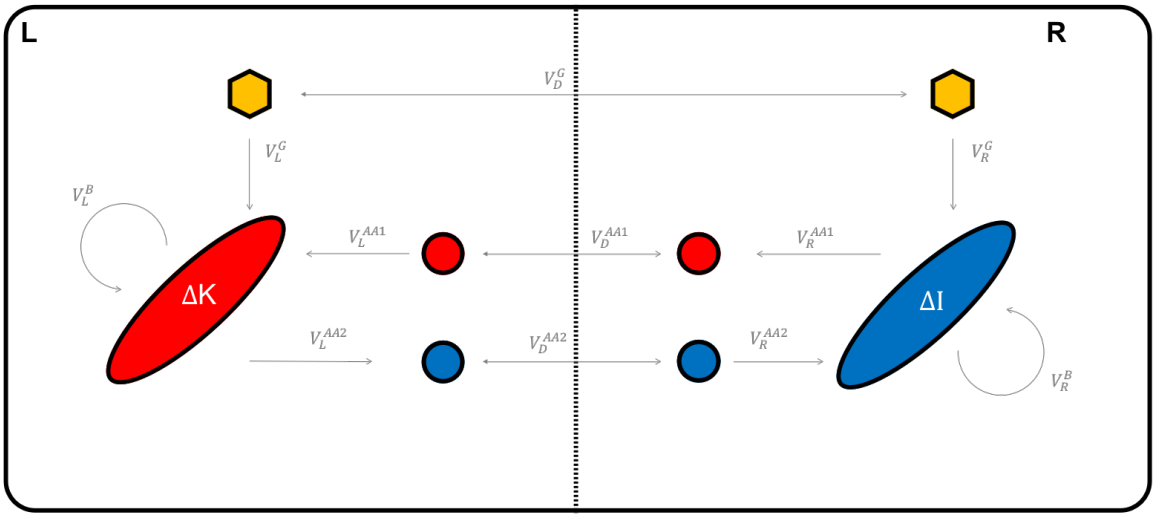

Figure 26: Theoretical framework of the syntrophic co-culture model (ΔK = red oval, ΔI = blue oval, lysine = red circle, isoleucine = blue circle, glucose = yellow hexagon). Uptake, growth, secretion, and diffusion parameters are appropriately labelled.

This model relies on six separate elements: (1) Two auxotroph populations confined to respective wells, (2) Glucose and (3) respective deficient amino acid uptake based on Michaelis-Menten kinetics, (4) Minimum/FBA inspired growth, (5) Biomass-dependent secretion, and (6) Concentration gradient driven diffusion across-membrane. The theoretical equations governing the developed model is provided in Figure C1.

Certain parameter values were found from literature, including the Michaelis-Menten Kinetics (v_{max}, k_m) and biomass stoichiometry parameters for both glucose & amino acid. For unknown parameters, the Monte Carlo method was used to randomly sample a space of values. For the amino acid secretion stoichiometry, a range of [10^{-2} – 10] was used, and for the membrane diffusion constant, [10^{-7} – 1] was used. Values are given in Table C1.

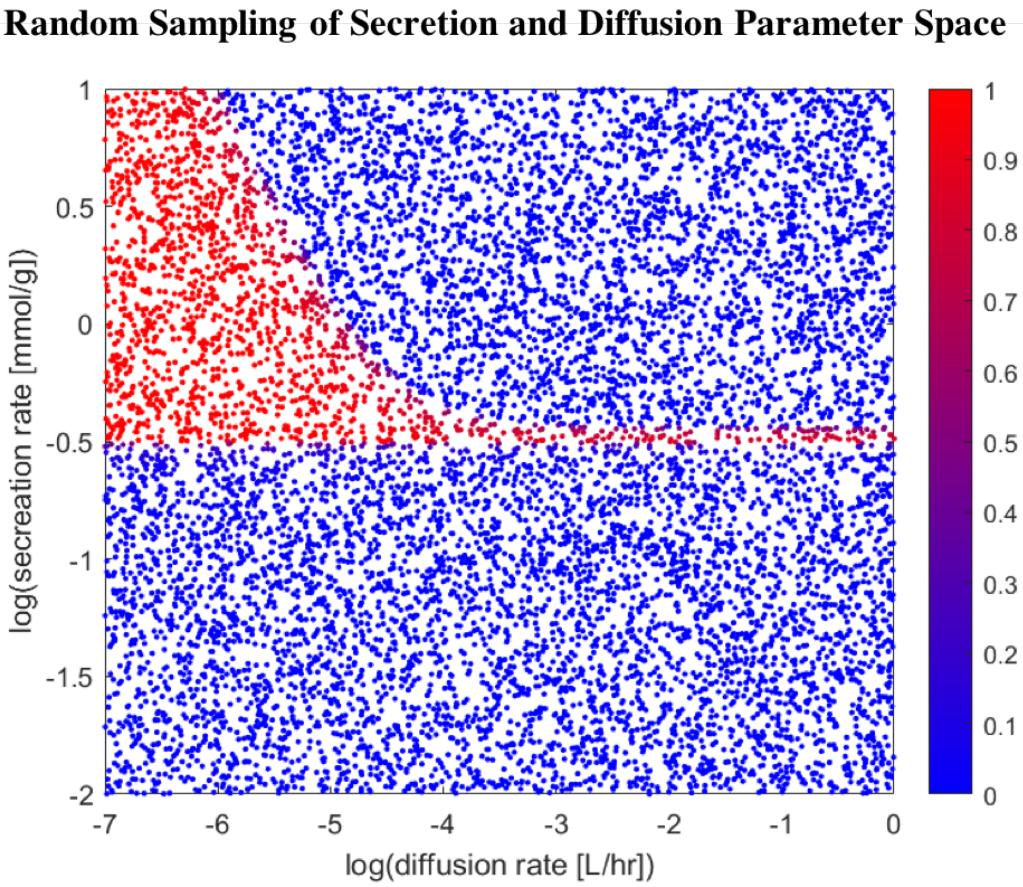

Figure 27: Monte Carlo results for the random sampling of secretion and diffusion parameter space

Monte Carlo method for the simulation of the proposed membrane-partitioned syntrophic model demonstrated a clear space of parameters where there is high growth in the same well (well-mixed co-culture) and low growth in opposite wells (across membranes in the BioMe plate).

Drosophila Gut Microbiome Co-Culture

Overview

The gut microbiome of *Drosophila melanogaster* (fruit flies) are usually composed of two bacterial genera: *Acetobacter* and *Lactobacillus* [55, 63, 64]. Bacterial strains acquired from *in vivo* fly gut samples showed two predominant (if not sole) members of the fly gut microbiome: *Acetobacter pasteurianus* and *Lactobacillus plantarum* [63]. Mutualistic cross-feeding was observed between two other paired species, *Acetobacter fabarum* and *Lactobacillus brevis,* also isolated from the gut of *Drosophila*. *A. fabarum* was shown to "utilize [and metabolize] multiple fermentation products of L. brevis" via gluconeogenesis [64]. A pairwise co-culture experiment was devised to test for mutualistic cross-feeding between *Acetobacter pasteurianus* and *Lactobacillus plantarum* or *Lactobacillus brevis.*

I hypothesize that *A. pasteurianus* will interact mutualistically for both *Lactobacillus* strains, but stronger for *L. plantarum*, due to their native isolation and co-evolution.

Materials & Methods

Identities of the bacterial strains isolated from fly gut samples were confirmed by species-specific primer PCR; the gels are pictured in Figure C3. Cultures were grown in YPD broth for liquid (10g/L peptone, 10g/L yeast extract, 8g/L dextrose) and solid (+15g/L agar) media. A BioMe was sterilized and assembled with membranes of 0.03 micron pore size, and seeded according to the schematic provided in Figure C2. A 96hr kinetic-read experiment was measured at 30^{o}C, with no shaking.

Results & Discussion

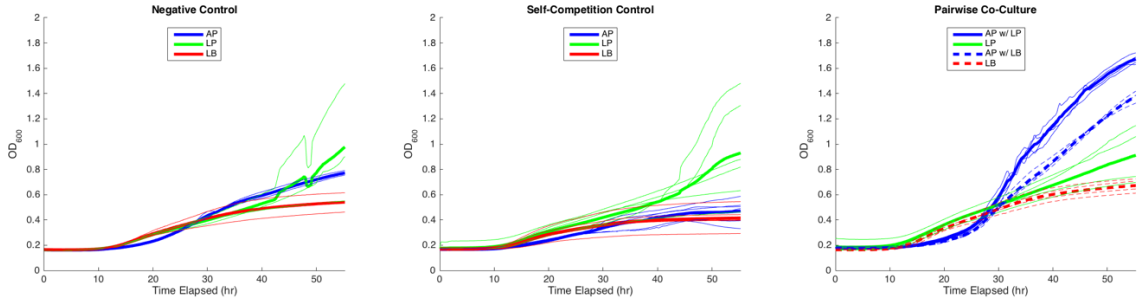

Figure 28: *Drosophila melanogaster* gut microbiota co-culture.

Initial results confirm that *A. pasteurianus* growth is greatly ameliorated by the presence of a *Lactobacillus* pair. Moreover, it supports the hypothesis that *A. pasteurianus* interacts more favorably with the *L. plantarum* strain in comparison to *L. brevis.* It is plausible that these pairs have mutually co-evolved to occupy mutually beneficial niches in the ecosystem. Interestingly, *L. plantarum* seems to demonstrate limited change in yield when co-cultured with no-one, itself, or *A. pasteurianus*. *L. brevis* yield was slightly improved when co-cultured with its *Acetobacter* pair. Results are preliminary and require further investigation.

APPENDIX A: BIOME DEVELOPMENT

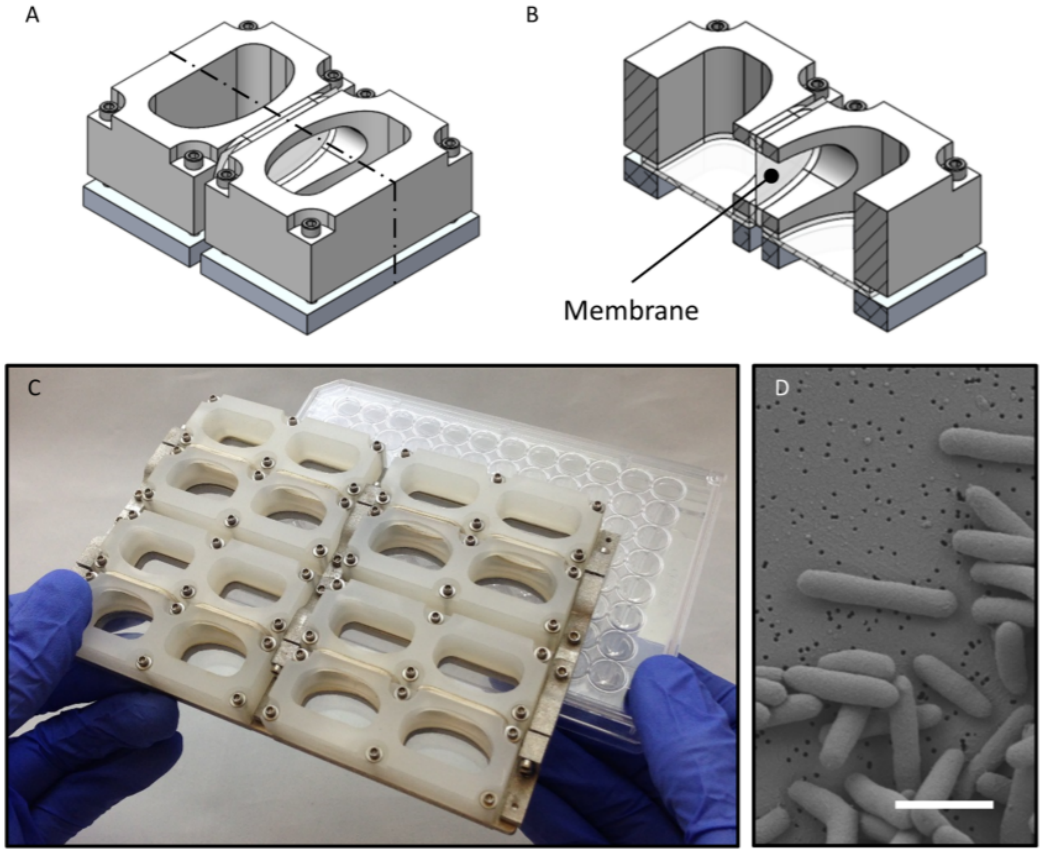

Figure A1: Moutinho et al.'s novel co-culture plate design [45].

Table A1: List of components, source, and catalogue number for the final BioMe plate

Component	Source	Catalogue #
Primary Body Segments	Machined: McMaster-Carr 3D-Printed: FormLabs Dental SG Resin	Machined: 8742K136 3D Printed: RS-F2-DGOR-01
Optically Clear Base	McMaster-Carr	8707K111
O-Rings	McMaster-Carr	5233T14
Rods	McMaster-Carr	95412A373
Nuts	McMaster-Carr	94758A102
Gasket	McMaster-Carr	86045K76
Screws	McMaster-Carr	90585A204
Porous Membranes	Sterlitech	*Custom Order*

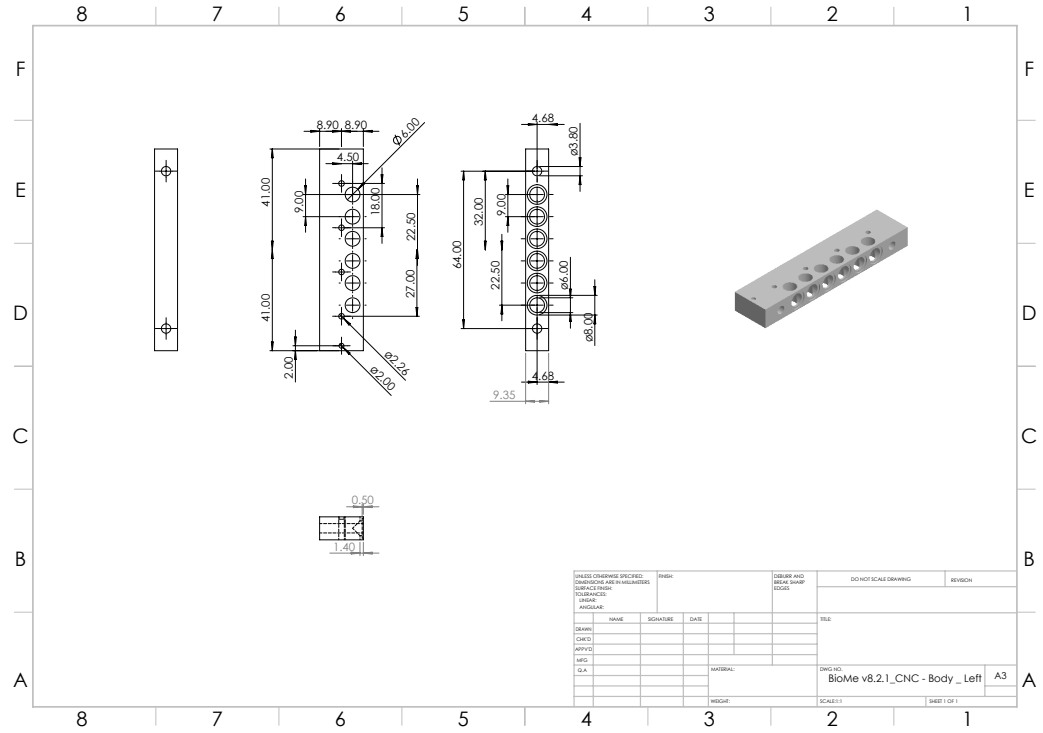

Figure A2: Left body segment SolidWorks CAD drawing used in final BioMe iteration (v8)

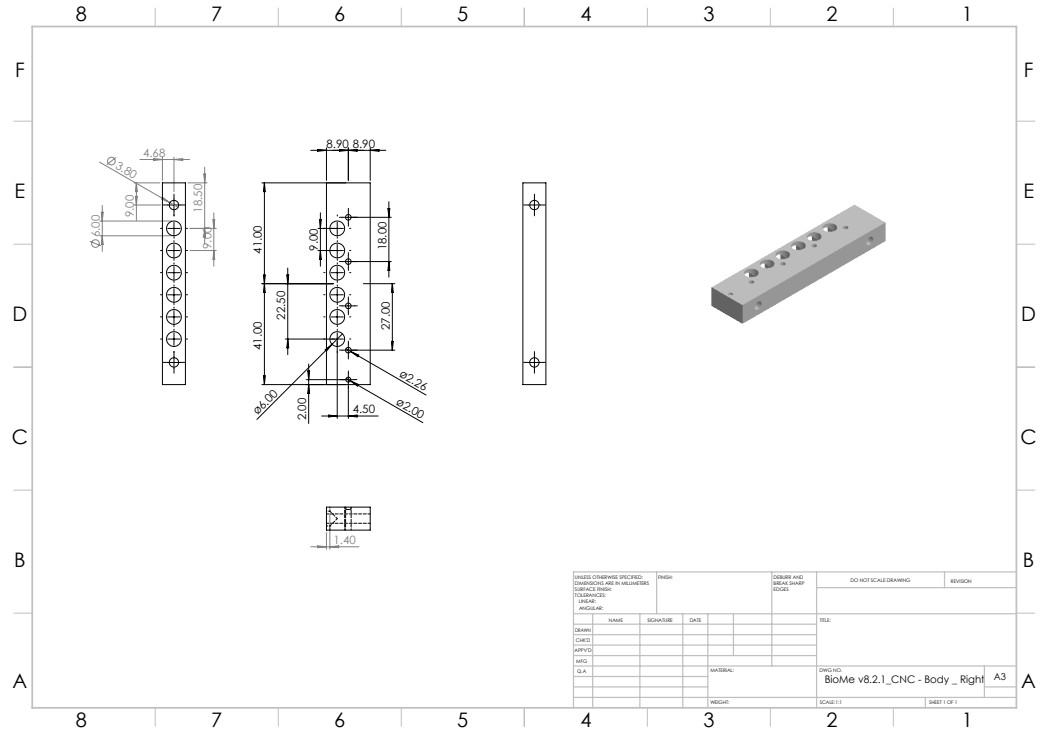

Figure A3:: Right body segment SolidWorks CAD drawing used in final BioMe iteration (v8)

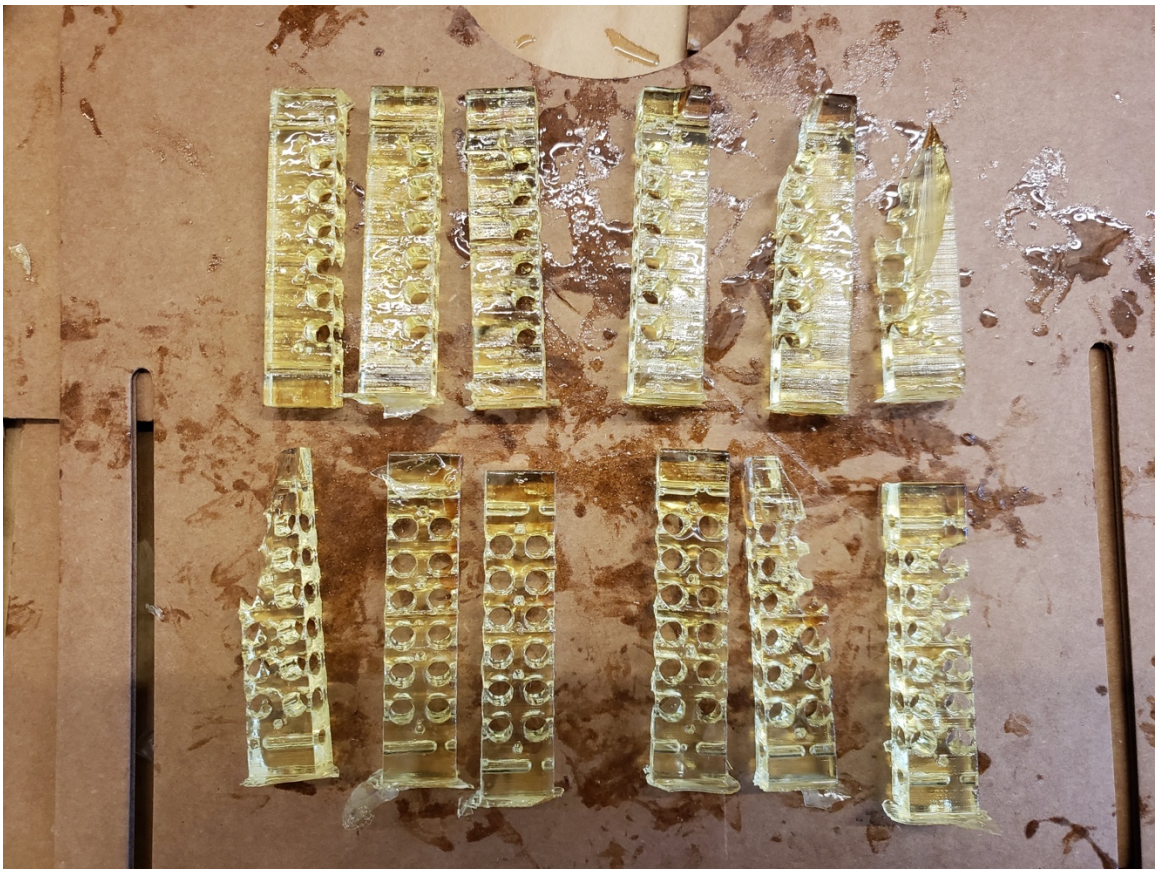

Figure A4: Example of failed body segment prints using the Form2 printer and Formlab's Dental SG Resin

BioMe Plate: Sterilization Validation v13 [Visual w/ Plating, w/ membranes]

GOALS:

- Confirm that the sterilization protocol eliminates microbial contamination from the BioMe device after use for E. Coli (MG1655, NR1, Lys-, Ile-, and Lys-&Ile-) culture.

PROCEDURE:

Pre-Sterilization Growth

Liquid Culture:

[1] Inoculate 5mL of LB w/o antibiotics broth in 12-well plate directly from glycerol stock of: **(1)** E. Coli K-12 MG1655, **(2)** E. Coli NR1 WT, **(3)** E. Coli Lys-, **(4)**, E. Coli Ile-, **(5)** E. Coli Lys- & Ile-

[2] Incubate in 30°C static incubator while assembling BioMe.

Non-Sterile BioMe Assembly, Inoculation, & Culture:

[3] Ethanol wipe-down benchtop. Fully assemble BioMe w/o membranes under non-sterile conditions.

[4] Once assembled, take 12-well plate out of incubator. Pipette up and down to mix liquid cultures. Seed the BioMe Plate w/ 250uL of appropriate culture according to the schematic below:

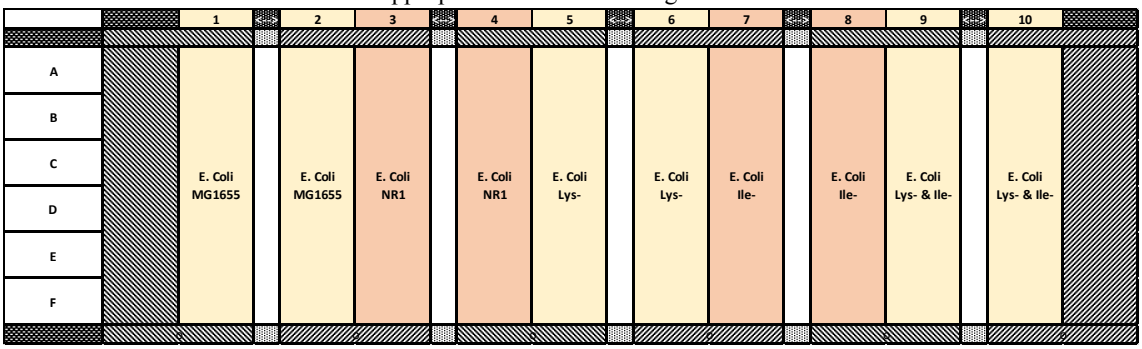

[5] Incubate BioMe in 30°C static incubator for 72hrs.

Sterilization Protocol

Ethanol Bath & Scrub:

[6] Once culturing time has elapsed, place BioMe device into sterile bag. Fill w/ ~200mL of 70% ethanol and shake vigorously. Let sit for 10mins, fully submerged.

[7] Drain the sterile bag directly down sink. Rinse BioMe w/ distilled water (DW).

[8] Disassemble BioMe device. Soap, scrub down, and rinse all device elements.

Dishwash & Autoclave:

[9] Dishwash all components except for screws: P2 [Plastic Wash] {1.5hr}

[10] Autoclave: P9 [Gravity, 121°C, 30mins exposure/15 mins dry] {1hr}

Side: Screws (50mL beaker) *Top: Gasket, Base (wrapped), Rods w/ O-rings, Allen Key, Tweezers*

Middle: Bodies *Bottom: Assembly body, Wrench*

BSC & Membrane Prep {During *Autoclave*}:

[11] Wipe down BSC with 70% ethanol. Sterile introduce: *Sterile bag (x2), reservoir*

[12] Wipe down bench top with ethanol and light Bunsen burner.

[13] Grab 5 weighing boats – one for each pairwise column [**PCTE:** 0.2um**]**.

[14] Ethanol spray down a weighing boat and fill with ~5mL of ethanol.
[15] Flame tweezers and use to pull out x6 membranes into respective boats.
[16] Wipe boats down with ethanol and introduce into BSC. Repeat for all pairwise columns.

BioMe Partial Assembly {After *Autoclave*}:

[17] Carefully introduce autoclaved rack w/ BioMe and beaker w/ screws into BSC.
[18] Place screws and allen key into first sterile bag.
[19] Place O-rings into reservoir and submerge in ~10mL of 70% ethanol.
[20] Partially assemble BioMe w/ O-rings and membranes in BSC.
[21] Place partially assembled BioMe, gasket, and base (wrapped) into second sterile bag.

Post- Sterilization Growth

BioMe Ethanol Bath, Full Assembly, & Experiment Prep:

[22] Turn on UV light for 20mins and then ethanol wipe down BSC.
[23] Ethanol wipe down and introduce into BSC: *sterile bags w/ BioMe components, 200mL of 70% ethanol, autoclave rack, reservoir.*
[24] Take out wrapped base and pour in ethanol into gasket//BioMe sterile bag and let sit for 10 minutes.
[25] Take out BioMe and let dry for ~1hr, upside-down on top rack, in far left corner of BSC.
[26] Fully assemble dried BioMe w/ screws, gasket, and base. Keep upside-down.
[27] Remove all items from BSC except BioMe.. Ethanol wipe down and introduce: *electronic multichannel pipette (1200uL), p1000, 1000uL tip box, tip waste, bottom tray, top lid, reagent reservoir, parafilm*
[28] Arrange USA Scientific 1000uL tip box w/o edge pipettes (rows and columns) in sterile BSC
[29] Turn on UV light for >20 mins, with fully assembled BioMe inside BSC (top rack).

Post- Sterilization Media Seeding:

[30] Ethanol wipe down and introduce: *LB w/o antibiotics Pyrex bottle*
[31] Pour out ~20mL of LB into reagent reservoir. Seed all wells of BioMe device w/ 250uL of LB.
[32] Cover w/ lid and seal with ethanol wiped parafilm.
[33] Place into 30ºC static incubator for 72hours.

Sterilization Validation

Visualization:

[34] Use visualization for initial sterilization verification. Take picture & report.

Plating:

[35] Plate 10uL of solution from all wells on (x5) LB w/o antibiotic agar plates, with each plate pinwheel divided into 12 sections.
[36] Incubate plates for 72hrs.
[37] Visualize and take pictures of plates to confirm no bacterial growth on any of the plates. Report.
    - Successful sterilization validation will demonstrate no growth on any of the plates.

APPENDIX B: BIOME EXPERIMENTS

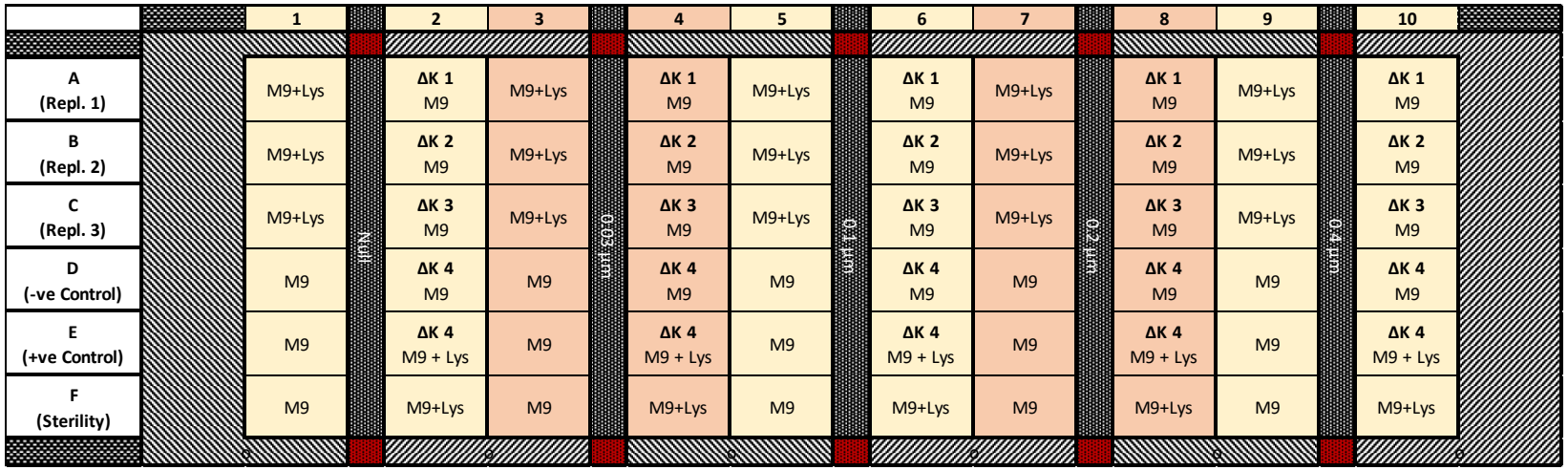

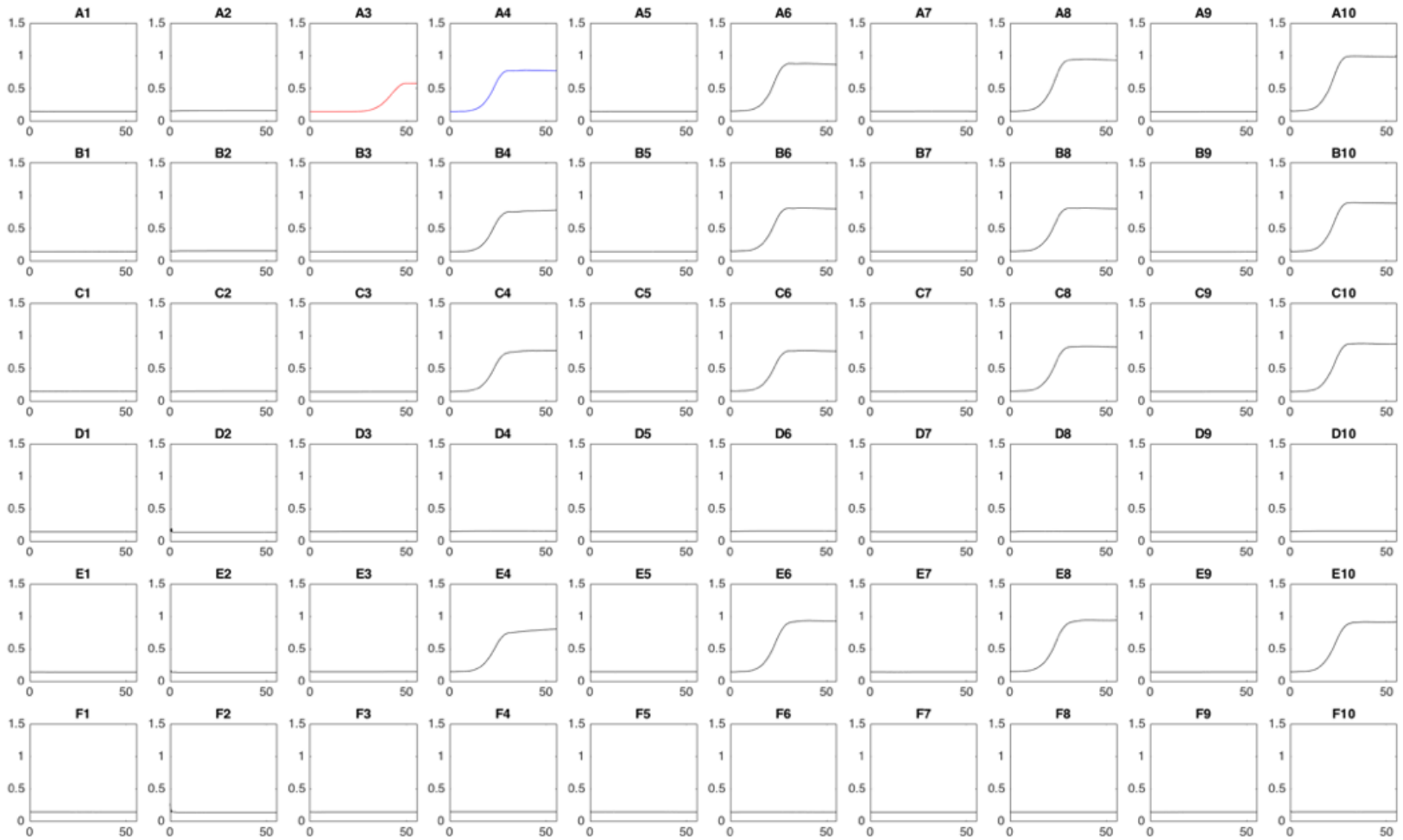

Figure B1: ΔK & Lysine Diffusion – Run 1. Each pairwise column separated by null, 0.03, 0.1, 0.2, or 0.4μm membrane. Top three rows are biological replicates, 4th row is negative control, 5th row is positive control, and sixth row is sterility control. (Top) Device schematic. (Bottom) Original OD_{600} data. Contaminated curves given in red, with data omitted curves given in blue.

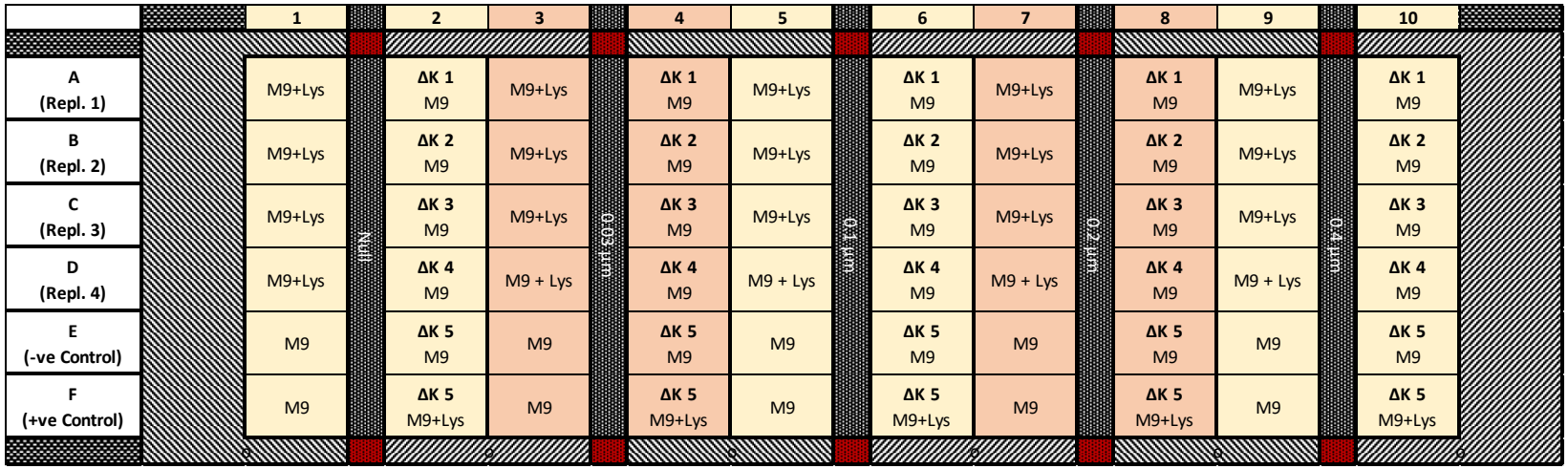
1
2
3
4
5
6
7
8
9
10
A (Repl. 1)
B (Repl. 2)
C (Repl. 3)
D (Repl. 4)
E (-ve Control)
F (+ve Control)
M9+Lys
ΔK 1 M9
ΔK 2 M9
ΔK 3 M9
ΔK 4 M9
ΔK 5 M9
M9 + Lys
M9
ΔK 5 M9+Lys
NaN
0.03 mm
0.1 mm
0.2 mm
0.4 mm

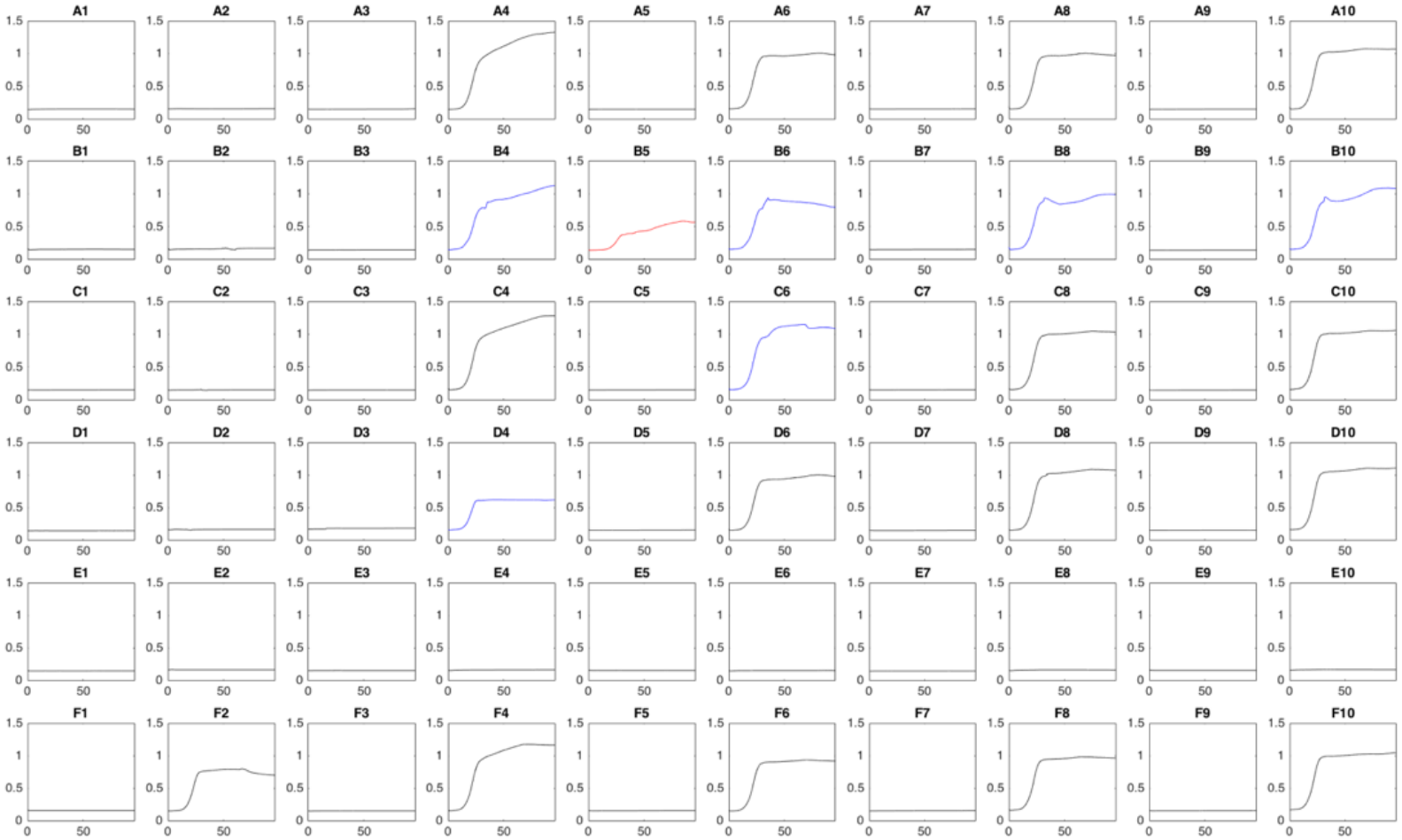

Figure B2: ΔK & Lysine Diffusion – Run 2. Each pairwise column separated by null, 0.03, 0.1, 0.2, or 0.4μm membrane. Top four rows are biological replicates, 5th row is negative control, and 6th row is positive control. (Top) Device schematic. (Bottom) Original OD_{600} data. Contaminated curves given in red, with data omitted curves given in blue.

	1		2	3		4	5		6	7		8	9		10
A (Repl. 1)	M9+Ile	Null	**ΔI 1** M9	M9+Ile	0.03 µm	**ΔI 1** M9	M9+Ile	0.1 µm	**ΔI 1** M9	M9+Ile	0.2 µm	**ΔI 1** M9	M9+Ile	0.4 µm	**ΔI 1** M9
B (Repl. 2)	M9+Ile		**ΔI 2** M9	M9+Ile		**ΔI 2** M9	M9+Ile		**ΔI 2** M9	M9+Ile		**ΔI 2** M9	M9+Ile		**ΔI 2** M9
C (Repl. 3)	M9+Ile		**ΔI 3** M9	M9+Ile		**ΔI 3** M9	M9+Ile		**ΔI 3** M9	M9+Ile		**ΔI 3** M9	M9+Ile		**ΔI 3** M9
D (-ve Control)	M9		**ΔI 4** M9	M9		**ΔI 4** M9	M9		**ΔI 4** M9	M9		**ΔI 4** M9	M9		**ΔI 4** M9
E (+ve Control)	M9		**ΔI 4** M9 + Ile	M9		**ΔI 4** M9 + Ile	M9		**ΔI 4** M9 + Ile	M9		**ΔI 4** M9 + Ile	M9		**ΔI 4** M9 + Ile
F (Sterility)	M9+Ile		M9	M9+Ile		M9	M9+Ile		M9	M9+Ile		M9	M9+Ile		M9

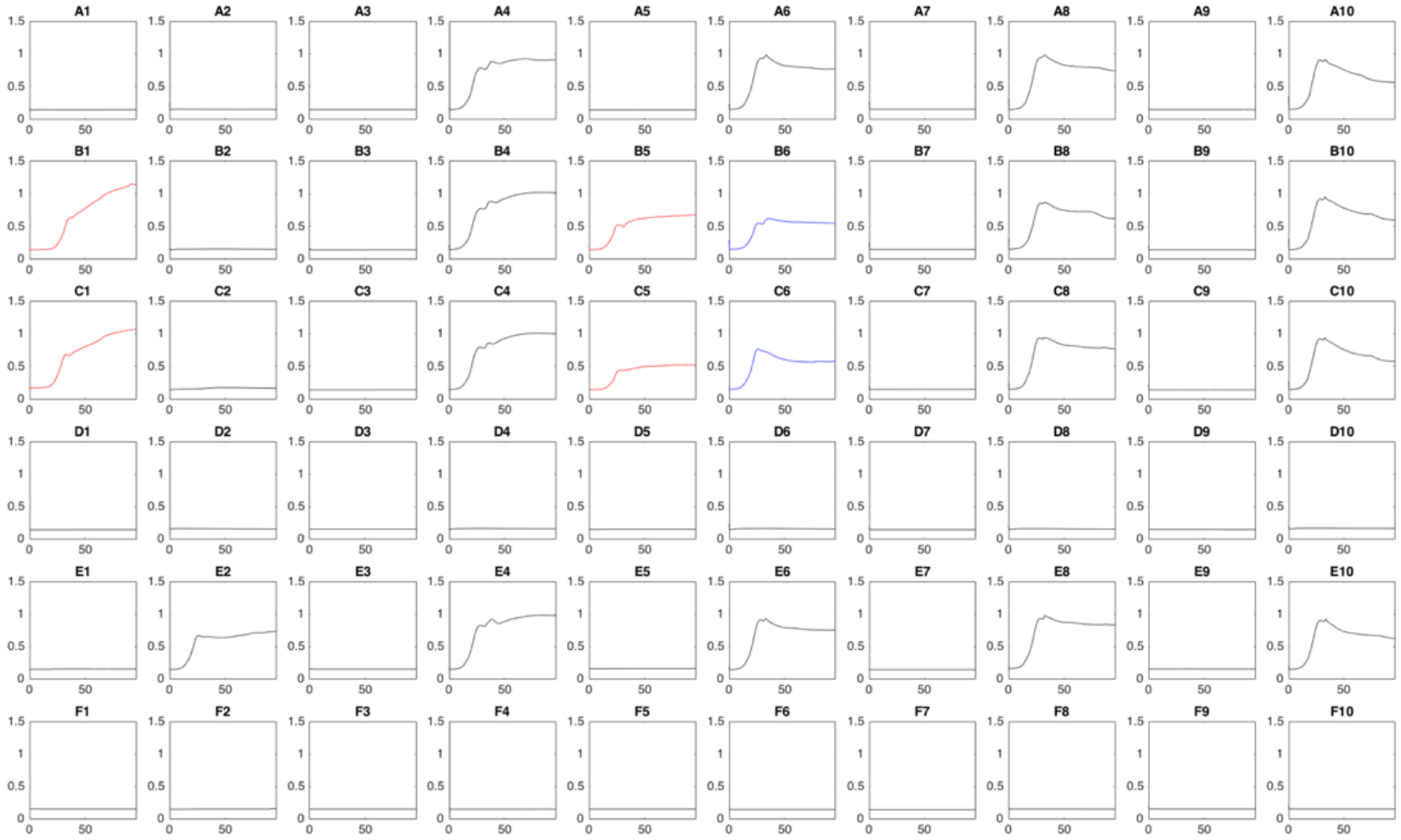

Figure B3: ΔI & Isoleucine Diffusion – Run 1. Each pairwise column separated by null, 0.03, 0.1, 0.2, or 0.4μm membrane. Top three rows are biological replicates, 4th row is negative control, 5th row is positive control, and sixth row is sterility control. (Top) Device schematic. (Bottom) Original OD_{600} data. Contaminated curves given in red, with data omitted curves given in blue.

	1	2	3	4	5	6	7	8	9	10
A (Repl. 1)	M9+Ile	**ΔI 1** M9	M9+Ile	**ΔI 1** M9	M9+Ile	**ΔI 1** M9	M9+Ile	**ΔI 1** M9	M9+Ile	**ΔI 1** M9
B (Repl. 2)	M9+Ile	**ΔI 2** M9	M9+Ile	**ΔI 2** M9	M9+Ile	**ΔI 2** M9	M9+Ile	**ΔI 2** M9	M9+Ile	**ΔI 2** M9
C (Repl. 3)	M9+Ile	**ΔI 3** M9	M9+Ile	**ΔI 3** M9	M9+Ile	**ΔI 3** M9	M9+Ile	**ΔI 3** M9	M9+Ile	**ΔI 3** M9
D (Repl. 4)	M9+Ile	**ΔI 4** M9	M9+Ile	**ΔI 4** M9	M9+Ile	**ΔI 4** M9	M9+Ile	**ΔI 4** M9	M9+Ile	**ΔI 4** M9
E (-ve Control)	M9	**ΔI 5** M9	M9	**ΔI 5** M9	M9	**ΔI 5** M9	M9	**ΔI 5** M9	M9	**ΔI 5** M9
F (+ve Control)	M9	**ΔI 5** M9+Ile	M9	**ΔI 5** M9+Ile	M9	**ΔI 5** M9+Ile	M9	**ΔI 5** M9+Ile	M9	**ΔI 5** M9+Ile

0.4 mm | 0.2 mm | 0.1 mm | 0.05 mm | Nil

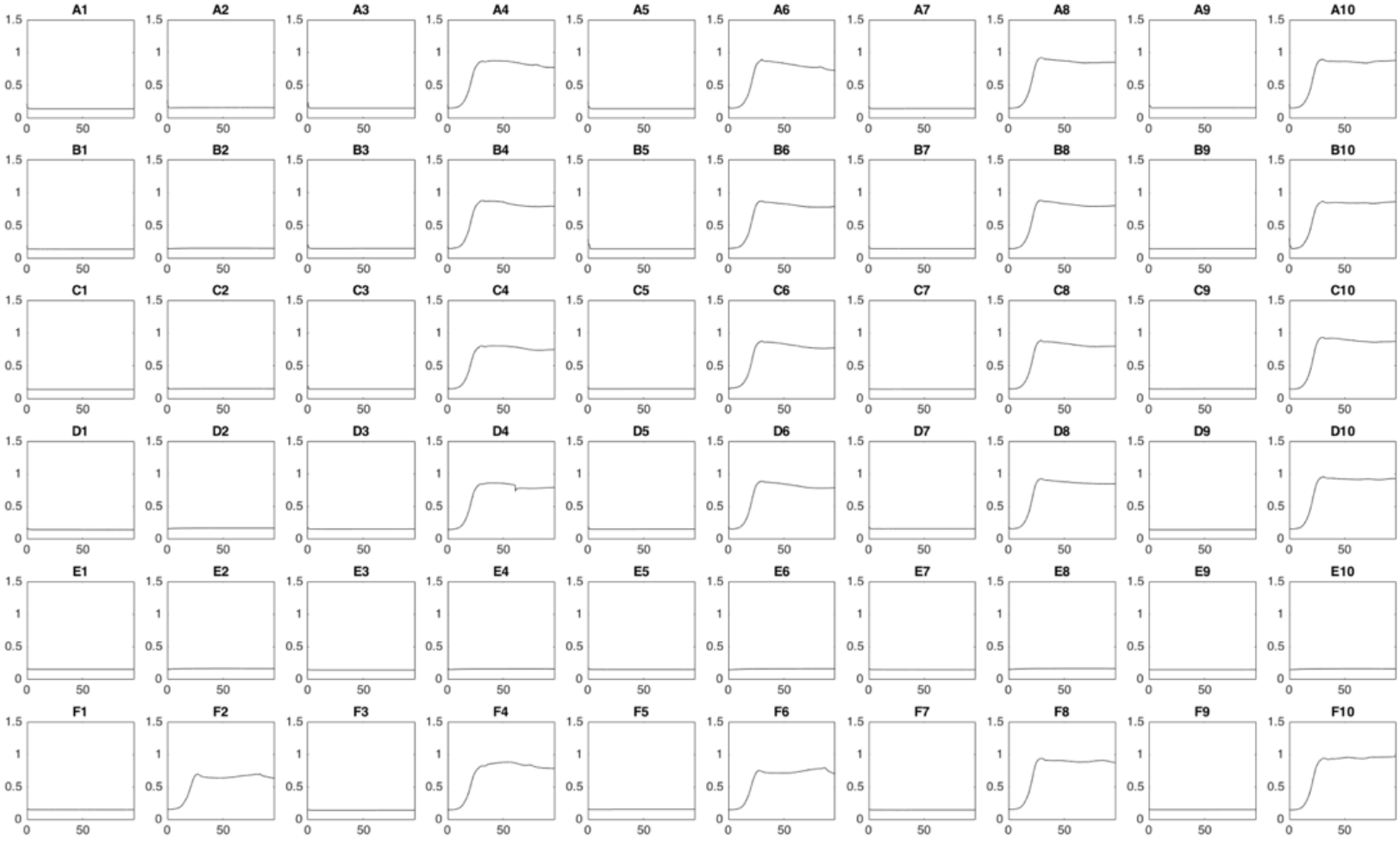

Figure B4: ΔI & Isoleucine Diffusion – Run 2. Each pairwise column separated by null, 0.03, 0.1, 0.2, or 0.4μm membrane. Top four rows are biological replicates, 5th row is negative control, and 6th row is positive control. (Top) Device schematic. (Bottom) Original OD_{600} data. Contaminated curves given in red, with data omitted curves given in blue.

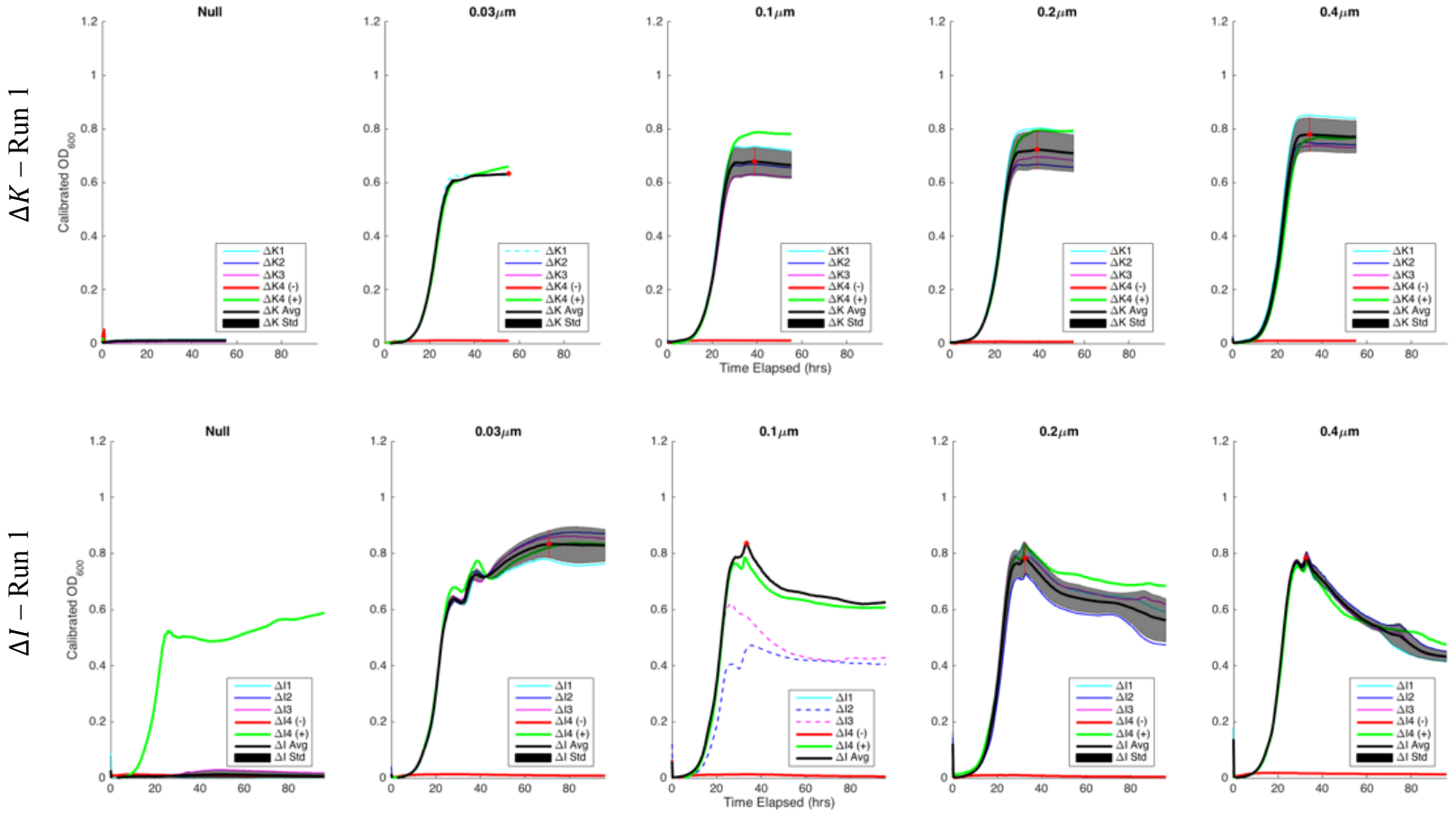

Figure B5: E. Coli *Auxotroph Growth Curves for first run of diffusion experiments: replicates (blue, cyan, magenta, yellow), negative control (red), positive control (green), average of replicates (black line), standard deviation of replicates (grey shading). Replicates that were not included in further analysis are shown in dotted lines.*

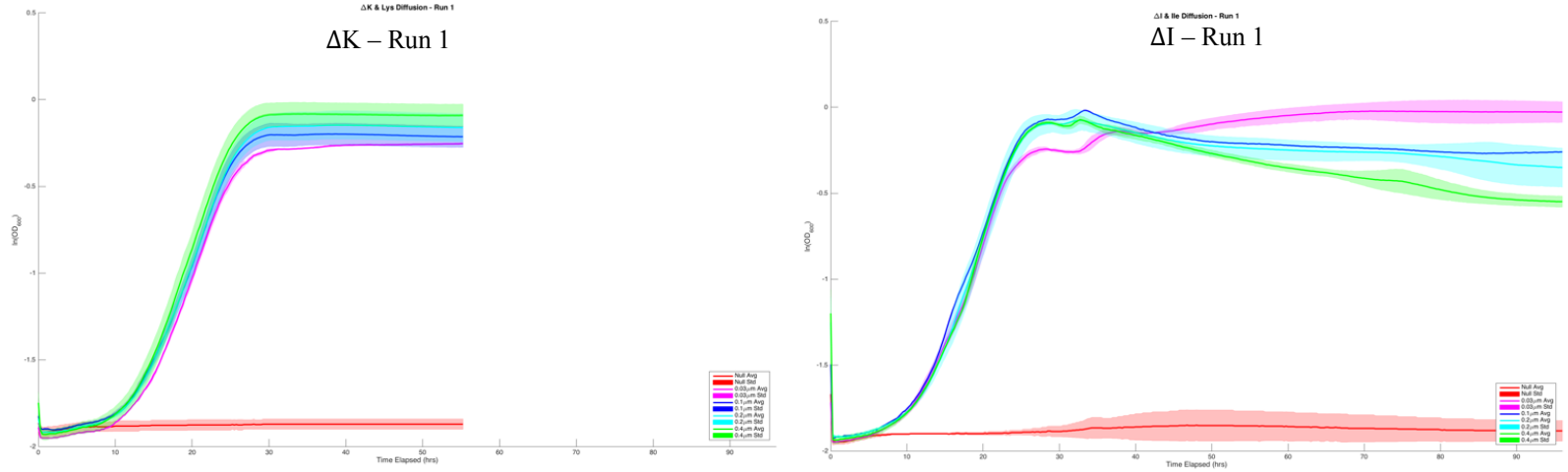

Figure B6: Semi-log plots for the average ln(OD_{600}) growth curves for all membrane pore size (Run 1); Null (red), 0.03μm (magenta), 0.1 μm (blue), 0.2 μm (cyan), 0.4 μm (green).

	ΔK & Lys Diffusion – Run 1					ΔK & Lys Diffusion – Run 2				
Pore Size (µm)	**Null**	**0.03**	**0.1**	**0.2**	**0.4**	**Null**	**0.03**	**0.1**	**0.2**	**0.4**
Max $OD_{600,C}$ Avg	0.0112	0.6330	0.6783	0.7224	0.7793	0.0102	1.1535	0.8544	0.8937	0.9278
Max $OD_{600,C}$ STD	0.0046	0.0028	0.0523	0.0712	0.0632	0.0127	0.0318	0.0028	0.0435	0.0251
Time @ Max (hr:min)	31:45	55:15 (End)	38:45	39:00	34:30	51:15	95:45	82:00	74:15	95:15
	ΔI & Ile Diffusion – Run 1					**ΔI & Ile Diffusion – Run 1**				
Pore Size (µm)	**Null**	**0.03**	**0.1**	**0.2**	**0.4**	**Null**	**0.03**	**0.1**	**0.2**	**0.4**
Max $OD_{600,C}$ Avg	0.0269	0.8339	0.8369	0.7829	0.7853	0.0169	0.7073	0.7375	0.7590	0.7676
Max $OD_{600,C}$ STD	0.0527	0.0469	0	0.0563	0.0210	0.0524	0.0321	0.0076	0.0212	0.0388
Time @ Max (hr:min)	0:00	70:45	33:30	32:30	32:45	0:00	40:00	30:00	29:25	30:25

Table B1: Max average calibrated OD_{600}, STD, and time @max for all diffusion experiments and diffusion culture sets as a function of membrane pore size.

ΔK & Lys Diffusion – Run 1				
Pore Size (μm)	**0.03**	**0.1**	**0.2**	**0.4**
Sample Size, n	2	3	3	3
μ_{max} (Avg±Std)	0.1243 ±0.0029	0.1226 ±0.0022	0.1238 ±0.0017	0.1291 ±0.0009
R^2 (Avg±Std)	0.9997 ±0.0000	0.9989 ±0.0011	0.9994 ±0.0004	0.9996 ±0.0001
ΔK & Lys Diffusion – Run 2				
Pore Size (μm)	**0.03**	**0.1**	**0.2**	**0.4**
Sample Size, n	2	2	3	3
μ_{max} (Avg±Std)	0.1368 ±0.0031	0.1326 ±0.0017	0.1359 ±0.0022	0.1380 ±0.0008
R^2 (Avg±Std)	0.9999 ±0.0001	0.9992 ±0.0002	0.9990 ±0.0010	0.9995 ±0.0003
ΔI & Ile Diffusion – Run 1				
Pore Size (μm)	**0.03**	**0.1**	**0.2**	**0.4**
Sample Size, n	3	1	3	3
μ_{max} (Avg±Std)	0.1176 ±0.0178	0.1230	0.1335 ±0.0071	0.1170 ±0.0284
R^2 (Avg±Std)	0.9961 ±0.0007	0.9979	0.9976 ±0.0017	0.9959 ±0.0011
ΔI & Ile Diffusion – Run 2				
Pore Size (μm)	**0.03**	**0.1**	**0.2**	**0.4**
Sample Size, n	4	4	4	4
μ_{max} (Avg±Std)	0.1257 ±0.0021	0.1279 ±0.0035	0.1299 ±0.0023	0.1297 ±0.0038
R^2 (Avg±Std)	0.9981 ±0.0022	0.9983 ±0.0006	0.9988 ±0.0003	0.9985 ±0.0008

Table B2: Max specific growth rate during exponential phase, μ_{max}, and its associated standard deviation, sample size, and R^2 for all diffusion experiments and diffusion culture sets as a function of membrane pore size.

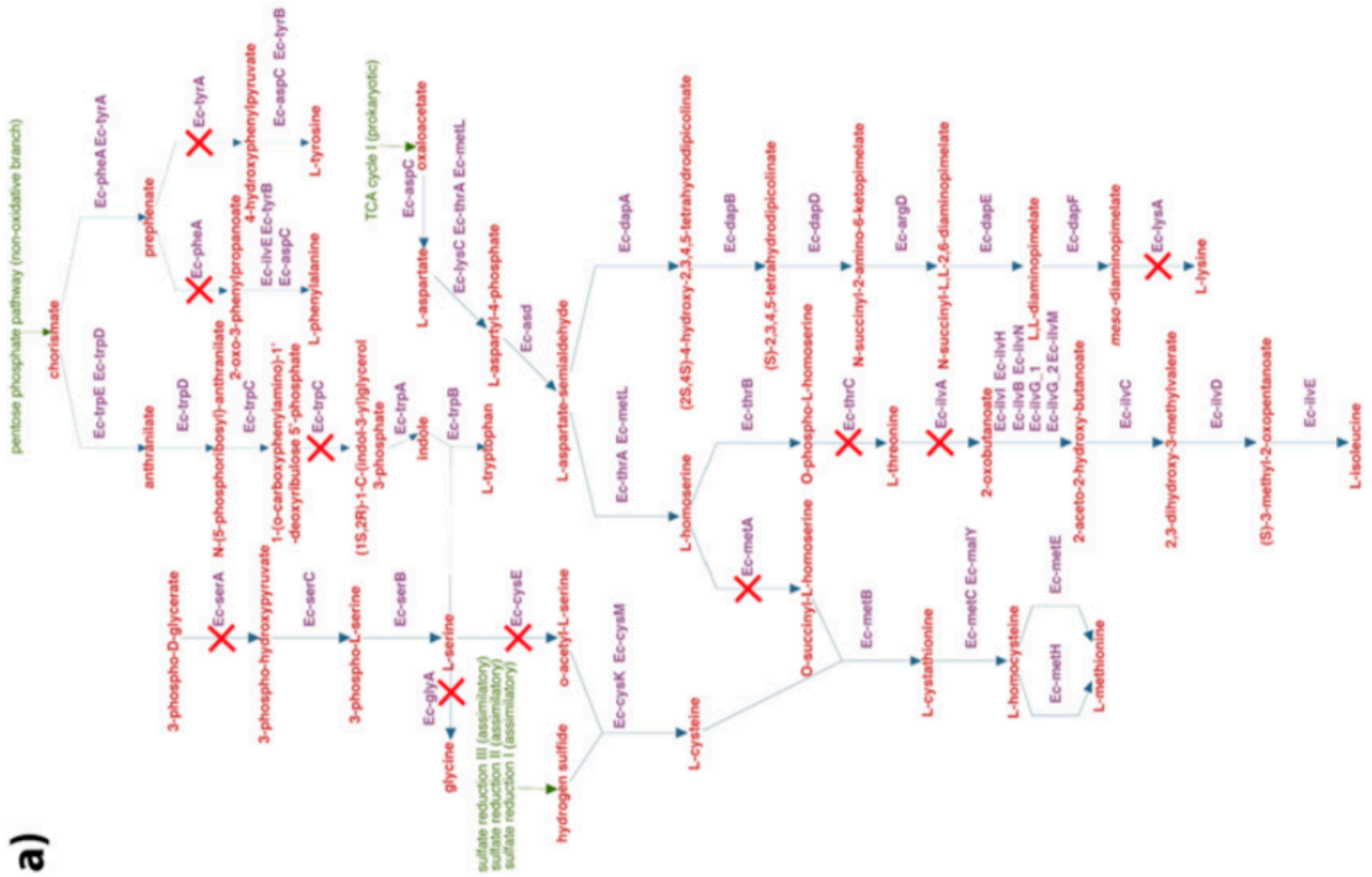

Figure B7: Metabolic pathways with red crosses indicating the location of gene knockout for amino acid auxotrophy generation

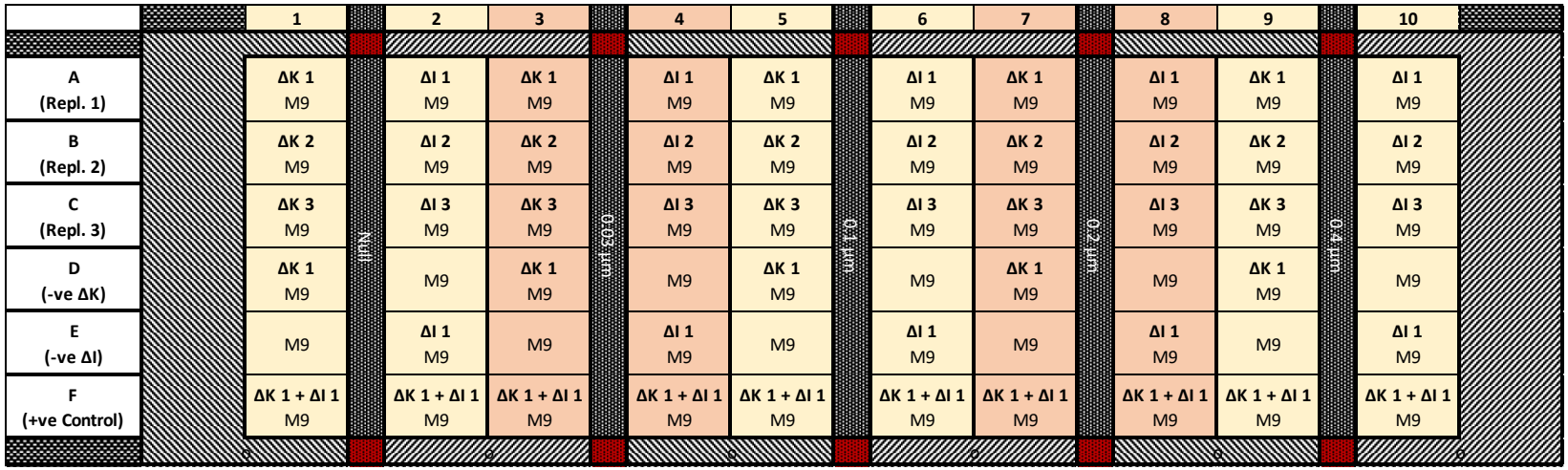
1
2
3
4
5
6
7
8
9
10
A (Repl. 1)
B (Repl. 2)
C (Repl. 3)
D (-ve ΔK)
E (-ve ΔI)
F (+ve Control)
ΔK 1 M9
ΔI 1 M9
ΔK 2 M9
ΔI 2 M9
ΔK 3 M9
ΔI 3 M9
ΔK 1 + ΔI 1 M9
M9
Nil
0.03 µm
0.1 µm
0.2 µm
0.4 µm

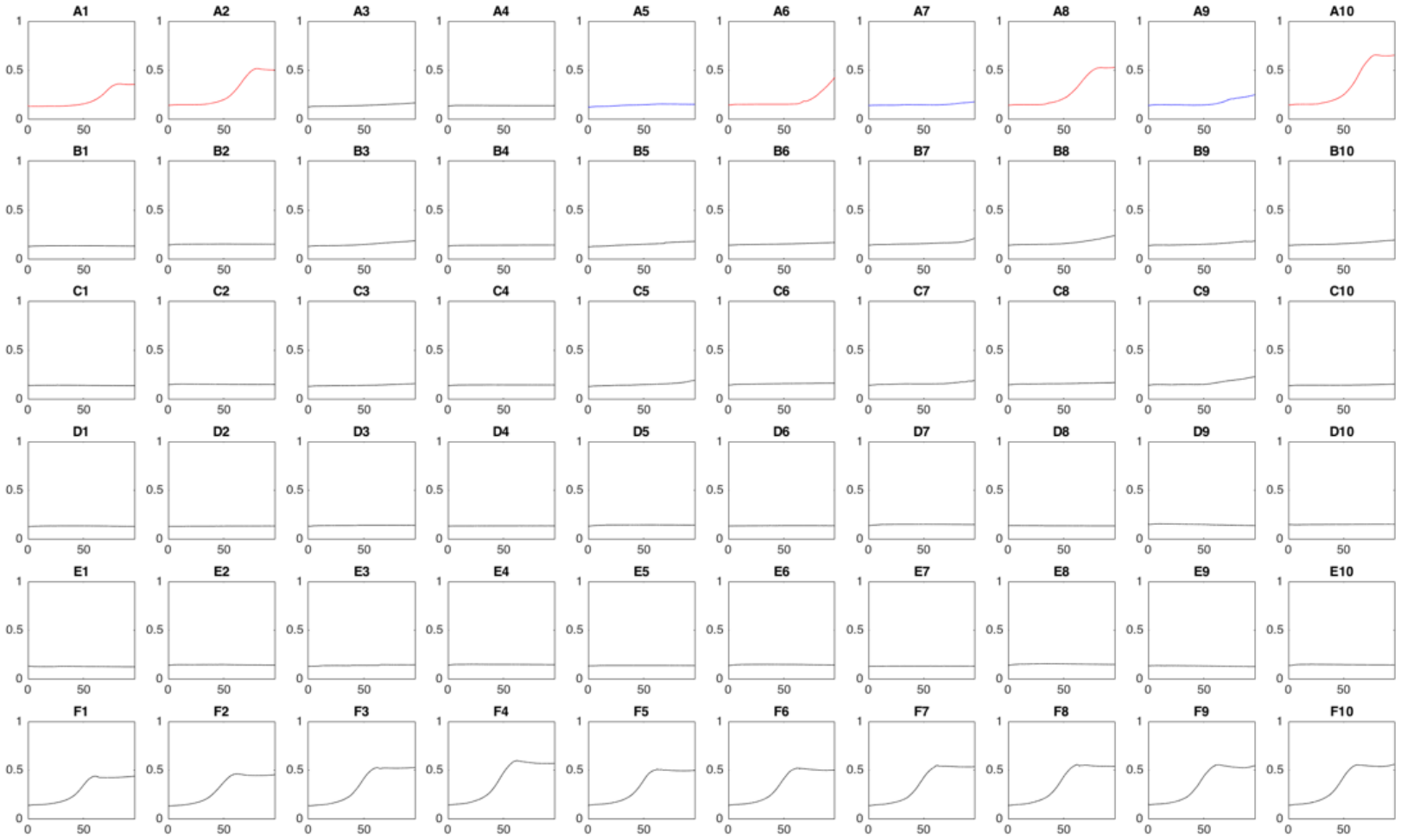

Figure B8: ΔK & ΔI Co-Culture Variable Pore Size – Run 1. Each pairwise column separated by null, 0.03, 0.1, 0.2, or 0.4μm membrane. Top three rows are biological replicates, 4th&5th rows are negative control, and 6th row is positive control. (Top) Device schematic. (Bottom) Original OD_{600} data. Contaminated curves given in red, with data omitted curves given in blue.

	1	2	3	4	5	6	7	8	9	10
A (Repl. 1)	**ΔK 1** M9	**ΔI 1** M9	**ΔK 1** K&I (10^3)	**ΔI 1** K&I (10^3)	**ΔK 1** K&I (10^6)	**ΔI 1** K&I (10^6)	**ΔK 1** K (10^6)	**ΔI 1** K (10^6)	**ΔK 1** I (10^6)	**ΔI 1** I (10^6)
B (Repl. 2)	**ΔK 2** M9	**ΔI 2** M9	**ΔK 2** K&I (10^3)	**ΔI 2** K&I (10^3)	**ΔK 2** K&I (10^6)	**ΔI 2** K&I (10^6)	**ΔK 2** K (10^6)	**ΔI 2** K (10^6)	**ΔK 2** I (10^6)	**ΔI 2** I (10^6)
C (Repl. 3)	**ΔK 3** M9	**ΔI 3** M9	**ΔK 3** K&I (10^3)	**ΔI 3** K&I (10^3)	**ΔK 3** K&I (10^6)	**ΔI 3** K&I (10^6)	**ΔK 3** K (10^6)	**ΔI 3** K (10^6)	**ΔK 3** I (10^6)	**ΔI 3** I (10^6)
D (-ve ΔK)	**ΔK 4** M9	M9	**ΔK 4** K&I (10^3)	K&I (10^3)	**ΔK 4** K&I (10^6)	K&I (10^6)	**ΔK 4** K (10^6)	K (10^6)	**ΔK 4** I (10^6)	I (10^6)
E (-ve ΔI)	M9	**ΔI 4** M9	K&I (10^3)	**ΔI 4** K&I (10^3)	K&I (10^6)	**ΔI 4** K&I (10^6)	K (10^6)	**ΔI 4** K (10^6)	I (10^6)	**ΔI 4** I (10^6)
F (+ve Control)	**ΔK 4 + ΔI 4** M9	**ΔK 4 + ΔI 4** M9	**ΔK 4 + ΔI 4** K&I (10^3)	**ΔK 4 + ΔI 4** K&I (10^3)	**ΔK 4 + ΔI 4** K&I (10^6)	**ΔK 4 + ΔI 4** K&I (10^6)	**ΔK 4 + ΔI 4** K (10^6)	**ΔK 4 + ΔI 4** K (10^6)	**ΔK 4 + ΔI 4** I (10^6)	**ΔK 4 + ΔI 4** I (10^6)

0.2 µm 0.2 µm 0.2 µm 0.2 µm 0.2 µm

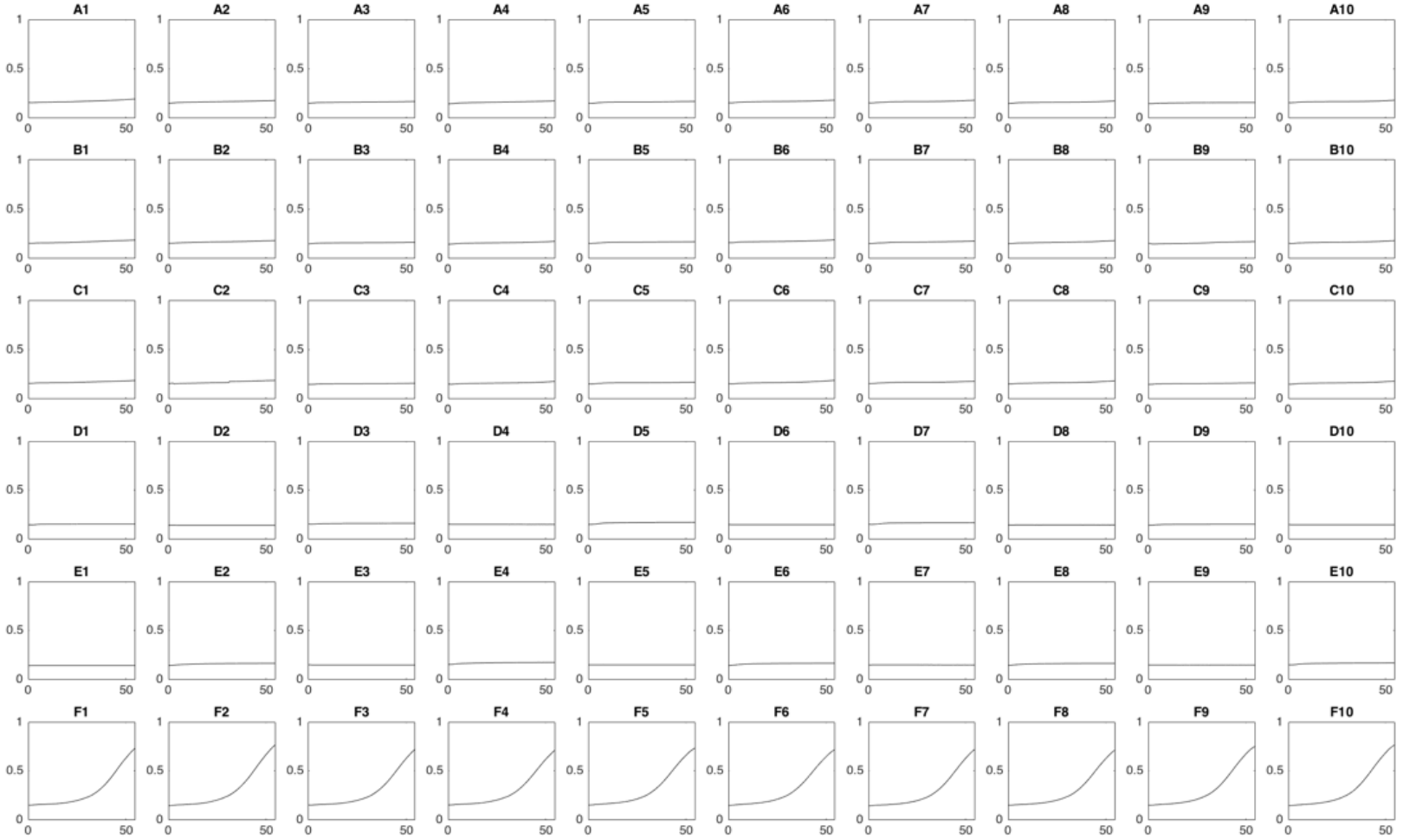

Figure B9: ΔK & ΔI Co-Culture: Variable Amino Acid – Run 1. Each pairwise column separated by 0.2μm membranes. Top three rows are biological replicates, 4th&5th rows are negative control, and 6th row is positive control. (Top) Device schematic. (Bottom) Original OD_{600} data. Contaminated curves given in red, with data omitted curves given in blue.

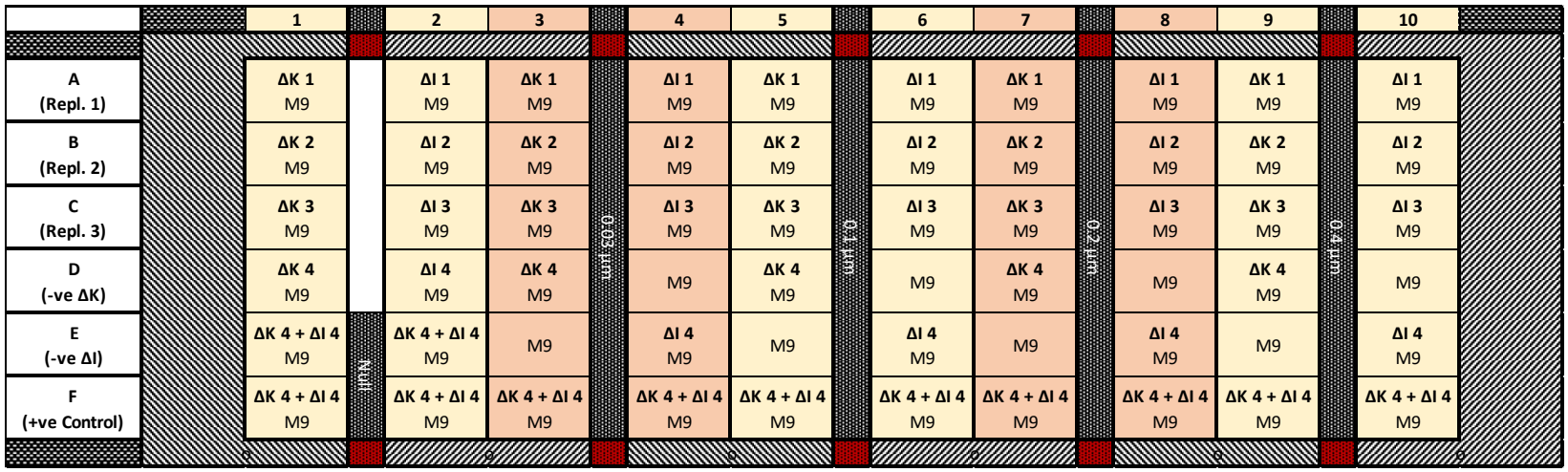
1
2
3
4
5
6
7
8
9
10
A (Repl. 1)
B (Repl. 2)
C (Repl. 3)
D (-ve ΔK)
E (-ve ΔI)
F (+ve Control)
ΔK 1 M9
ΔI 1 M9
ΔK 2 M9
ΔI 2 M9
ΔK 3 M9
ΔI 3 M9
ΔK 4 M9
ΔI 4 M9
ΔK 4 + ΔI 4 M9
M9
Neat
0.05 µm
0.1 µm
0.2 µm
0.4 µm
0

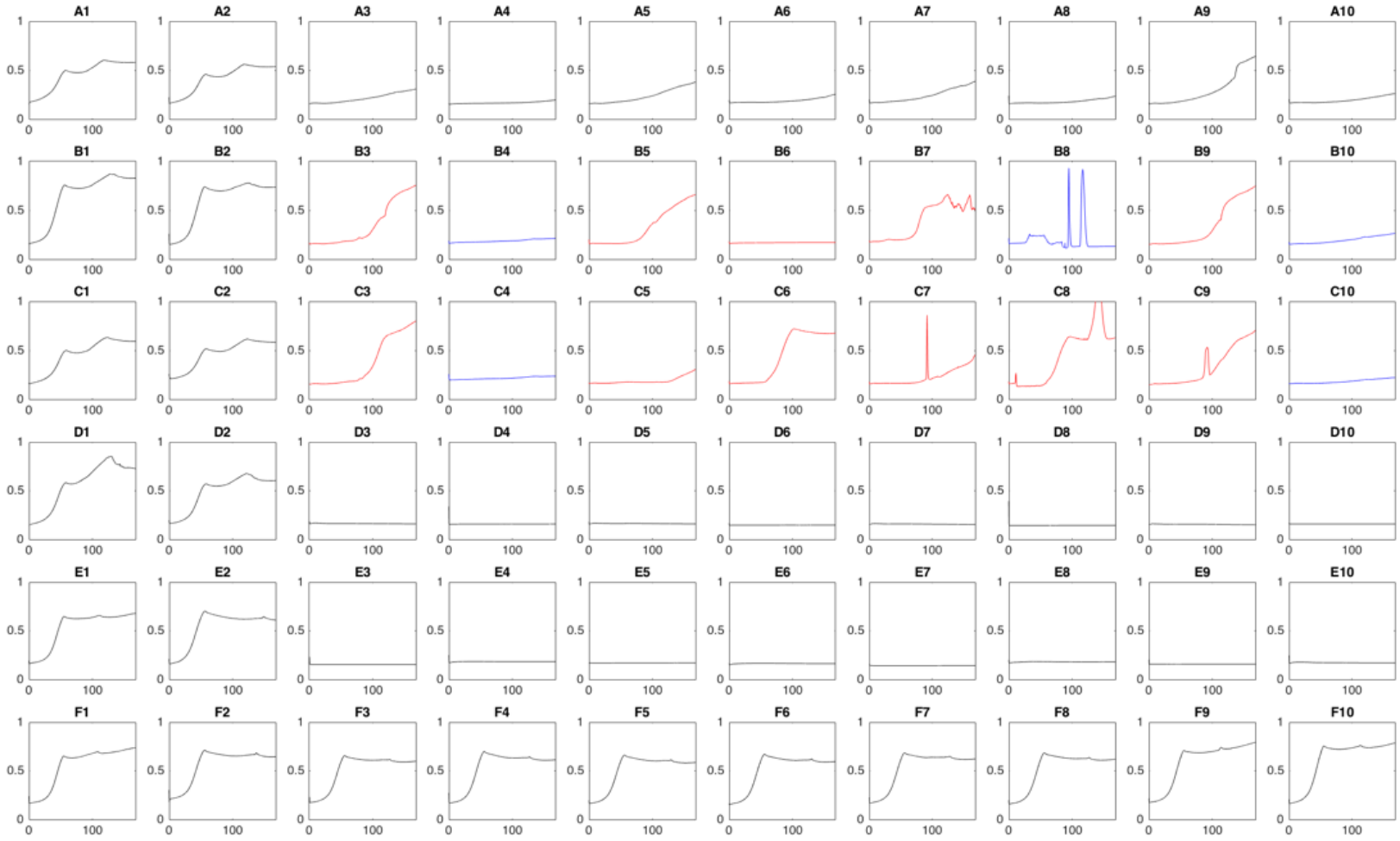

Figure B10: ΔK & ΔI Co-Culture: Variable Pore Size – Run 1. Each pairwise column separated by null, 0.03, 0.1, 0.2, or 0.4μm membrane. Top three rows are biological replicates, 4th&5th rows are negative control, and 6th row is positive control. (Top) Device schematic. (Bottom) Original OD_{600} data. Contaminated curves given in red, with data omitted curves given in blue.

	1	2	3	4	5	6	7	8	9	10
A (Repl. 1)	**ΔK 1** M9	**ΔI 1** M9	**ΔK 1** K&I (10^3)	**ΔI 1** K&I (10^3)	**ΔK 1** K&I (10^6)	**ΔI 1** K&I (10^6)	**ΔK 1** K (10^6)	**ΔI 1** K (10^6)	**ΔK 1** I (10^6)	**ΔI 1** I (10^6)
B (Repl. 2)	**ΔK 2** M9	**ΔI 2** M9	**ΔK 2** K&I (10^3)	**ΔI 2** K&I (10^3)	**ΔK 2** K&I (10^6)	**ΔI 2** K&I (10^6)	**ΔK 2** K (10^6)	**ΔI 2** K (10^6)	**ΔK 2** I (10^6)	**ΔI 2** I (10^6)
C (Repl. 3)	**ΔK 3** M9	**ΔI 3** M9	**ΔK 3** K&I (10^3)	**ΔI 3** K&I (10^3)	**ΔK 3** K&I (10^6)	**ΔI 3** K&I (10^6)	**ΔK 3** K (10^6)	**ΔI 3** K (10^6)	**ΔK 3** I (10^6)	**ΔI 3** I (10^6)
D (-ve ΔK)	**ΔK 4** M9	M9	**ΔK 4** K&I (10^3)	K&I (10^3)	**ΔK 4** K&I (10^6)	K&I (10^6)	**ΔK 4** K (10^6)	K (10^6)	**ΔK 4** I (10^6)	I (10^6)
E (-ve ΔI)	M9	**ΔI 4** M9	K&I (10^3)	**ΔI 4** K&I (10^3)	K&I (10^6)	**ΔI 4** K&I (10^6)	K (10^6)	**ΔI 4** K (10^6)	I (10^6)	**ΔI 4** I (10^6)
F (+ve Control)	**ΔK 4 + ΔI 4** M9	**ΔK 4 + ΔI 4** M9	**ΔK 4 + ΔI 4** K&I (10^3)	**ΔK 4 + ΔI 4** K&I (10^3)	**ΔK 4 + ΔI 4** K&I (10^6)	**ΔK 4 + ΔI 4** K&I (10^6)	**ΔK 4 + ΔI 4** K (10^6)	**ΔK 4 + ΔI 4** K (10^6)	**ΔK 4 + ΔI 4** I (10^6)	**ΔK 4 + ΔI 4** I (10^6)

0.2 µm 0.2 µm 0.2 µm 0.2 µm 0.2 µm

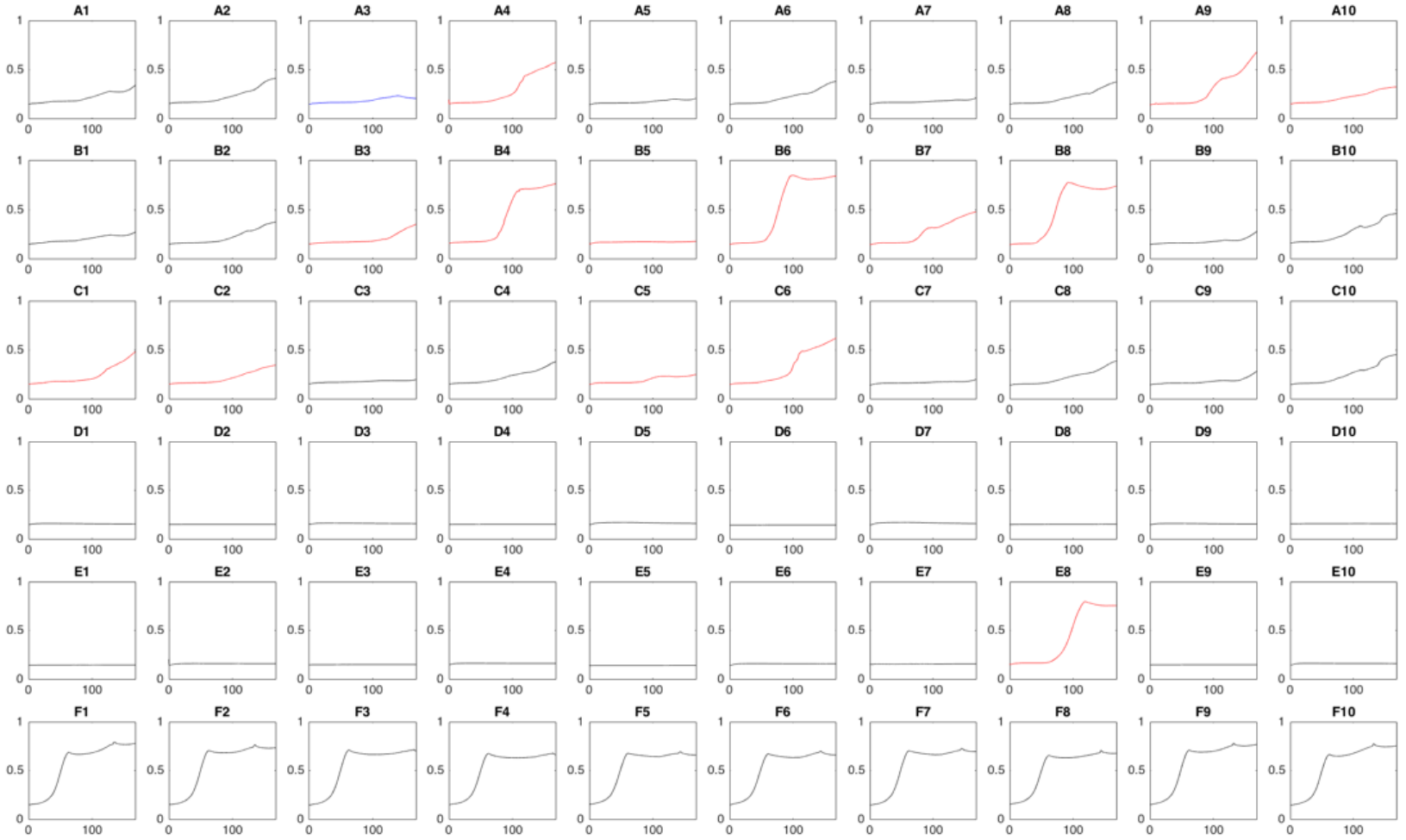

Figure B11: ΔK & ΔI Co-Culture: Variable Amino Acid – Run 2. Each pairwise column separated by 0.03μm membranes. Top three rows are biological replicates, 4th&5th rows are negative control, and 6th row is positive control. (Top) Device schematic. (Bottom) Original OD_{600} data. Contaminated curves given in red, with data omitted curves given in blue.

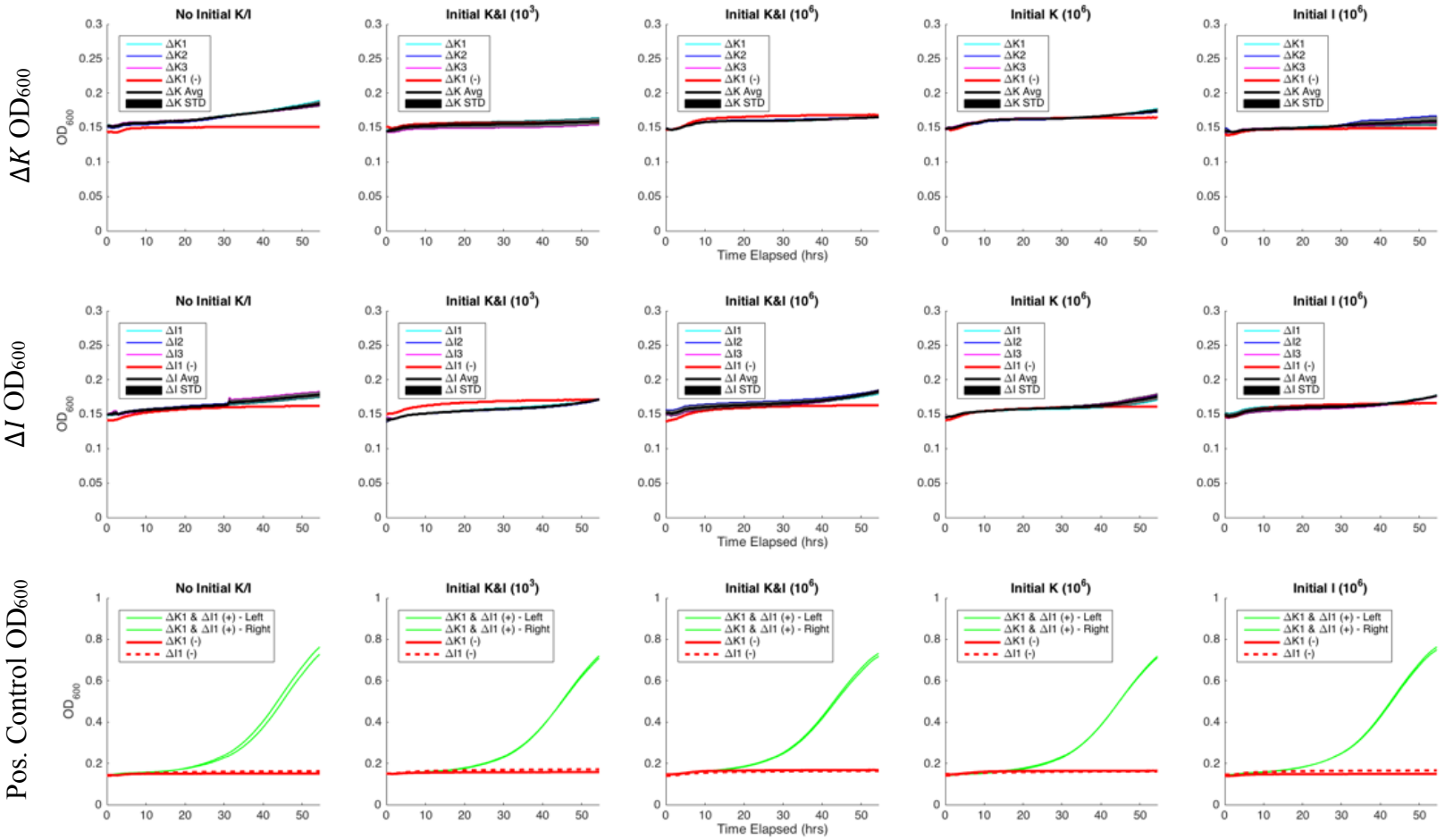

Figure B12: Δ*K*&Δ*I* – Var.AA 1: Original OD_{600} growth curves. (*Top Row*) OD_{600} growth curves of the Δ*K* auxotroph (y-axis = [0 0.3]), (*Middle Row*) OD_{600} growth curves of the Δ*I* auxotroph (y-axis = [0 0.3]), (*Bottom Row*) OD_{600} growth curves of the positive control co-culture, where Δ*K* and Δ*I* auxotrophs are in the same well (y-axis = [0 1]). Data omitted for analysis is depicted by dotted lines.

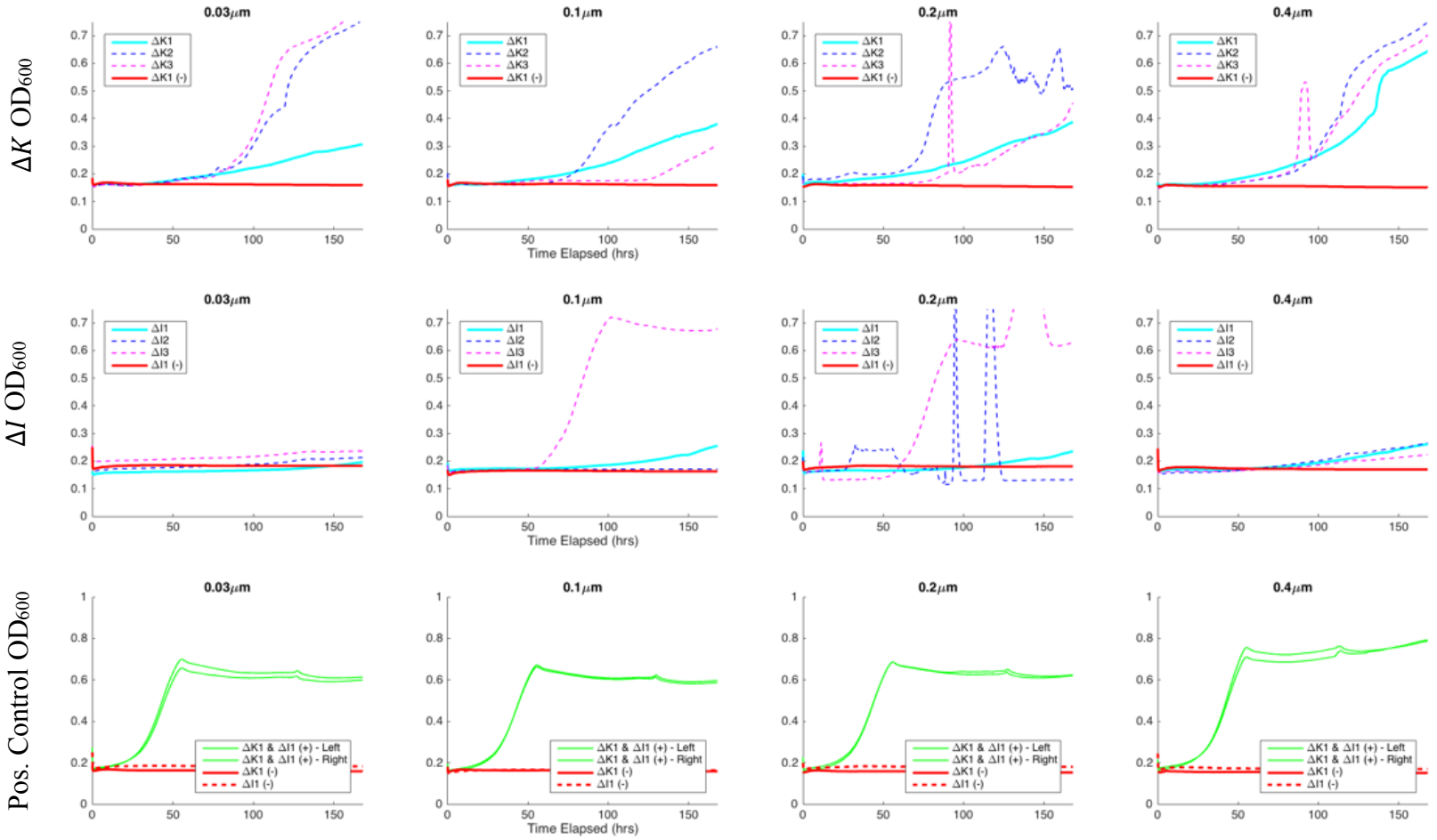

Figure B13: Δ*K*&Δ*I* – Var. Pore Size – Run 2: Original OD_{600} growth curves. (*Top Row*) OD_{600} growth curves of the Δ*K* auxotroph (y-axis = [0 0.5]), (*Middle Row*) OD_{600} growth curves of the Δ*I* auxotroph (y-axis = [0 0.5]), (*Bottom Row*) OD_{600} growth curves of the positive control co-culture, where Δ*K* and Δ*I* auxotrophs are in the same well (y-axis = [0 1]). Data omitted for analysis is depicted by dotted lines.

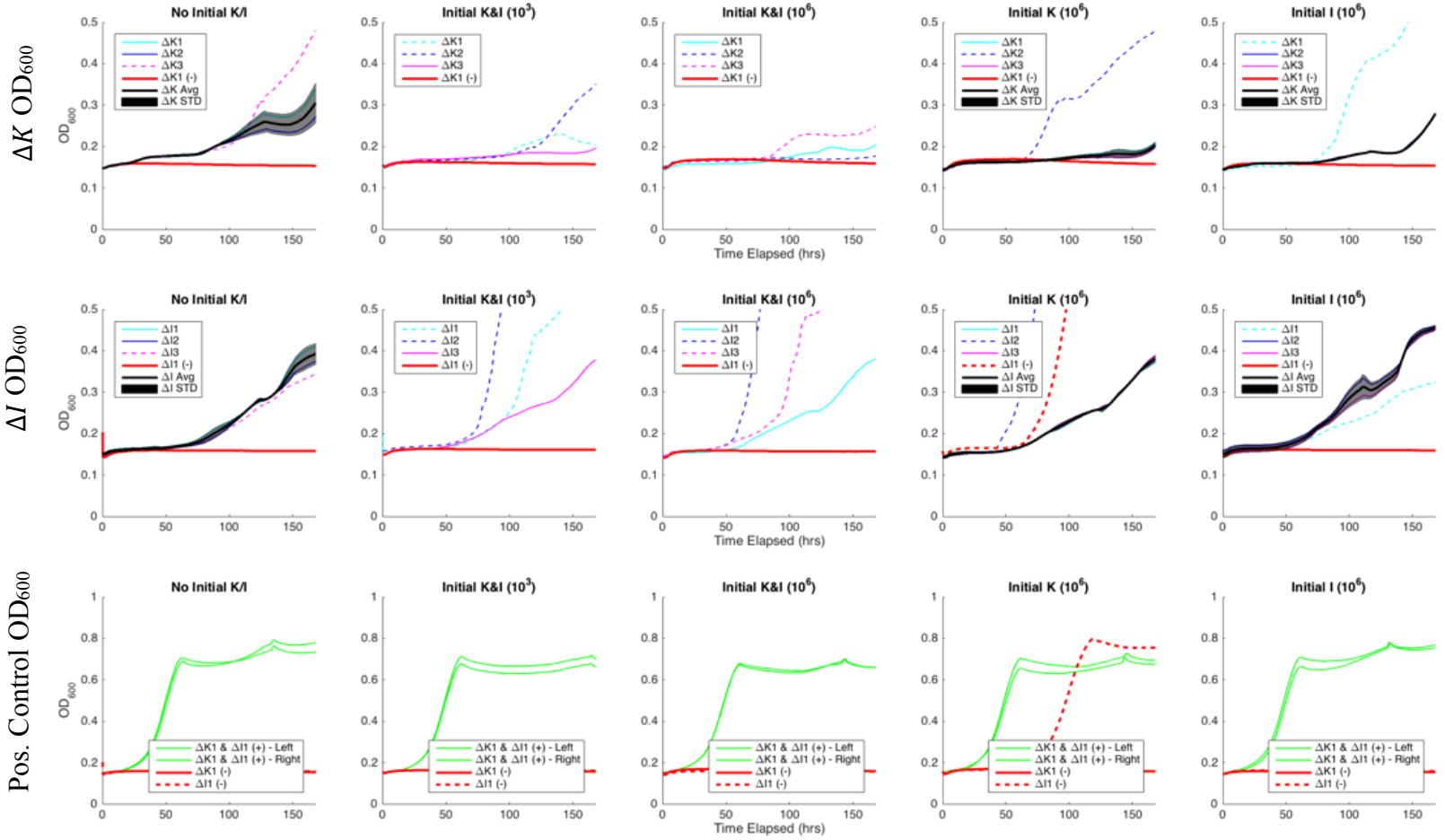

Figure B14: Δ*K*&Δ*I* – Var.AA – Run 2: Original OD_{600} growth curves. (*Top Row*) OD_{600} growth curves of the Δ*K* auxotroph (y-axis = [0 0.5]), (*Middle Row*) OD_{600} growth curves of the Δ*I* auxotroph (y-axis = [0 0.5]), (*Bottom Row*) OD_{600} growth curves of the positive control co-culture, where Δ*K* and Δ*I* auxotrophs are in the same well (y-axis = [0 1]). Data omitted for analysis is depicted by dotted lines.

APPENDIX C: ONGOING & FUTURE WORK

Stoichiometry

$$\alpha_{1(2)} AA1(2) + \alpha_G G = B_{L(R)} + \beta_{2(1)} AA2(1)$$

Fluxes

$$V^B_{L(R)} = min\left(\frac{\frac{vmax_G * \left(\frac{G_{L(R)}}{vol}\right)}{K_G + G_{L(R)}}}{\alpha_G}, \frac{\frac{vmax_{1(2)} * \left(\frac{AA1(2)_{L(R)}}{vol}\right)}{K_{1(2)} + AA1(2)_{L(R)}}}{\alpha_{1(2)}}\right)$$

$$V^G_{L(R)} = V^B_{L(R)} * \alpha_G \qquad V^{AA1(2)}_{L(R)} = V^B_{L(R)} * \alpha_{1(2)} \qquad V^{AA2(1)}_{L(R)} = V^B_{L(R)} * \beta_{2(1)}$$

Diffusion

$$V^{G(AA1)(AA2)}_D = D * \left(\frac{G(AA1)(AA2)_L}{vol} - \frac{G(AA1)(AA2)_R}{vol}\right)$$

Dynamics

$$\frac{dG_L}{dt} = -V^G_L * B_L - V^G_D \qquad \frac{dG_R}{dt} = -V^G_R * B_R + V^G_D$$

$$\frac{dAA1_L}{dt} = -V^{AA1}_L * B_L - V^{AA1}_D \qquad \frac{dAA1_R}{dt} = V^{AA1}_R * B_R + V^{AA1}_D$$

$$\frac{dAA2_L}{dt} = V^{AA2}_L * B_L - V^{AA2}_D \qquad \frac{dAA2_R}{dt} = -V^{AA2}_R * B_R - V^{AA2}_D$$

$$\frac{dB_L}{dt} = V^B_L * B_L \qquad \frac{dB_R}{dt} = V^B_R * B_R$$

Figure C1: Theoretical equations of the syntrophic co-culture model.

	Carbon	Lysine	Isoleucine
v_{max}	10	10	10
k_{max}	10^{-3}	10^{-3}	10^{-3}
α $-$*Stoich. Constant*	0.0901	2.7374	4.0148
$\beta - Secretion\ Rate$	$-$	$[10^{-4} - 1]$	$[10^{-4} - 1]$

Table C1: Parameter values for theoretical model

	1		2	3		4	5		6	7		8	9		10
A	AP 1	0.03μm	LP 1	AP 1	0.03μm	LB 1	LP 1	0.03μm	LB 1	AP 1	0.03μm	AP 1	LB 1	0.03μm	LB 1
B	AP 2		LP 2	AP 2		LB 2	LP 2		LB 2	AP 2		AP 2	LB 2		LB 2
C	AP 3		LP 3	AP 3		LB 3	LP 3		LB 3	AP 3		AP 3	LB 3		LB 3
D	AP 4		LP 4	AP 4		LB 4	LP 4		LB 4	LP 1		LP 1	AP 1		
E	LP 1			LP 3			LB 2		LB 2	LP 2		LP 2	AP 2		
F	LP 2			LB 1		LB 1	LB 3		LB 3	LP 3		LP 3	AP 3		

Figure C2: Device schematic for the *Drosophila* gut microbiome co-culture experiment

Lanes

Top: (Left to right)
1 Ladder
LB primers
2 LP
3 LC
4 LB
5 AP
6 no template control
7 empty
Negative controls (no primers)
8 LP
9 LC
10 LB
11 AP
12 no template

Lanes

Bottom: (Left to right)
1 Ladder
LP primers
2 LP
3 LC
4 LB
5 AP
6 no template control
7 empty
LC primers
8 LP
9 LC
10 LB
11 AP
12 no template

Underline (correct product). We see bands corresponding to correct size (~150bp) products. (Red dot from ipad camera)

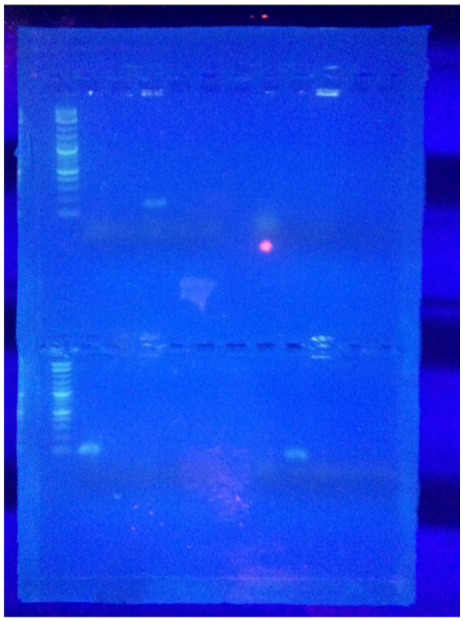

Figure C3: Gel images for the PCR with species-specific primers to confirm bacterial species identity

BIBLIOGRAPHY

1. Aylagas, Eva, et al. "A Bacterial Community-Based Index to Assess the Ecological Status of Estuarine and Coastal Environments." *Marine Pollution Bulletin*, vol. 114, no. 2, Jan. 2017, pp. 679–688. *Crossref*, doi:10.1016/j.marpolbul.2016.10.050.

2. Ben Said, Sami, and Dani Or. "Synthetic Microbial Ecology: Engineering Habitats for Modular Consortia." *Frontiers in Microbiology*, vol. 8, June 2017. *Crossref*, doi:10.3389/fmicb.2017.01125.

3. Berdy, Brittany, et al. "In Situ Cultivation of Previously Uncultivable Microorganisms Using the Ichip." *Nature Protocols*, vol. 12, no. 10, Oct. 2017, pp. 2232–2242. *Crossref*, doi:10.1038/nprot.2017.074.

4. Bittihn, Philip, et al. "Rational Engineering of Synthetic Microbial Systems: From Single Cells to Consortia." *Current Opinion in Microbiology*, vol. 45, Oct. 2018, pp. 92–99. *Crossref*, doi:10.1016/j.mib.2018.02.009.

5. Blaser, Martin J., et al. "Toward a Predictive Understanding of Earth's Microbiomes to Address 21st Century Challenges." *mBio*, vol. 7, no. 3, July 2016. *Crossref*, doi:10.1128/mBio.00714-16.

6. Boon, Eva, et al. "Interactions in the Microbiome: Communities of Organisms and Communities of Genes." *FEMS Microbiology Reviews*, vol. 38, no. 1, Jan. 2014, pp. 90–118. *Crossref*, doi:10.1111/1574-6976.12035.

7. Caspi, Ron, et al. "The MetaCyc Database of Metabolic Pathways and Enzymes." *Nucleic Acids Research*, vol. 46, no. D1, Jan. 2018, pp. D633–639. *Crossref*, doi:10.1093/nar/gkx935.

8. Chacón, Jeremy M., et al. "The Spatial and Metabolic Basis of Colony Size Variation." *The ISME Journal*, vol. 12, no. 3, Mar. 2018, pp. 669–680. *Crossref*, doi:10.1038/s41396-017-0038-0.

9. Chodkowski, John L., and Ashley Shade. "A Synthetic Community System for Probing Microbial Interactions Driven by Exometabolites." *mSystems*, edited by Pieter C. Dorrestein, vol. 2, no. 6, Nov. 2017. *Crossref*, doi:10.1128/mSystems.00129-17.

10. Chu, Hoi Yee, et al. "Assessing the Benefits of Horizontal Gene Transfer by Laboratory Evolution and Genome Sequencing." *BMC Evolutionary Biology*, vol. 18, no. 1, Dec. 2018. *Crossref*, doi:10.1186/s12862-018-1164-7.

11. Cordero, Otto X., and Manoshi S. Datta. “Microbial Interactions and Community Assembly at Microscales.” *Current Opinion in Microbiology*, vol. 31, June 2016, pp. 227–234. *Crossref*, doi:10.1016/j.mib.2016.03.015.

12. Datta, Manoshi S., et al. “Microbial Interactions Lead to Rapid Micro-Scale Successions on Model Marine Particles.” *Nature Communications*, vol. 7, no. 1, Sept. 2016. *Crossref*, doi:10.1038/ncomms11965.

13. Davison, Brian H., and Gregory Stephanopoulos. “Coexistence ofS. Cerevisiae andE. Coli in Chemostat under Substrate Competition and Product Inhibition.” *Biotechnology and Bioengineering*, vol. 28, no. 11, Nov. 1986, pp. 1742–1752. *Crossref*, doi:10.1002/bit.260281119.

14. Dietert, Rodney Reynolds, and Ellen Kovner Silbergeld. “Biomarkers for the 21st Century: Listening to the Microbiome.” *Toxicological Sciences*, vol. 144, no. 2, Apr. 2015, pp. 208–216. *Crossref*, doi:10.1093/toxsci/kfv013.

15. Dittami, Simon M., et al. “A Metabolic Approach to Study Algal-Bacterial Interactions in Changing Environments.” *Molecular Ecology*, vol. 23, no. 7, Apr. 2014, pp. 1656–1660. *Crossref*, doi:10.1111/mec.12670.

16. Dohlman, Anders B., and Xiling Shen. “Mapping the Microbial Interactome: Statistical and Experimental Approaches for Microbiome Network Inference.” *Experimental Biology and Medicine*, edited by Horst von Recum, vol. 244, no. 6, Apr. 2019, pp. 445–458. *Crossref*, doi:10.1177/1535370219836771.

17. Elmqvist, Thomas, et al. “Response Diversity, Ecosystem Change, and Resilience.” *Frontiers in Ecology and the Environment*, vol. 1, no. 9, Nov. 2003, pp. 488–494. *Crossref*, doi:10.1890/1540-9295(2003)001[0488:RDECAR]2.0.CO;2.

18. Embree, Mallory, et al. “Networks of Energetic and Metabolic Interactions Define Dynamics in Microbial Communities.” *Proceedings of the National Academy of Sciences of the United States of America*, vol. 112, no. 50, Dec. 2015, pp. 15450–15455. *Crossref*, doi:10.1073/pnas.1506034112.

19. Estrela, Sylvie, and Sam P. Brown. “Metabolic and Demographic Feedbacks Shape the Emergent Spatial Structure and Function of Microbial Communities.” *PLoS Computational Biology*, edited by Stefano Allesina, vol. 9, no. 12, Dec. 2013, p. e1003398. *Crossref*, doi:10.1371/journal.pcbi.1003398.

20. Faust, Karoline, and Jeroen Raes. “Microbial Interactions: From Networks to Models.” *Nature Reviews. Microbiology*, vol. 10, no. 8, Aug. 2012, pp. 538–550. *Crossref*, doi:10.1038/nrmicro2832.

21. Freilich, Shiri, et al. “Competitive and Cooperative Metabolic Interactions in Bacterial Communities.” *Nature Communications*, vol. 2, no. 1, Sept. 2011. *Crossref*, doi:10.1038/ncomms1597.

22. Friedman, Jonathan, et al. “Community Structure Follows Simple Assembly Rules in Microbial Microcosms.” *Nature Ecology & Evolution*, vol. 1, no. 5, May 2017. *Crossref*, doi:10.1038/s41559-017-0109.

23. Ge, Zhifei, et al. “Nanoporous Microscale Microbial Incubators.” *Lab on a Chip*, vol. 16, no. 3, 2016, pp. 480–488. *Crossref*, doi:10.1039/C5LC00978B.

24. Ghoul, Melanie, and Sara Mitri. “The Ecology and Evolution of Microbial Competition.” *Trends in Microbiology*, vol. 24, no. 10, Oct. 2016, pp. 833–845. *Crossref*, doi:10.1016/j.tim.2016.06.011.

25. Gibbons, Sean M., and Jack A. Gilbert. “Microbial Diversity—exploration of Natural Ecosystems and Microbiomes.” *Current Opinion in Genetics & Development*, vol. 35, Dec. 2015, pp. 66–72. *Crossref*, doi:10.1016/j.gde.2015.10.003.

26. Goers, Lisa, et al. “Co-Culture Systems and Technologies: Taking Synthetic Biology to the next Level.” *Journal of the Royal Society, Interface*, vol. 11, no. 96, July 2014. *PubMed*, doi:10.1098/rsif.2014.0065.

27. Goldford, Joshua E., et al. “Emergent Simplicity in Microbial Community Assembly.” *Science*, vol. 361, no. 6401, Aug. 2018, pp. 469–474. *Crossref*, doi:10.1126/science.aat1168.

28. Griffith, Gary P., et al. “Climate Change Alters Stability and Species Potential Interactions in a Large Marine Ecosystem.” *Global Change Biology*, vol. 24, no. 1, Jan. 2018, pp. e90–100. *Crossref*, doi:10.1111/gcb.13891.

29. Grilli, Jacopo, et al. “Higher-Order Interactions Stabilize Dynamics in Competitive Network Models.” *Nature*, vol. 548, no. 7666, Aug. 2017, pp. 210–213. *Crossref*, doi:10.1038/nature23273.

30. Hall, B. G., et al. “Growth Rates Made Easy.” *Molecular Biology and Evolution*, vol. 31, no. 1, Jan. 2014, pp. 232–238. *Crossref*, doi:10.1093/molbev/mst187.

31. Harcombe, William. “Novel Cooperation Experimentally Evolved between Species.” *Evolution*, Feb. 2010. *Crossref*, doi:10.1111/j.1558-5646.2010.00959.x.

32. Harcombe, William R., et al. “Metabolic Resource Allocation in Individual Microbes Determines Ecosystem Interactions and Spatial Dynamics.” *Cell Reports*, vol. 7, no. 4, May 2014, pp. 1104–1115. *Crossref*, doi:10.1016/j.celrep.2014.03.070.

33. Hunting, Ellard R., et al. “Resource Niche Overlap Promotes Stability of Bacterial Community Metabolism in Experimental Microcosms.” *Frontiers in Microbiology*, vol. 6, Feb. 2015. *Crossref*, doi:10.3389/fmicb.2015.00105.

34. Johns, Nathan I., et al. “Principles for Designing Synthetic Microbial Communities.” *Current Opinion in Microbiology*, vol. 31, June 2016, pp. 146–153. *Crossref*, doi:10.1016/j.mib.2016.03.010.

35. Kallus, Yoav, et al. “Paradoxes in Leaky Microbial Trade.” *Nature Communications*, vol. 8, no. 1, Dec. 2017. *Crossref*, doi:10.1038/s41467-017-01628-8.

36. Kehe, Jared, et al. “Massively Parallel Screening of Synthetic Microbial Communities.” *Proceedings of the National Academy of Sciences*, vol. 116, no. 26, June 2019, pp. 12804–12809. *Crossref*, doi:10.1073/pnas.1900102116.

37. Kinnunen, Marta, et al. “Stochastic Processes Govern Invasion Success in Microbial Communities When the Invader Is Phylogenetically close to Resident Bacteria.” *The ISME Journal*, vol. 12, no. 11, Nov. 2018, pp. 2748–2756. *Crossref*, doi:10.1038/s41396-018-0202-1.

38. Klitgord, Niels, and Daniel Segrè. “Environments That Induce Synthetic Microbial Ecosystems.” *PLoS Computational Biology*, edited by Jason A. Papin, vol. 6, no. 11, Nov. 2010, p. e1001002. *Crossref*, doi:10.1371/journal.pcbi.1001002.

39. Levine, Jonathan M., et al. “Beyond Pairwise Mechanisms of Species Coexistence in Complex Communities.” *Nature*, vol. 546, no. 7656, June 2017, pp. 56–64. *Crossref*, doi:10.1038/nature22898.

40. Levy, R., and E. Borenstein. “Metabolic Modeling of Species Interaction in the Human Microbiome Elucidates Community-Level Assembly Rules.” *Proceedings of the National Academy of Sciences of the United States of America*, vol. 110, no. 31, July 2013, pp. 12804–12809. *Crossref*, doi:10.1073/pnas.1300926110.

41. Lidicker, William Z. “A Clarification of Interactions in Ecological Systems.” *BioScience*, vol. 29, no. 8, Aug. 1979, pp. 475–477. *Crossref*, doi:10.2307/1307540.

42. Lindemann, Stephen R., et al. “Engineering Microbial Consortia for Controllable Outputs.” *The ISME Journal*, vol. 10, no. 9, Sept. 2016, pp. 2077–2084. *Crossref*, doi:10.1038/ismej.2016.26.

43. Mazumdar, Varun, et al. “Metabolic Proximity in the Order of Colonization of a Microbial Community.” *PLoS ONE*, edited by Jens Kreth, vol. 8, no. 10, Oct. 2013, p. e77617. *Crossref*, doi:10.1371/journal.pone.0077617.

44. McNally, Luke, and Sam P. Brown. “Building the Microbiome in Health and Disease: Niche Construction and Social Conflict in Bacteria.” *Philosophical Transactions of the Royal Society B: Biological Sciences*, vol. 370, no. 1675, Aug. 2015, p. 20140298. *Crossref*, doi:10.1098/rstb.2014.0298.

45. Mee, Michael T., et al. “Syntrophic Exchange in Synthetic Microbial Communities.” *Proceedings of the National Academy of Sciences of the United States of America*, vol. 111, no. 20, May 2014, pp. E2149–2156. doi:10.1073/pnas.1405641111.

46. Mee, Michael T., and Harris H. Wang. “Engineering Ecosystems and Synthetic Ecologies.” *Molecular BioSystems*, vol. 8, no. 10, 2012, p. 2470. *Crossref*, doi:10.1039/c2mb25133g.

47. Mendes-Soares, Helena, et al. “MMinte: An Application for Predicting Metabolic Interactions among the Microbial Species in a Community.” *BMC Bioinformatics*, vol. 17, no. 1, Dec. 2016. *Crossref*, doi:10.1186/s12859-016-1230-3.

48. Moutinho, Thomas J., et al. “Novel Co-Culture Plate Enables Growth Dynamic-Based Assessment of Contact-Independent Microbial Interactions.” *PLoS ONE*, edited by Jacob Guy Bundy, vol. 12, no. 8, Aug. 2017, p. e0182163. *Crossref*, doi:10.1371/journal.pone.0182163.

49. Mueller, U. G., and J. L. Sachs. “Engineering Microbiomes to Improve Plant and Animal Health.” *Trends in Microbiology*, vol. 23, no. 10, Oct. 2015, pp. 606–617. *Crossref*, doi:10.1016/j.tim.2015.07.009.

50. Muller, Emilie E. L., et al. “Using Metabolic Networks to Resolve Ecological Properties of Microbiomes.” *Current Opinion in Systems Biology*, vol. 8, Apr. 2018, pp. 73–80. *Crossref*, doi:10.1016/j.coisb.2017.12.004.

51. Nichols, D., et al. “Use of Ichip for High-Throughput In Situ Cultivation of ‘Uncultivable’ Microbial Species.” *Applied and Environmental Microbiology*, vol. 76, no. 8, Apr. 2010, pp. 2445–2450. *Crossref*, doi:10.1128/AEM.01754-09.

52. Pacheco, Alan R., et al. “Costless Metabolic Secretions as Drivers of Interspecies Interactions in Microbial Ecosystems.” *Nature Communications*, vol. 10, no. 1, Jan. 2019, pp. 1–12. doi:10.1038/s41467-018-07946-9.

53. Pacheco, Alan R., and Daniel Segrè. “A Multidimensional Perspective on Microbial Interactions.” *FEMS Microbiology Letters*, vol. 366, no. 11, June 2019. *Crossref*, doi:10.1093/femsle/fnz125.

54. Paczia, Nicole, et al. “Extensive Exometabolome Analysis Reveals Extended Overflow Metabolism in Various Microorganisms.” *Microbial Cell Factories*, vol. 11, no. 1, 2012, p. 122. *Crossref*, doi:10.1186/1475-2859-11-122.

55. Pais, Inês S., et al. “Drosophila Melanogaster Establishes a Species-Specific Mutualistic Interaction with Stable Gut-Colonizing Bacteria.” *PLoS Biology*, edited by Nancy Moran, vol. 16, no. 7, July 2018, p. e2005710. *Crossref*, doi:10.1371/journal.pbio.2005710.

56. Ponomarova, Olga, and Kiran Raosaheb Patil. “Metabolic Interactions in Microbial Communities: Untangling the Gordian Knot.” *Current Opinion in Microbiology*, vol. 27, Oct. 2015, pp. 37–44. *Crossref*, doi:10.1016/j.mib.2015.06.014.

57. Relman, David A. “The Human Microbiome: Ecosystem Resilience and Health.” *Nutrition Reviews*, vol. 70, Aug. 2012, pp. S2–9. *Crossref*, doi:10.1111/j.1753-4887.2012.00489.x.

58. Rosenthal, Adam Z., et al. “Metabolic Interactions between Dynamic Bacterial Subpopulations.” *eLife*, 2018. *DataCite*, doi:10.7554/elife.33099.001.

59. Russel, Jakob, et al. “Antagonism Correlates with Metabolic Similarity in Diverse Bacteria.” *Proceedings of the National Academy of Sciences of the United States of America*, vol. 114, no. 40, Oct. 2017, pp. 10684–10688. *Crossref*, doi:10.1073/pnas.1706016114.

60. Sachs, Joel L., et al. “The Evolution of Cooperation.” *The Quarterly Review of Biology*, vol. 79, no. 2, June 2004, pp. 135–160. *Crossref*, doi:10.1086/383541.

61. Sanchez-Gorostiaga, Alicia, et al. “High-Order Interactions Dominate the Functional Landscape of Microbial Consortia.” *bioRxiv*, May 2018. *DataCite*, doi:10.1101/333534.

62. Seth, Erica C., and Michiko E. Taga. “Nutrient Cross-Feeding in the Microbial World.” *Frontiers in Microbiology*, vol. 5, July 2014. *Crossref*, doi:10.3389/fmicb.2014.00350.

63. Simhadri, Rama K., et al. “The Gut Commensal Microbiome of *Drosophila Melanogaster* Is Modified by the Endosymbiont *Wolbachia*.” *mSphere*, edited by Karen L. Visick, vol. 2, no. 5, Oct. 2017. *Crossref*, doi:10.1128/mSphere.00287-17.

64. Sommer, Andrew J., and Peter D. Newell. “Metabolic Basis for Mutualism between Gut Bacteria and Its Impact on the *Drosophila Melanogaster* Host.” *Applied and Environmental Microbiology*, edited by Shuang-Jiang Liu, vol. 85, no. 2, Nov. 2018. *Crossref*, doi:10.1128/AEM.01882-18.

65. Stachowicz, John J., et al. “Understanding the Effects of Marine Biodiversity on Communities and Ecosystems.” *Annual Review of Ecology, Evolution, and Systematics*, vol. 38, no. 1, Dec. 2007, pp. 739–766. *Crossref*, doi:10.1146/annurev.ecolsys.38.091206.095659.

66. Steinway, Steven N., et al. “Inference of Network Dynamics and Metabolic Interactions in the Gut Microbiome.” *PLoS Computational Biology*, edited by Costas D. Maranas, vol. 11, no. 6, June 2015, p. e1004338. *Crossref*, doi:10.1371/journal.pcbi.1004338.

67. Stevenson, Keiran, et al. “General Calibration of Microbial Growth in Microplate Readers.” *Scientific Reports*, vol. 6, no. 1, Dec. 2016. *Crossref*, doi:10.1038/srep38828.

68. Sung, Jaeyun, et al. “Global Metabolic Interaction Network of the Human Gut Microbiota for Context-Specific Community-Scale Analysis.” *Nature Communications*, vol. 8, no. 1, Aug. 2017. *Crossref*, doi:10.1038/ncomms15393.

69. Vance, W., et al. “Determination of Causal Connectivities of Species in Reaction Networks.” *Proceedings of the National Academy of Sciences of the United States of America*, vol. 99, no. 9, Apr. 2002, pp. 5816–5821. doi:10.1073/pnas.022049699.

70. Vemuri, G. N., et al. “Overflow Metabolism in Escherichia Coli during Steady-State Growth: Transcriptional Regulation and Effect of the Redox Ratio.” *Applied and Environmental Microbiology*, vol. 72, no. 5, May 2006, pp. 3653–3661. *Crossref*, doi:10.1128/AEM.72.5.3653-3661.2006.

71. Venturelli, Ophelia S., et al. “Deciphering Microbial Interactions in Synthetic Human Gut Microbiome Communities.” *Molecular Systems Biology*, vol. 14, no. 6, June 2018. *Crossref*, doi:10.15252/msb.20178157.

72. Vet, Stefan, et al. “Bistability in a System of Two Species Interacting through Mutualism as Well as Competition: Chemostat vs. Lotka-Volterra Equations.” *PLoS ONE*, edited by Ramon Grima, vol. 13, no. 6, June 2018, p. e0197462. *Crossref*, doi:10.1371/journal.pone.0197462.

73. Vetsigian, Kalin, et al. “Structure and Evolution of Streptomyces Interaction Networks in Soil and In Silico.” *PLoS Biology*, edited by Jonathan A. Eisen, vol. 9, no. 10, Oct. 2011, p. e1001184. *Crossref*, doi:10.1371/journal.pbio.1001184.

74. Watkins, Eleanor R., et al. “Metabolic Competition as a Driver of Bacterial Population Structure.” *Future Microbiology*, vol. 11, no. 10, Oct. 2016, pp. 1339–1357. *Crossref*, doi:10.2217/fmb-2016-0079.

75. White, Richard Allen, et al. “The Past, Present and Future of Microbiome Analyses.” *Nature Protocols*, vol. 11, no. 11, Nov. 2016, pp. 2049–2053. *Crossref*, doi:10.1038/nprot.2016.148.

76. Wintermute, Edwin H., and Pamela A. Silver. “Emergent Cooperation in Microbial Metabolism.” *Molecular Systems Biology*, vol. 6, no. 1, Jan. 2010, p. 407. *Crossref*, doi:10.1038/msb.2010.66.

77. Xiao, Yandong, et al. “Mapping the Ecological Networks of Microbial Communities.” *Nature Communications*, vol. 8, no. 1, Dec. 2017. *Crossref*, doi:10.1038/s41467-017-02090-2.

78. Xu, B., et al. “Modeling of Overflow Metabolism in Batch and Fed-Batch Cultures of Escherichia Coli.” *Biotechnology Progress*, vol. 15, no. 1, Feb. 1999, pp. 81–90. *Crossref*, doi:10.1021/bp9801087.

79. Zaneveld, Jesse R., et al. “Stress and Stability: Applying the Anna Karenina Principle to Animal Microbiomes.” *Nature Microbiology*, vol. 2, no. 9, Sept. 2017. *Crossref*, doi:10.1038/nmicrobiol.2017.121.

80. Zelezniak, Aleksej, et al. “Metabolic Dependencies Drive Species Co-Occurrence in Diverse Microbial Communities.” *Proceedings of the National Academy of Sciences of the United States of America*, vol. 112, no. 20, May 2015, pp. 6449–6454. *Crossref*, doi:10.1073/pnas.1421834112.

81. Ziegler, Maren, et al. “Bacterial Community Dynamics Are Linked to Patterns of Coral Heat Tolerance.” *Nature Communications*, vol. 8, no. 1, Apr. 2017. *Crossref*, doi:10.1038/ncomms14213.

82. Zomorrodi, Ali R., and Daniel Segrè. “Synthetic Ecology of Microbes: Mathematical Models and Applications.” *Journal of Molecular Biology*, vol. 428, no. 5, Feb. 2016, pp. 837–861. *Crossref*, doi:10.1016/j.jmb.2015.10.019.

CURRICULUM VITAE